PETROLOGY AND MINERAL CHEMISTRY OF SOME JAN MAYEN VOLCANICS

A thesis presented to the Faculty
of the State University of New York
at Albany
in partial fulfillment of the requirements
for the degree of
Master of Science

School of Arts and Sciences
Department of Geological Sciences

Carla A. White

1979

ACKNOWLEDGMENTS

The author wishes to thank Dr. Steve DeLong for providing the thin sections from Jan Mayen and for advising this research project. Dr. George Putman and Dr. Akiho Miyashiro are gratefully thanked for their advice, discussions and criticism. Dr. Dave Walker is kindly thanked for instruction and assistance in the operation of the electron microprobe at the Harvard University Geology Department. Samples used in this study were provided to Dr. DeLong by Mr. Frank J. Fitch, Birkbeck College, University of London. Computer programming and photographic techniques were kindly demonstrated by Frieda Malcolm. Computer time was provided by the State University of New York at Albany Computer Center. A teaching assistantship provided by the Department of Geological Sciences at the State University of New York at Albany is gratefully acknowledged.

PETROLOGY AND MINERAL CHEMISTRY OF SOME JAN MAYEN VOLCANICS

Abstract of
a thesis presented to the Faculty
of the State University of New York
at Albany
in partial fulfillment of the requirements
for the degree of
Master of Science

School of Arts and Sciences
Department of Geological Sciences

Carla A. White

1979

ABSTRACT

The island of Jan Mayen is the northernmost active volcano on the Mid-Atlantic Ridge. The rocks of Jan Mayen belong to the potassic series of the alkaline rocks and appear to belong to the straddle type association. The ankaramites and alkali olivine basalts are characterized by the presence of large xenocrysts of rimmed chromium diopside, titaniferous salite, olivine (Fo_{83} to Fo_{88}), magnetite and sometimes plagioclase (bytownite rimmed by labradorite). Phenocrysts of olivine (Fo_{74}) and plagioclase (andesine) are present in several rocks. These xenocrysts and phenocrysts lie in a matrix composed of titaniferous salite, olivine (Fo_{58}), plagioclase (andesine), magnetite, biotite and sometimes ilmenite. Latite andesites contain large crystals of plagioclase of an andesine-oligoclase composition rimmed by oligoclase or alkali feldspar, magnetite, biotite, hornblende and sometimes highly altered clinopyroxene. The trachytes are characterized by phenocrysts of aegirine-augite, anorthoclase, magnetite, biotite and sometimes andesine rimmed by an alkali feldspar. The phenocrysts of the latite andesites and trachyte lie in a groundmass consisting of andesine, alkali feldspar, magnetite, hematite and biotite.

Trace element whole rock geochemistry indicates that the rocks of Jan Mayen were probably derived from the mantle from slightly different source regions based on different Rb/Sr ratios for the mafic rocks of Nord Jan and Sor Jan. The rocks formed by the partial accumulation of titaniferous salite, plagioclase, olivine and magnetite from an alkali basalt magma followed by the intrusion and capture of xenoliths and xenocrysts of ultramafic or mafic rocks, which may have been in the process of accumulation. This accumulation process is supported by the results of least squares magma mixing models and Rayleigh fractionation curves.

TABLE OF CONTENTS

LIST OF FIGURES

LIST OF TABLES

LIST OF PLATES

I. LOCATION AND PHYSICAL FEATURES OF JAN MAYEN

The tiny island of Jan Mayen is the northernmost, active volcanic island on the Mid-Atlantic Ridge system (71°N, 8-9°W). It lies at the northernmost end of the Jan Mayen Ridge just south of the intersection of the western segment of the Jan Mayen Fracture Zone and the southern end of the Mohns Ridge (Figure 1).

Jan Mayen rises about 5.3 km from the ocean floor to its highest peak on the Beerenberg volcano 2277 m above sea level. The island is elongated NE-SW 53.6 km, has a maximum width of 16 km, and covers an area of 380 km^2.

Nord Jan is dominated by the Beerenberg volcano. The gently sloping basal dome of Beerenberg is 25 km in diameter at sealevel and is capped by a steep sided cone. This upper cone is characterized by a crater about 1.3 km in diameter and smaller parasitic cones of lava or ash surrounding it on the southwest, west, and northeast sides. Beerenberg is covered by twenty glaciers which extend radially from the summit to the base. The glaciers occupy shallow, wide valleys to the south and deep valleys to the north.

Beerenberg terminates to the north, east and west in steep coastal cliffs. The northeastern extremity of Nord Jan is a coastal platform which extends 0.5 to 1.0 mi

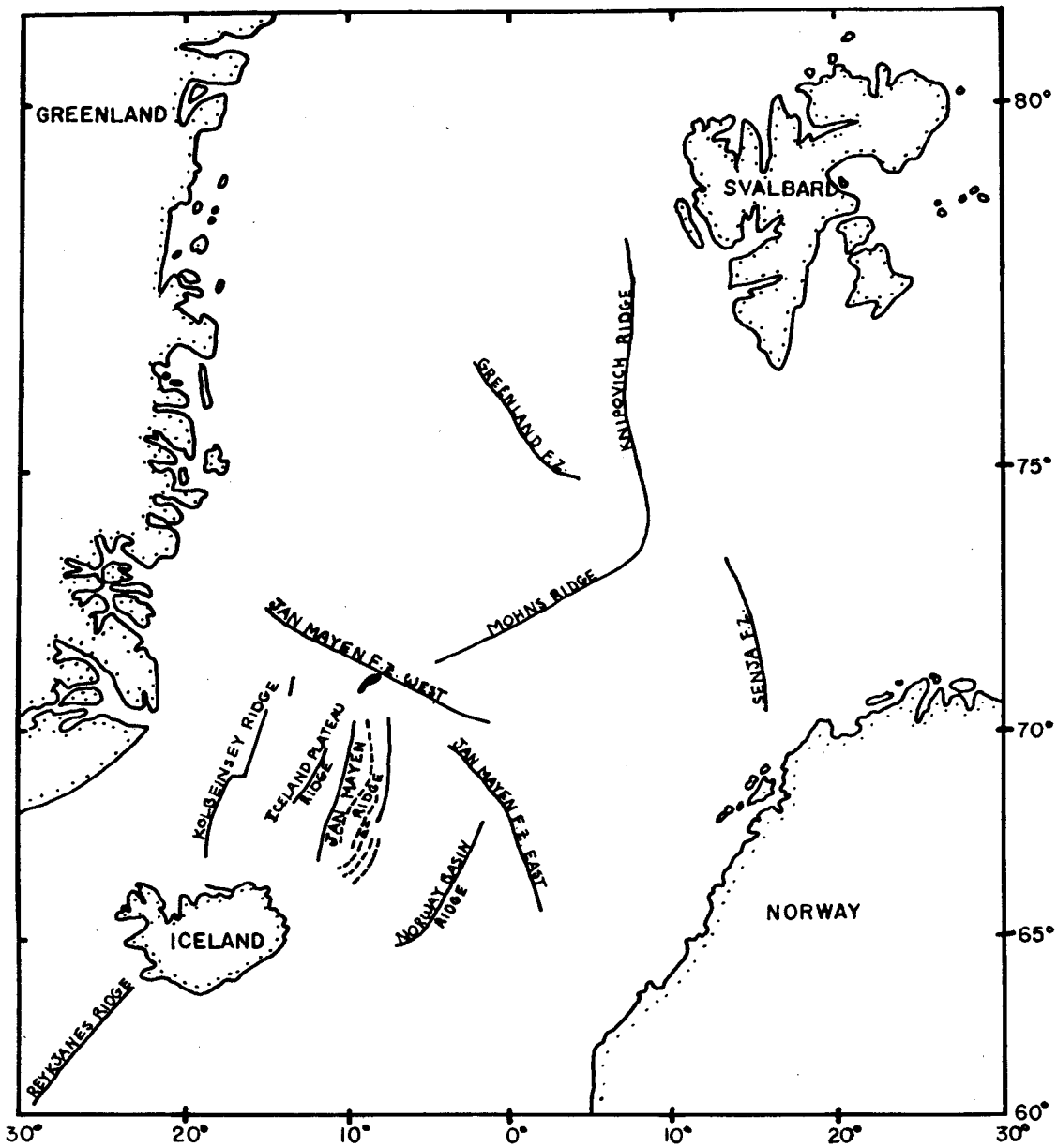

Figure 1. The tectonic location of Jan Mayen Island in the Northern Atlantic Ocean (adapted from Talwani and Eldholm, 1977).

toward the sea, and along the coast to the west and south. A northeast trending volcanic rift zone (Nordkapp Rift Zone), originating from Beerenberg, ends just south of the coastal platform. The rift is bounded by two 500 m cliffs. Two subsidiary rifts extend southeast and southwest giving Beerenberg the typical tribrachial structure of volcanoes. Most minor rifts, dikes, faults, fractures, and fissures also follow the dominant NE-SW trend, but two minor sets trend NW-SE and E-W.

The Central Region is very narrow and the smallest width is only 2 miles. The area is characterized by long beaches, lagoons, and a high pillar (volcanic neck) called the Saule.

Sor Jan is a low, relatively narrow, volcanic tableland (500 m above sea level). Linearly trending trachyte domes and volcanic craters or depressions are common. The domes are oval shaped (100 m by 600-800 m) at the base and are flattened on the top. The tops of some domes are characterized by small circular depressions. Sor Jan rises steeply from the sea except for a few bays on the southwest coast.

II. HISTORY OF JAN MAYEN

The island of Jan Mayen was "discovered" many times by English and Dutch seamen searching for a northern passage to the East. The island has therefore been known by several different names throughout its known existence: 1) Hudson Tutches (1607, Henry Hudson), 2) Trinity Island (1611, Thomas Marmaduke), 3) Isle de Richelieu (1612, Jean Vrolicz), 4) Sir Thomas Smith's Island (1615, Robert Fotherby), and 5) Jan Mayen Island (1614, Jan Jacobsz May). The search for the northern passage was unsuccessful, but the seamen found a very rich whaling-ground. The Dutch even went so far as to build several whaling stations on Jan Mayen. The whaling-ground was so extensively used that by 1650 most of the whales were exterminated.

Modern scientific work on Jan Mayen began in 1920 with the establishment of a wireless radio and a weather station by the Norwegian government (Norway annexed Jan Mayen in 1929). An Austrian expedition to Jan Mayen in the Polar Year 1882-1883 completed a topographic map of the island and brought back geological specimens. Magnetic, meteorological, and biological data were also collected. The Cambridge party expedition in 1921, including geologist J.M. Wordie, brought back a collection of 60 rock specimens (described by Tyrrell in 1926), a biological collection, and completed a general geological survey. Another Austrian

party revisited Jan Mayen for magnetic measurements in the Polar Year 1932-1933. The Imperial College Expedition in 1938 studied glaciology (J.N. Jennings, 1948), geology (detailed geologic map at 1:25,000 scale of the central part of the island), botany, ornithology, and marine biology (A. King, 1939) of Jan Mayen. G.D. Nicholls visited Jan Mayen in 1950 and developed a short unnamed volcanic stratigraphy for Nord Jan. During the 1960's several trips to Jan Mayen (notably the University of London 1961 Beerenberg Expedition) were made by different groups of geologists. Glaciology, glacial history, petrography, geology, geologic history, volcanic stratigraphy, tectonics, and paleomagnetism were studied at this time.

The 1970 eruption on the northeastern slope of Beerenberg renewed interest in the tectonics, seismicity, and petrography of Jan Mayen.

Current surveillance of activity on Jan Mayen includes a seismographic network of 3 stations, crustal movement studies (6 tiltmeters), measurement of the temperature of gas emitted at Eggoya and 19 gravity stations (Sylvester, 1975).

III. GEOLOGIC AND GLACIAL HISTORY OF JAN MAYEN

The first major contribution to the understanding of the geology of Jan Mayen was presented by Wordie in 1926. Since then the geologic history and volcanic stratigraphy of Jan Mayen have been established by Fitch, Grasty and Miller (1965), Roberts and Hawkins (1965), Fitch, Nairn and Talbot (1965), Fitch (1962), Nicholls (1955), Sylvester (1975), Carstens (1962), and Dollar (1965). The glacial history was established by Kinsman and Sheard (1962), Fitch (1962), Lamb, Probert-Jones and Sheard (1962), and Kinsman, Sheard and Fitch (1962). The following is an abbreviated account of the geologic history, glacial history, and stratigraphy from the above mentionned sources.

The oldest rocks on Jan Mayen are located in Sor Jan and comprise three separate formations: the Lower, Middle, and Upper Groups. The rocks of the Lower Group represent the formation of the volcanic basement upon which the island of Jan Mayen lies. The age of the volcanic basement is believed to be at the earliest, Mid-Tertiary and at the latest Pleistocene, 12,000 years BP (Fitch, Grasty and Miller, 1965; Fitch, 1962). This age range, however, is much too broad. The age of the volcanic basement is probably more accurately defined by the Pleistocene age. The Lower Group consists of basaltic lavas and pyroclastics, which were extruded through a N50°E fissure swarm, and are crosscut by later dikes.

The Sor Jan plateau was constructed during a long period of fissure eruptions notably occurring at the junctions of the old N50°E fissure swarm and a newly developed N40°E fissure swarm. These Middle Group lavas consist of trachybasalt, trachyandesite, latite, and trachyte and are crosscut by dikes of trachybasalt and trachyandesite, which may have acted as feeders to the lavas. The development of the trachybasaltic plateau is separated from the younger dome building stage of the Upper Group by an erosional period and another short period of phyric trachybasalt extrusion.

The trachyte and latite domes of the Upper Group represent the plugging of the basaltic necks (at the junctions of N40°E and N50°E fissures) in Sor Jan and Central Jan Mayen (the Saule). The lavas probably originated from around the base of the dome or from the central depression and are probably the most recent volcanics on Sor Jan.

A period of volcanic quiescence and extensive erosion followed the volcanic activity in Sor Jan.

Volcanism on Jan Mayen subsequently moved northeastward from Sor Jan to the volcano Beerenberg on Nord Jan which was constructed in three stages. The submarine foundation of Nord Jan is unexposed, but trachybasaltic xenoliths in some lavas, bombs, lapilli tuffs, and xenoliths of ankaramite in the Kapp Fishburn Tillite indicate that it may consist of a basalt to trachyte sequence.

The lower volcanic dome of Beerenberg developed by explosive fissure eruptions from the N40°E fissure swarm followed by the subaerial extrusion of ankaramite from the central vent and radial fissures. The Kapp Muyen group, the lavas of the lower cone, consists of the Krossbukta formation, the Kapp Fishburn Tillite, the Storfjellet formation, the Havhestberget formation and the Nordvestkapp formation (from oldest to youngest).

The Krossbukta formation is the oldest volcanic sequence in Nord Jan and consists of two ankaramitic basalt aa flows separated by a well compacted fossil talus of angular, ankaramitic basalt fragments.

The Kapp Fishburn Tillite is the first evidence of glaciation on Jan Mayen and overlies eroded Krossbukta lavas. The basaltic tillite is believed to be a product of the last Pleistocene glaciation (Fitch, 1962) and contain fragments of ankaramitic basalt and nonporphyritic basalt. It is divisible into two distinguishable units: 1) the lower tillite, which is believed to have formed about 12,000 years BP and 2) the upper tillite, which formed 10,000 to 10,500 years BP (Kinsman and Sheard, 1962). At the present there is no direct evidence of another glaciation in the volcanic stratigraphy of Jan Mayen until the formation of the summit cone and crater of Beerenberg 6,000 to 7,000 years BP (Fitch, Nairn and Talbot, 1965). The tillite is unconformably overlain by the Storfjellet formation.

The Storfjellet formation, extruded about 9,000 years BP (Fitch, Nairn and Talbot, 1965), consists of pyroclastic cones and whaleback mounds of ash, scoriae, and agglutinate overlying a sequence of ankaramitic basalts and nonporphyritic basalts. Dikes are most abundant in the Storfjellet formation and cut through both pyroclastic and lava sequences. They vary in thickness from a few centimeters (sinuous) to about 4 m (constant strike over distances greater than one kilometer). The dikes in the Storfjellet formation generally do not extend upward into the overlying Nordvestkapp formation and are thus probably feeders from which the Storfjellet formation and/or Nordvestkapp formation were derived. Many dikes appear to have orientations similar to the fissure swarms and actually may be filled in fissures or tension gashes.

The Havhestberget formation unconformably overlies the Storfjellet formation and represents a major explosive stage in the development of the lower dome. It consists of a basalt pumice-tuff and a sillar or agglomerate. The Havhestberget formation is overlain by the Nordvestkapp formation which constitute the major part of the lower ankaramitic cone. The Nordvestkapp aa lavas are highly porphyritic ankaramitic basalts which are sometimes interbedded with ankaramites, nonporphyritic basalts, cinders, and tuff. A single sill (2 m thick), characterized by well developed columnar jointing, intrudes the lavas of the Nordvestkapp formation. The Havhestberget and Nordvestkapp

formations were deposited about 7,000 to 8,000 years BP (Fitch, Nairn and Talbot, 1965).

The steep trachybasaltic upper cone of Beerenberg was constructed from the Sentralkrateret lavas about 6,000 to 7,000 years BP (Fitch, Nairn and Talbot, 1965) after a short interval of erosion. The lavas extruded from the upper cone are distinct from the ankaramitic basalt of the lower dome in that they consist primarily of glomeroporphyritic plagioclase trachybasalt interbedded with a few ankaramite flows. The Sentralkrateret lavas rest unconformably on the Nordvestkapp formation. Another period of erosion after the formation of the summit cone cut steep sea cliffs about the volcano.

Subsequent volcanism, occurring on the flanks of Beerenberg, was structurally controlled by reactivation of the N40°E fissure swarm and by activation of radial fissures on the south and southeast flanks. Violent pyroclastic eruptions followed by gentle lava flows were typical of this flank volcanism. During the later stages of this period of volcanism a new set of fissures developed in the northeastern part of Nord Jan parallel to N65°E. The Nordkapp Group represents the parasitic and fissure eruptions on the flanks of Beerenberg since the end of the extrusion of the Sentralkrateret formation to the present. It includes the Tromsoryggen formation, the Kokssletta formation, and the Smithbreen formation.

The Tromsoryggen lavas, extruded about 4,000 to 5,000 years BP (Fitch, Nairn and Talbot, 1965) consist of ankaramitic basalts overlain by a thick and variable sequence of pyroclastics. The pyroclastics, consisting of scoriae, bombs, and agglutinate, form large ridges parallel to the fissures.

An extensive glacial advance, the Krogness Advance, probably occurred after the extrusion of the Tromsoryggen lavas (Kinsman and Sheard, 1962). Most moraines formed by this glaciation were buried by the Kokssletta lavas.

The Kokssletta lavas represent the last major cycle of eruption about 2,500 to 3,00 years BP (Fitch, 1964). They occur as aa flows, but pahoehoe type lavas are also present (which usually overlie the aa flows). To the north the lavas are glomeroporphyritic plagioclase trachybasalts and ankaramitic basalts; to the south only glomeroporphyritic plagioclase trachybasalts are observed. Sylvester (1975) disputes Fitch's age of the Kokssletta lavas and concludes, based on old maps and lava forms, that the lavas probably formed between 1820 and 1882.

The Smithbreen formation consists of all nonvolcanic deposits younger than the Kokssletta lavas. It includes primarily morainic debris, with talus or outwash fans, lagoon silts and muds, present day beach material, and recent volcanics.

The Joris glacial advance occurred after the deposition of the Kokssletta formation, possibly about 2,500 years BP (Kinsman and Sheard, 1962).

Most of the moraines of the Joris Advance were broken up by the later Sorbreen Advance and are not well preserved. The moraines of the Joris Advance, where present, lie outside of those of the Sorbreen Advance.

The glacial activity of the past 350 years on Beerenberg is known as the Sorbreen Advance or the "Little Ice Age". A summary of observations on the minor advances and retreats of the Sorbreen Advance has been compiled from Lamb, Probert-Jones and Sheard (1962), Jennings (1948), Fitch, (1962), Kinsman, Sheard and Fitch (1962), and Kinsman and Sheard (1962).

Sorbreen Advance

1750	Climax of an advance. Retreat and formation of outer series moraine (I).
1810-20	Small readvance. Slow retreat and formation of hummocky moraines.
1850-70	Large readvance. Rapid retreat and formation of inner series moraine (II) which are less developed than the outer series moraine.
1910-20	Readvance. Retreat and formation of innermost series moraine (III).
1938-42	Rapid retreat.
1954	Estimated beginning of an advance.
1959	Acceleration of advance.
1961-	Glaciers still advancing.

Documented eruptions on Jan Mayen have occurred in 1732 (Jan Jacobsen Laab, a Dutch sailor), in 1818

(the British sailor William Scoresby, Jr.) and in 1970. These eruptions took place along the northeastern flank of Beerenberg. The eruptions of 1732 and 1818 have been subjected to some doubt as to their authenticity because neither produced lava. However, based on the recent eruption in 1970, these eruptions may have been accurately reported.

The most recent volcanic activity on Jan Mayen began on 18 September 1970. The eruption may have begun either simultaneously with or shortly after an earthquake. Birkenmajer (1972) reports a magnitude of 5.1 on the Richter scale for this earthquake and Sylvester (1974) calculated the depth of its epicenter to be 28 km. Zobin (1972) reports a magnitude of 5.0, and 33 km as the depth of the epicenter (with nearly vertical nodal planes at 85°WSW and 75°SSE orientations). This earthquake was the first and strongest of the following earthquake swarm. Seismicity throughout the eruption was very high.

It has been disputed whether four, short fissures opened up initially or whether there was simply a single, long fissure. Aerial photographs taken 20 and 21 September appear to be ambiguous and can be interpreted in either manner. Birkenmajer (1972) supports the formation of four fissures and the following discussion assumes the same.

The fissures first opened up above Austbukta and Clandeboyebukta varying from a height of 40 m to 500 m above sea level. The fissures had a NNE-SSW strike of about

30° (azimuth) and extended for about 6 km in this direction. Birkenmajer (1972) interprets the fissures as being stepped tension gashes that opened along a dextral strike slip fault.

Lava erupted from the four fissures as gentle flows or lava fountains. Ejected pyroclastic debris (bombs and ash) was also spread over the eruption site. This type of activity probably continued until 21 September. By 23 September five major craters from which lava was explosively erupted developed along the initial fissure system. A 500 m wide and 3.5 km long subaerial platform developed from the coalescing lavas.

A set of secondary fissures developed, after the initial fissures filled in with volcanic material, connecting the craters in a single line. The azimuth at the northern end of this line (80°) corresponds approximately to the 85°WSW nodal plane of the first earthquake. The development of the secondary fissure and later post-eruptive fissures is suggested by Birkenmajer (1972) and Sylvester (1972) to be caused primarily by the same tectonic processes that formed the initial pre-eruptive fissures.

Three of the craters ceased to be active by the end of September 1970, while the other two remained active until sometime in the beginning of 1971.

An emission of smoke and vapor over the northeastern part of Jan Mayen on 16 March 1971 was preceded by an earthquake. A second, larger earthquake (5.7 on the Richter scale) on 23 March 1971 preceded an eruption of volcanic

dust and emission of sulphuric gases from the fissures near Eggoya. In January 1973 fumarolic activity and faulting was observed in the eruption area of 1970. Eggoya, Sigurdbreen, Skrukkelia, and Beerenberg (Sentralkrateret) still emit steam, and minor fumarolic activity is common in the parasitic cones and in other areas on the northeastern slopes of Beerenberg.

IV. PETROGRAPHY OF THE VOLCANIC ROCKS OF JAN MAYEN

Introduction

The rocks of Jan Mayen are ankaramites, alkali basalts, trachybasalts, tristanites (trachyandesite), and trachytes according to the classification of Irvine and Baragar (1971) for the potassic series of the alkaline rocks. The names originally given to the rocks by Fitch (written commun.) are retained in this study to be consistent with previous publications. It is found, however, that alkali olivine basalts of Sor Jan (SJ13A, SJ5A, SJ6 and SJ9B) and Nord Jan (NC12C, NC12C*, NC17*, NJ17*, NC27K, NC27K*, NC13 and 4^T) are ankaramites; trachyandesites are trachybasalts, except for NC22 which falls in the alkali basalt region; and latite andesites are tristanites according to this classification (Appendix II).

Representative rock textures and minerals are shown in Plates 1 to 5 (magnification of 3x) and Appendix I, respectively. Whole rock chemical analyses and the locations of each rock sample are listed in Appendices II, III and VII. Sample rock descriptions (this study) are listed in Appendix VIII.

Ankaramites

Ankaramites are dark gray, vesicular rocks containing megaxenocrysts of yellow green olivine and dark green clinopyroxene. Petrographically, they are holocrystalline, seriate porphyritic, and weakly pilotaxitic with an intergranular groundmass.

The ankaramites consist of xenocrysts of chromium diopside, titaniferous salite, olivine, magnetite, and rarely, plagioclase.

Chromium diopside xenocrysts are anhedral to subhedral, pale yellow green to colorless crystals up to 6.0 mm in size. They are strongly resorbed and are rimmed (0.02-0.10 mm) by a light to medium purple brown titaniferous augite. Chromium diopside crystals are unzoned and may be simply twinned. They exhibit features of polygonization or straining and may contain inclusions of plagioclase, olivine or magnetite.

Titaniferous salite xenocrysts are light purple brown to colorless, euhedral to resorbed crystals attaining sizes up to 6.0 mm. They are rimmed (0.02-0.10 mm) by purple brown titaniferous augite and are reversely zoned or sector zoned. They may contain inclusions of unaltered red-brown glass and yellow brown-red brown pleochroic kaersutite(?). The kaersutite(?) occurs as rounded inclusions, usually associated with tiny opaques and their cleavage is parallel to that of the titaniferous salite. Titaniferous salite is

Plate 1. Rock Textures
Ankaramite

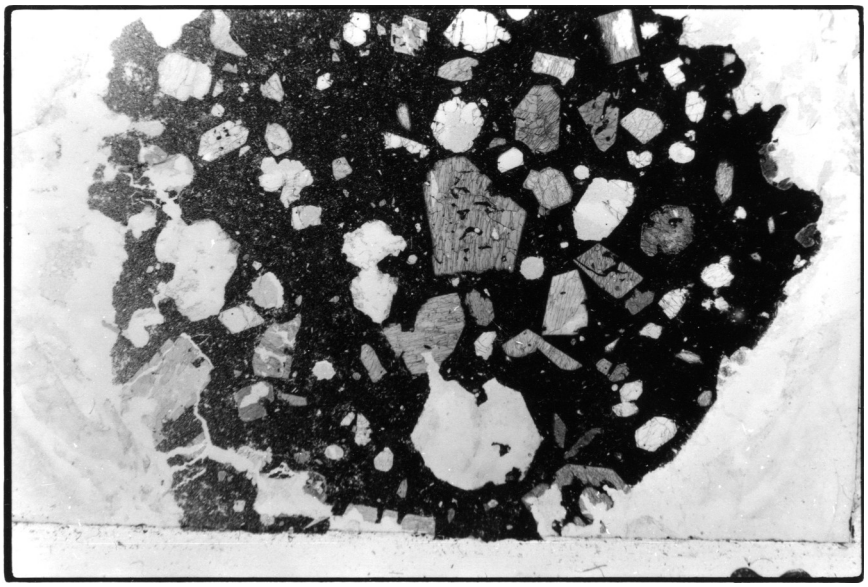

SJ15A

commonly poikilitic in the core or rim with devitrified glass or partially crystallized glass (which appears similar to the groundmass). Kaersutite(?) occurs as rounded inclusions, usually associated with tiny opaques. Their cleavage is often parallel to that of the titaniferous salite host.

Olivine xenocrysts are rounded and resorbed semi-equant crystals sometimes bounded by a rim of iddingsite. They are polygonized, unzoned, and form crystals up to 3.5 mm. They may have inclusions of magnetite or devitrified glass.

Rare plagioclase xenocrysts (bytownite) in the ankaramites are anhedral, rounded remnants of tabular laths or glomerocrysts that have been intensely resorbed. They are commonly rimmed (0.01 mm) by labradorite, have obscure albite twins and may be normally zoned (usually little developed or absent). A few may contain devitrified glass inclusions. Plagioclase xenocrysts are usually less than 0.75 mm in size.

Microxenocrysts of magnetite are resorbed and rounded or even skeletal. Magnetite grains may attain sizes up to 0.60 mm.

Groundmass minerals are: titaniferous augite, olivine, labradorite, magnetite, biotite, $\pm$ alkali feldspar, $\pm$ analcite, and $\pm$ ilmenite. Titaniferous augite crystals are purple brown, sector zoned, euhedral equant prisms or plates. Olivines are euhedral to subhedral hexagons that are unzoned

and sometimes partially iddingsitized. Labradorite laths are euhedral to subhedral and are characterized by albite twinning. Magnetite occurs as tiny opaque euhedral cubes evenly distributed in the groundmass. Anhedral, tabular biotite crystals are pleochroic dark brown-green brown, dark brown-yellow brown, have a reaction rim of magnetite and are up to 0.75 mm long. Roberts and Hawkins (1965) and Hawkins and Roberts (1972) report groundmass alkali feldspar, analcite, and ilmenite rods. Alkali feldspar occurs in interstitial shapeless pools that are untwinned and exhibit undulatory extinction. They contain minute needles of apatite. Analcite is found to occur rarely with alkali feldspar.

Clinopyroxene glomerocrysts are most abundant in the ankaramites, but smaller amounts of clinopyroxene+olivine, olivine, and even more rarely, plagioclase and clinopyroxene+plagioclase are present. Generally, the amounts of clinopyroxene > olivine = plagioclase.

Alkali Olivine Basalt - Sor Jan

The alkali olivine basalts of Sor Jan include trachybasalt, doleritic basalt, and basanite. They are typically light to dark gray, vesicular, phyric rocks. Petrographically, they are holocrystalline with groundmass textures varying from pilotaxitic to trachytic and are seriate porphyritic.

The alkali olivine basalts contain xenocrysts of chromium diopside, titaniferous salite, olivine, plagioclase and magnetite.

Xenocrysts of chromium diopside are pale yellow green to colorless, subhedral to anhedral crystals up to 4.0 mm in size. They are resorbed and rimmed (0.06-0.10 mm) by a light purple brown titaniferous augite. They are unzoned and sometimes simply twinned. Polygonization features are present and they may contain inclusions of plagioclase, olivine, magnetite or carbonate (possibly from the alteration of plagioclase inclusions).

Xenocrysts of purple brown titaniferous salite are euhedral and resorbed crystals displaying reverse zonation. They may also be sector zoned and may have inclusions of olivine and red brown-yellow brown pleochroic kaersutite(?). They are commonly poikilitic with devitrified glass or partially crystallized glass (appearing like the groundmass of the rock) along the rims or in the core.

Olivine xenocrysts occur as resorbed and rounded crystals up to 4.0 mm in size, usually surrounded by a rim

Plate 2. Rock Textures
Alkali Olivine Basalt – Sor Jan

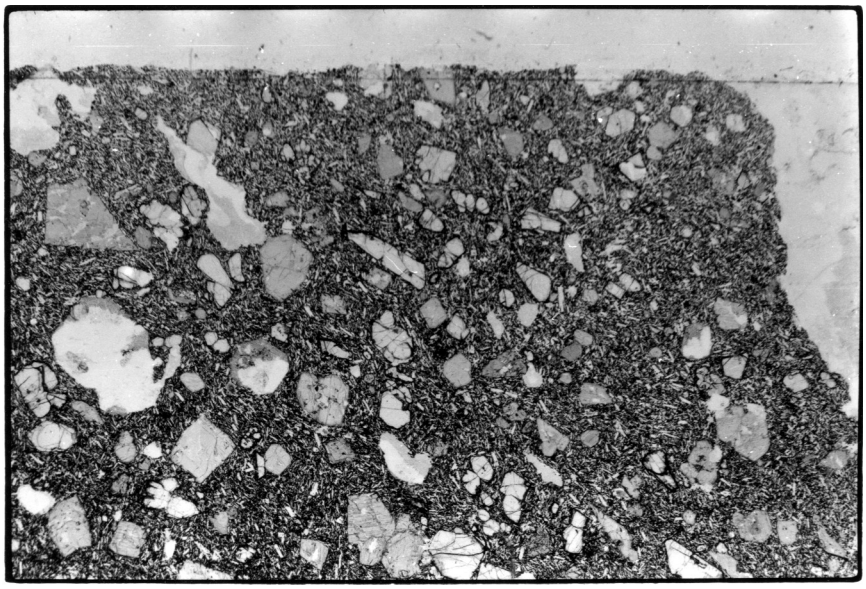

SJ6

of iddingsite and sometimes a reaction rim of magnetite. All olivine xenocrysts are unzoned. Some are polygonized and may exist as intergrown crystals.

Plagioclase xenocrysts (bytownite) are resorbed, anhedral remnants of larger laths rimmed (0.01-0.02 mm) by labradorite. The crystals are up to 1.5 mm in size and display weak normal zoning (may be absent), obscure albite twins, and may contain inclusions of divitrified glass.

Microxenocrysts of magnetite are resorbed and rounded equant crystals up to 0.35 mm.

The matrix in which the xenocrysts lie is composed of titaniferous augite, olivine, labradorite, magnetite, ilmenite, biotite, ± alkali feldspar, ± analcite, ± leucite, ± kaersutite, ± magnesite, ± apatite and very rarely, glass. Titaniferous augite crystals are purple brown, sector zoned, euhedral to subhedral prisms or plates. Forked needles of olivine and diamond shaped olivine are unzoned. The diamond shaped olivines appear to have crystallized about tiny opaque minerals. Labradorite laths are subhedral to euhedral with albite twins. Magnetite occurs as euhedral equant grains evenly distributed throughout the groundmass. Ilmenite rods are also present. Ragged plates of red brown pleochroic biotite are up to 0.35 mm long. Tyrrell (1926) and Carstens (1961) report the presence of analcite rarely occurring with untwinned interstitial pools of feldspar and brownish cryptocrystalline interstitial glass. Carstens (1961) also indicates the presence of kaersutite and magnesite in

1 to 2 mm diameter vesicles. In 1962 Carstens reported observing interstitial leucite associated with analcite. Needles of euhedral interstitial apatite are reported by Tyrrell (1926).

Glomerocrysts of clinopyroxene are most abundant, but some plagioclase glomerocrysts are observed. Generally, the amounts of clinopyroxene and plagioclase are nearly the same, but both are in greater abundance than olivine. The large amount of clinopyroxene and olivine xenocrysts makes these rocks appear more similar to the ankaramites of Nord Jan than alkali olivine basalts.

Alkali Olivine Basalt - Nord Jan

Alkali olivine basalts of Nord Jan include potash basalt, trachybasalt, and basanitoid trachybasalt. They are light to dark gray, vesicular rocks containing yellow green olivine and dark green clinopyroxene xenocrysts. In thin section the alkali olivine basalts are holocrystalline and seriate porphyritic with groundmass textures that are generally intergranular and pilotaxitic.

Xenocrysts occurring in these rocks are chromium diopside, titaniferous salite, olivine, plagioclase and magnetite with phenocrysts of olivine and plagioclase.

Chromium diopside xenocrysts are anhedral to subhedral, pale yellow green to colorless, broken and rounded (resorbed) crystals up to 6.0 mm in size. They are rimmed (0.02-0.07 mm) by light to dark purple brown titaniferous augite and are unzoned and sometimes simply twinned. They also exhibit polygonization features and may contain inclusions of magnetite or olivine.

Titaniferous salite xenocrysts are purple brown euhedral to resorbed crystals up to 6.0 mm in size. They are rimmed (0.02-0.07 mm) by purple brown titaniferous augite, are sector zoned or reversely zoned. They may contain inclusions of magnetite or olivine. In NC23 titaniferous salite has poikilitic rims of partially crystallized or devitrified glass and contains inclusions of altered kaersutite(?).

Plate 3. Rock Textures
Alkali Olivine Basalt – Nord Jan

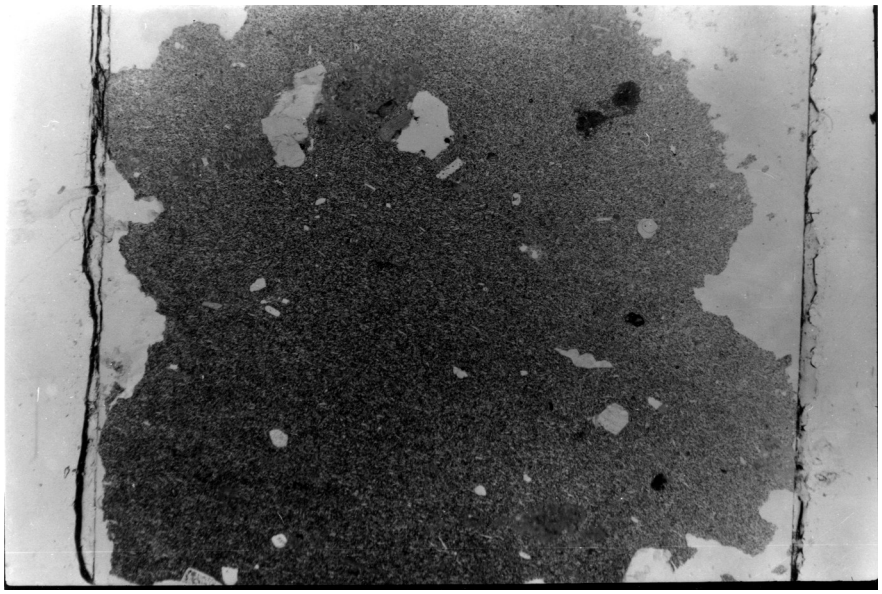

NC22

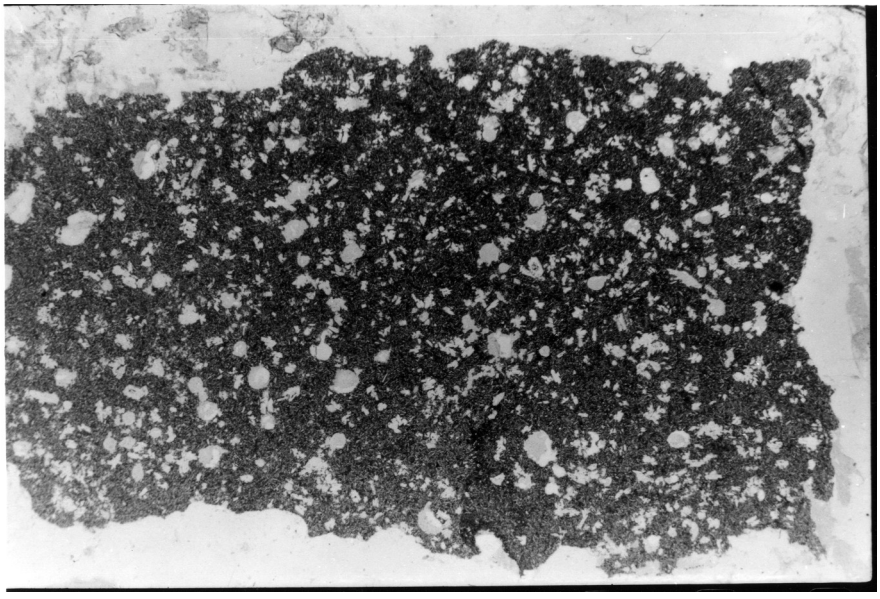

NC34B

Plate 3. Rock Textures (cont.)

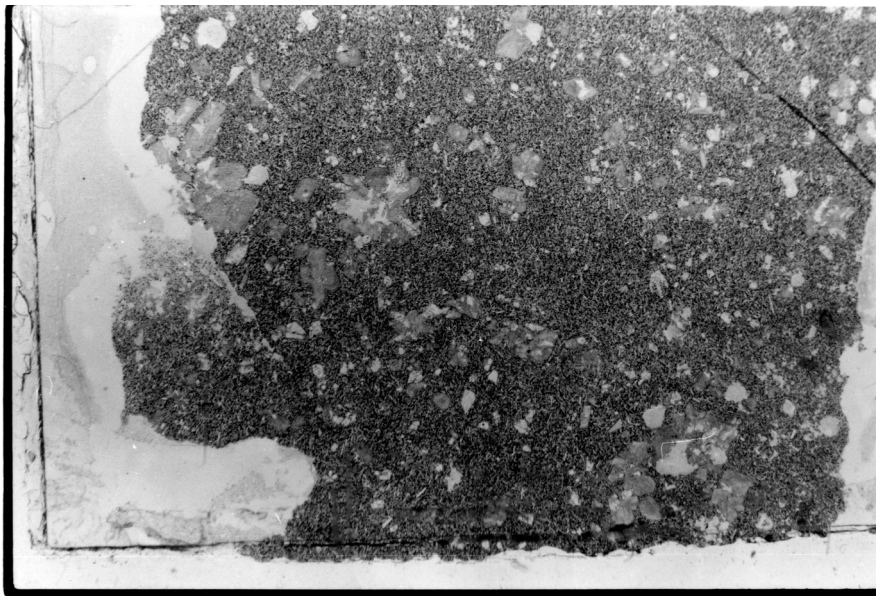

NC12C

Xenocrysts of olivine are resorbed equant crystals up to 3-4 mm in size. They are unzoned, polygonized, iddingsitized (some have a reaction rim of magnetite) and contain inclusions of magnetite.

Bytownite xenocrysts (up to 3.0 mm) are resorbed anhedral remnants of larger laths that are rimmed (0.01 mm) by labradorite. They display weak normal zoning with albite twins.

Magnetite microxenocrysts are resorbed and rounded equant grains up to 0.75 mm long.

Olivine phenocrysts are unzoned euhedral equant grains 1-2 mm across. Phenocrysts of labradorite are found in NC12C, as are euhedral phenocrysts of bytownite zoned to labradorite found in NC34B and JB202. Some bytownite phenocrysts may contain inclusions of devitrified glass (Weigand in 1970 reports these inclusions as simply opaque minerals).

The groundmass consists of titaniferous augite, olivine, labradorite, magnetite, ilmenite, biotite, $\pm$ analcite, and $\pm$ alkali feldspar. Titaniferous augite crystals are purple brown and sector zoned. Olivines may be hexagonal or diamond shaped (with an opaque core). Plagioclase laths of labradorite (0.01-0.15 mm long) are subhedral to euhedral and display albite twins. Euhedral grains of magnetite are evenly disseminated throughout the groundmass. Ragged plates of yellow brown-red brown pleochroic biotite occur in crystals up to 0.15 mm long. Tyrrell (1926), Hawkins and

Roberts (1972), and Roberts and Hawkins (1965) report that analcite occurs rarely with alkali feldspar (forms in interstitial pools that are untwinned and may be turbid). Skeletal rods of ilmenite are reported by Tyrrell (1926) and Hawkins and Roberts (1972).

The most common glomerocrysts present in the alkali olivine basalts are composed of clinopyroxene. In general, the amount of clinopyroxene = plagioclase > olivine, but in the extreme case of NC34B and JB202 plagioclase > clinopyroxene > olivine, since they consist almost entirely of plagioclase glomerocrysts.

Latite Andesites

Latite andesites are light gray to gray, nonvesicular rocks sometimes containing phenocrysts of clinopyroxene. Petrographically, these rocks are holocrystalline, porphyritic to seriate porphyritic with the groundmass texture varying from intergranular to trachytic.

Phenocryst phases occurring in these rocks are plagioclase (andesine), magnetite, biotite, hornblende, and ± clinopyroxene.

Clinopyroxene phenocrysts are euhedral, tabular crystals up to 1.2 mm across. They are completely altered to calcite and a felty mass of actinolite-tremolite(?). Simple twins are observable in the altered clinopyroxene crystals and they may contain inclusions of plagioclase, magnetite, and biotite.

Subhedral to anhedral phenocrysts of andesine are rounded, rimmed (0.02 mm) by an alkali feldspar, and occur as crystals up to 3.0 mm in size. They display normal zoning to an oligoclase composition and some appear to have a perthite texture. Andesine may contain inclusions of clinopyroxene and magnetite.

Magnetite microphenocrysts are subhedral to euhedral equant grains that sometimes appear resorbed and skeletal. They are commonly up to 0.5 mm in size and are pseudomorphic after biotite and hornblende.

Anhedral to subhedral, tabular biotite phenocrysts, up to 1.5 mm long, are dark brown-yellow brown pleochroic.

Plate 4. Rock Textures
Latite Andesite

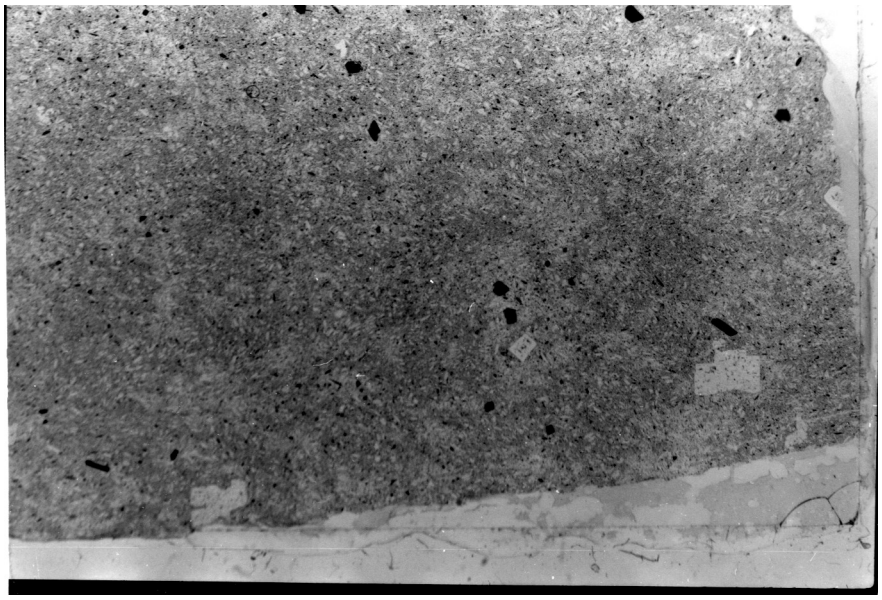

SJ2B

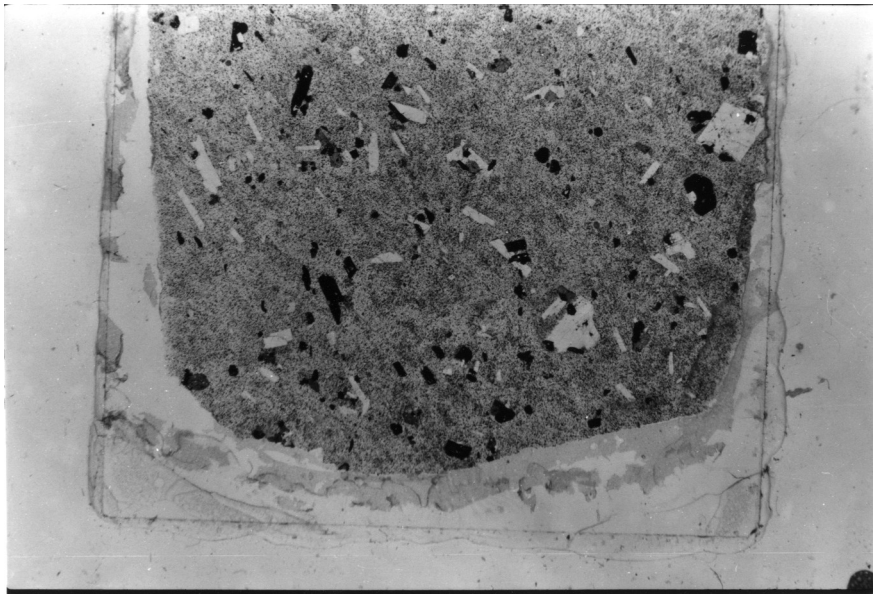

JB1I

They contain inclusions of magnetite dust and have a reaction rim of magnetite.

Anhedral, prismatic hornblende phenocrysts have a reaction rim of magnetite, are pleochroic dark brown-dark red brown, and are up to 1.5 mm long.

The matrix in which the phenocrysts lie is composed of oligoclase, alkali feldspar, magnetite, hematite, biotite, and ± analcite. Oligoclase laths are subhedral to euhedral crystals up to 0.3 mm long that exhibit albite twinning. Laths of subhedral alkali feldspar are untwinned and occur interstitially between the plagioclase laths. Euhedral octahedral grains of magnetite are evenly distributed throughout the groundmass. Hematite (an alteration product of biotite, hornblende, and magnetite) stains the groundmass red. Ragged plates of biotite are present in the groundmass and in vesicles as 'worms' 3-4 mm long (Hawkins and Roberts, 1972; Carstens, 1961). Hawkins and Roberts (1972) also report analcite occurring rarely with alkali feldspar. Glomerocrysts usually consist of andesine, magnetite, biotite and hornblende.

Trachytes

Trachytes are light gray, friable, nonvesicular rocks containing small phenocrysts of anorthoclase and biotite. In thin section they are holocrystalline, seriate porphyritic, and trachytic.

The trachytes contain phenocrysts of aegirine-augite, anorthoclase, magnetite, biotite and ± plagioclase.

Aegirine-augite phenocrysts are bright green to yellow green, subhedral, tabular crystals up to 1.0 mm in size. They may contain inclusions of plagioclase and magnetite.

Anhedral, rounded, tabular plagioclase phenocrysts (andesine) may or may not be present. They occur up to 4.5 mm in size, are rimmed (0.12 mm) by alkali feldspar, are normally zoned, and are albite twinned.

Anorthoclase phenocrysts are anhedral, rounded, and rimmed (0.03 mm of alkali feldspar) crystals up to 5-6 mm in size. They may exhibit a perthite texture and may contain inclusions of magnetite, biotite, and aegirine-augite.

Magnetite microphenocrysts are anhedral to euhedral grains about 0.35 mm average in size. Some are rounded and some have a rim of hematite. Magnetite is pseudomorphic after biotite.

Tabular, anhedral to subhedral biotite flakes are up to 1.5 mm long and display red brown-dark brown and green brown-dark brown pleochroism. Biotite is sometimes opaque from inclusions of magnetite dust and is surrounded by a

Plate 2. Rock Textures
Alkali Olivine Basalt – Sor Jan

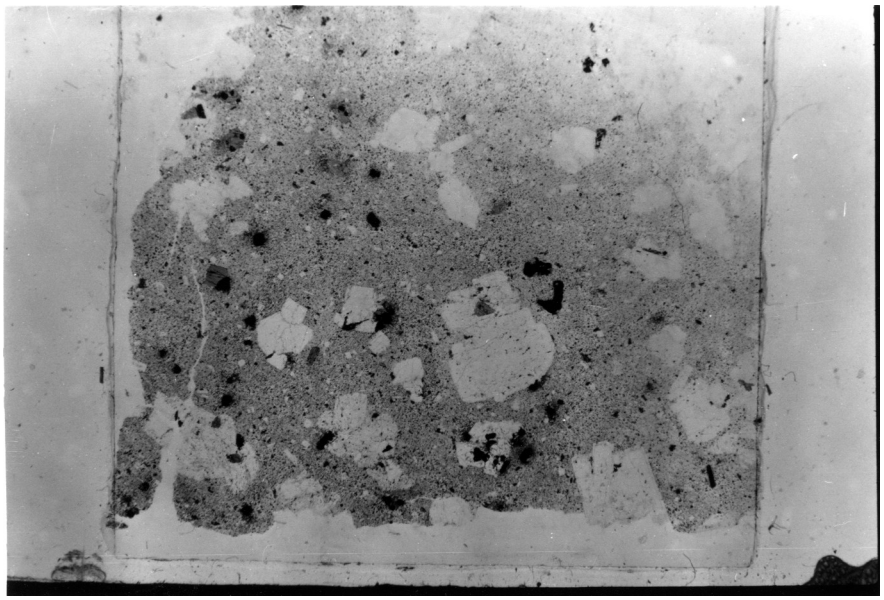

SJ25B

reaction rim of magnetite and hematite.

Groundmass minerals are: oligoclase, alkali feldspar, magnetite, sanidine, ± hematite, and ± cristobalite. Oligoclase laths are subhedral to euhedral and are albite twinned. Subhedral laths of alkali feldspar are untwinned and occur interstitially between the plagioclase laths. Euhedral grains of magnetite are equally distributed throughout the groundmass. Square, euhedral sanidine crystals occur up to 0.3 mm in size. Tyrrell (1926) also reports the presence of red, translucent flakes of hematite, and Carstens (1961) indicates the presence of anhedral cristobalite in the groundmass and in cavities.

Carstens (1961) reports the presence in a trachyte of a hornblende trachybasalt inclusion that consists of augite, olivine, plagioclase, hornblende and iron ore. Vesicles in this basic inclusion contain brown pyroxene, prehnite, and laths of feldspar in radial groups. Glomerocrysts in these rocks are combinations of anorthoclase, aegirine-augite, magnetite and biotite.

V. WHOLE ROCK CHEMISTRY OF THE VOLCANIC ROCKS OF JAN MAYEN

Whole Rock Major Oxide Chemistry

A total of 61 whole rock chemical analyses are plotted on MgO variation diagrams and other types of variation diagrams. The rocks are broken down into 6 major groups: 1) 9 ankaramites (Fitch, written commun.; Roberts and Hawkins, 1965; Tyrrell, 1926), 2) 7 alkali olivine basalts from Sor Jan (Fitch, written commun.; trachybasalt and doleritic basalt from Tyrrell, 1926), 3) 34 alkali olivine basalts from Nord Jan (trachybasalts from Roberts and Hawkins, 1965; Tyrrell, 1926; and Hawkins and Roberts, 1972; alkali basalt and basanite from Lussiaa-Berdou-Polve, 1973; potash basalt from Hawkins and Roberts, 1972; alkali olivine basalts from Siggerud, 1972; Weigand, 1972; and Fitch, written commun.), 4) 6 trachyandesites (Roberts and Hawkins, 1965; Carstens, 1961; Carstens, 1962; Tyrrell, 1926; Lussiaa-Berdou-Polve and Vidal, 1973), 5) 2 latite andesites (Fitch, written commun) and 6) 3 trachytes (Fitch, written commun.; Carstens, 1961; Tyrrell, (1926). The chemical analyses of these rocks were done by classical solution methods, by atomic absorption spectrophotometry, and/or by electron microprobe. Some replication by different authors indicates that the analyses are quite accurate (Roberts and Hawkins, 1965; Fitch, written commun.

TABLE 1.

WHOLE ROCK MAJOR OXIDE AVERAGES

	Ankaramite (9)	Alkali Olivine Basalt-Sor Jan (7)	Alkali Olivine Basalt-Nord Jan (34)
SiO_2	46.80 (0.34)[1]	45.70 (1.76)	46.98 (1.31)
TiO_2	2.08 (0.16)	2.40 (1.29)	2.73 (0.63)
Al_2O_3	9.55 (1.74)	14.73 (2.16)	15.48 (1.55)
FeO*	9.49 (0.94)	10.68 (0.49)	10.97 (1.13)
MnO	0.18 (0.05)	0.24 (0.10)	0.20 (0.03)
MgO	13.82 (1.47)	7.61 (3.10)	6.13 (1.89)
CaO	14.17 (0.66)	10.81 (1.10)	10.45 (1.26)
Na_2O	1.59 (0.31)	2.47 (0.75)	2.93 (0.57)
K_2O	1.20 (0.15)	1.71 (0.43)	2.36 (0.52)
P_2O_5	0.31 (0.04)	0.63 (0.16)	0.59 (0.19)

	Trachyandesite (6)	Latite Andesite (2)	Trachyte (3)
SiO_2	58.43 (2.53)	60.75 (2.05)	65.48 (0.52)
TiO_2	2.05 (0.35)	0.99 (0.27)	0.43 (0.18)
Al_2O_3	16.96 (1.41)	17.70 (0.14)	16.33 (0.40)
FeO*	8.36 (0.86)	4.19 (0.47)	3.35 (0.33)
MnO	0.25 (0.09)	0.21 (0.02)	0.20 (0.03)
MgO	3.17 (1.13)	0.95 (0.00)	0.57 (0.36)
CaO	6.29 (1.58)	2.80 (0.06)	1.46 (0.52)
Na_2O	4.47 (0.64)	5.52 (0.45)	5.63 (0.07)
K_2O	3.22 (0.12)	5.81 (0.29)	5.52 (0.45)
P_2O_5	0.57 (0.11)	0.37 (0.08)	0.08 (0.06)

---

[1] ( ) represents the standard deviation.
* Total iron as FeO.

The highly xenocrystic nature of these rocks (especially the ankaramites and alkali olivine basalts) may profoundly affect the shape of the curves obtained and thus their use is limited. Individual major oxide analyses are listed in Appendix II with their normative mineralogy, and averages are shown in Table 1. Normative mineralogies have been recalculated by DeLong (unpub.) from the chemical analyses in the leterature.

The rocks of Jan Mayen belong to the potassic series (Fig. 2) of the alkaline rocks (Fig. 3 and 4A). On the $K_2O + Na_2O$:SiO_2 diagram ankaramites and alkali olivine basalts SJ13A, SJ5A, SJ6, SJ9B and NC27K lie below the division lines given by MacDonald and Katsura (1964) and Irvine and Baragar (1971). This may be due to the enrichment of chromium diopside and magnesian olivine in these rocks which apparently decreases their relative alkalinity (MacDonald and Katsura, 1964).

Potash and soda are strongly and positively correlated (Fig. 4B) in all the rocks with an average Na_2O/K_2O ratio of 1.30 for the whole series. The ratio, however, tends to be higher for the alkali olivine basalts and ankaramites (1.29-1.46) than for the latite andesites and trachytes (0.95 and 1.02, respectively). The ternary diagram Na_2O-K_2O-CaO (Fig. 5) shows that the ratio of Na_2O/K_2O does remain nearly constant as CaO decreases continuously. The latite andesites and trachyte, though, appear to lie proportionately closer to the K_2O apex, as indicated by their lower ratios, than the alkali olivine basalts and ankaramites.

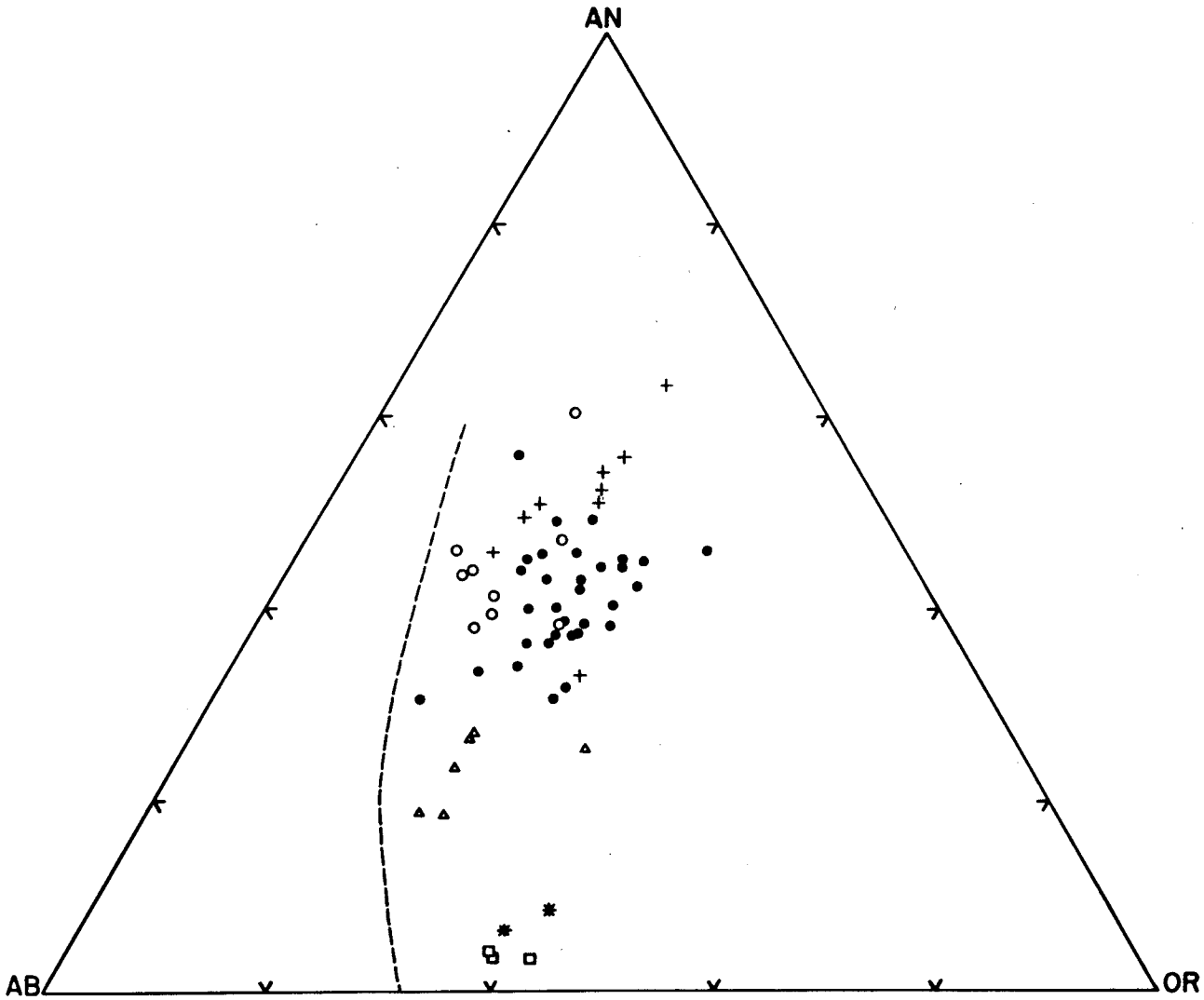

Figure 2. The Ab-An-Or diagram is based on the normative mineralogy of the Jan Mayen rocks. The dashed line (Irvine and Baragar, 1971) separates the sodic and potassic series for the alkaline rocks. The rocks of Jan Mayen belong to the potassic series. + ankaramite, o Sor Jan alkali olivine basalts, • Nord Jan alkali olivine basalts, △ trachyandesites, ✱ latite andesites, □ trachytes.

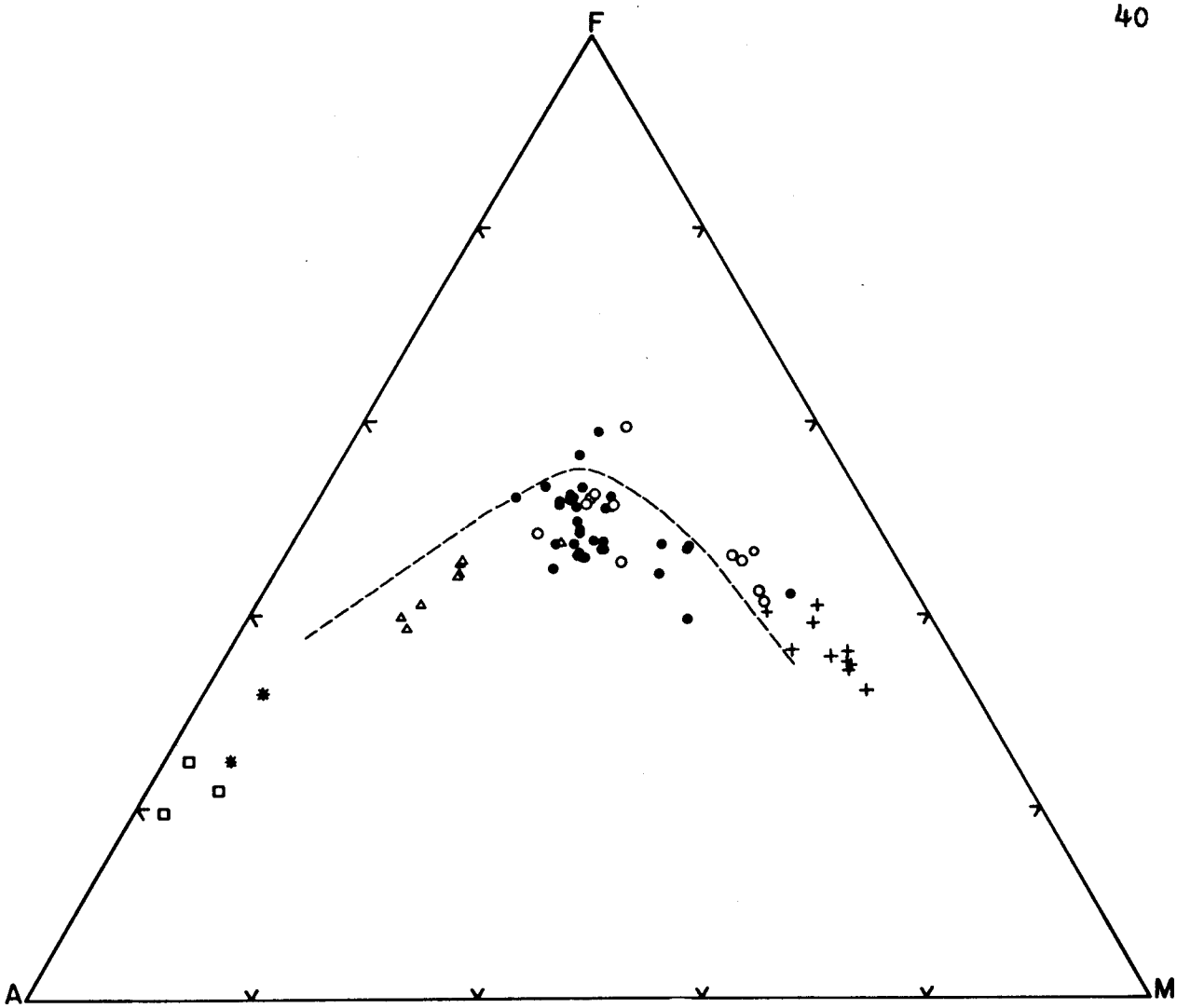

Figure 3. The AFM diagram is based on the whole rock analyses of the Jan Mayen rocks. The dashed line represents the division line between tholeiites and calc alkaline rocks (Irvine and Baragar, 1971). Caution must be exercised in explaining this trend due to the highly xenocrystic character of the rocks. A = Na_2O+K_2O, F = FeO total, and M = MgO. Symbols are the same as in Fig. 2.

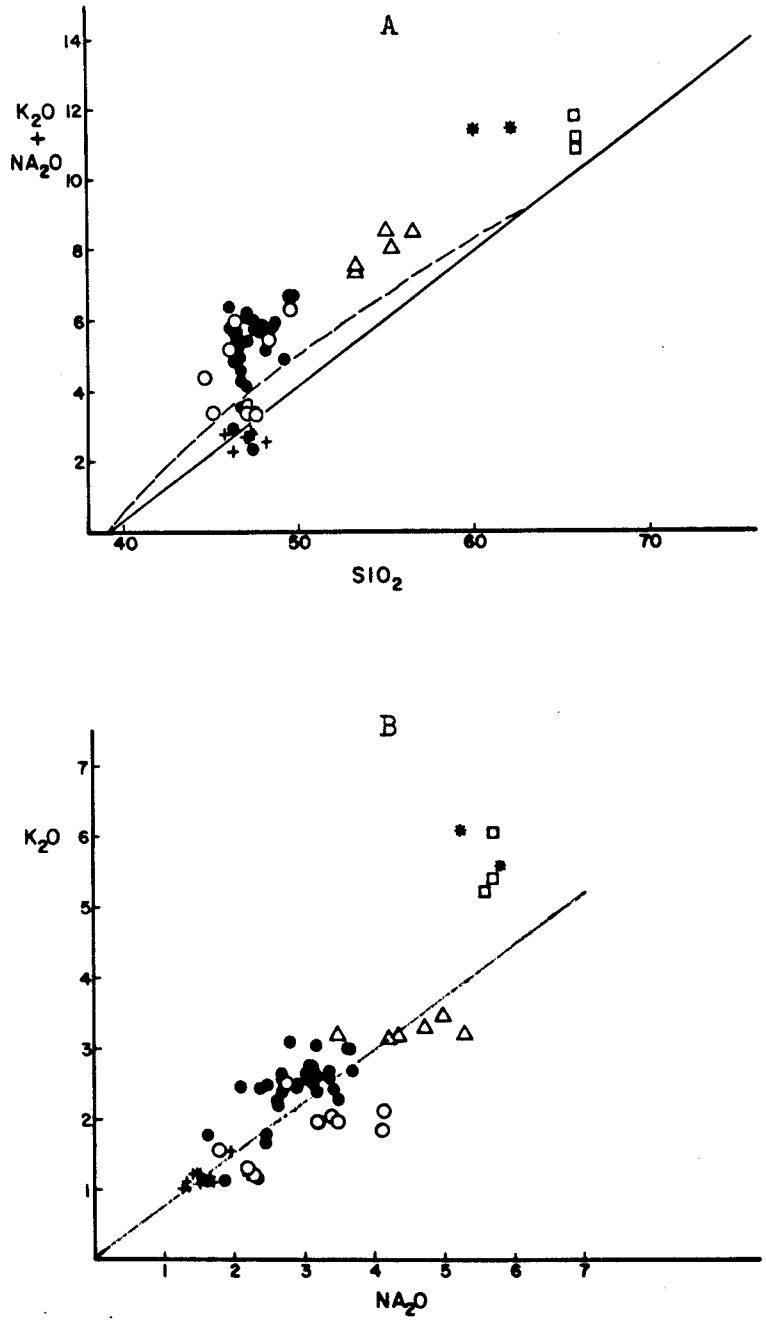

Figure 4. A. The $K_2O+Na_2O:SiO_2$ diagram indicates that the rocks of Jan Mayen are alkaline. The solid division line is from MacDonald and Katsura (1964) and the dashed line is from Irvine and Baragar (1971). See text for explanation for the ankaramites. B. The $K_2O:Na_2O$ diagram shows that soda and potash are positively correlated with a slightly higher soda content (Na_2O/K_2O = 1.30 average). Symbols are the same as in Fig. 2.

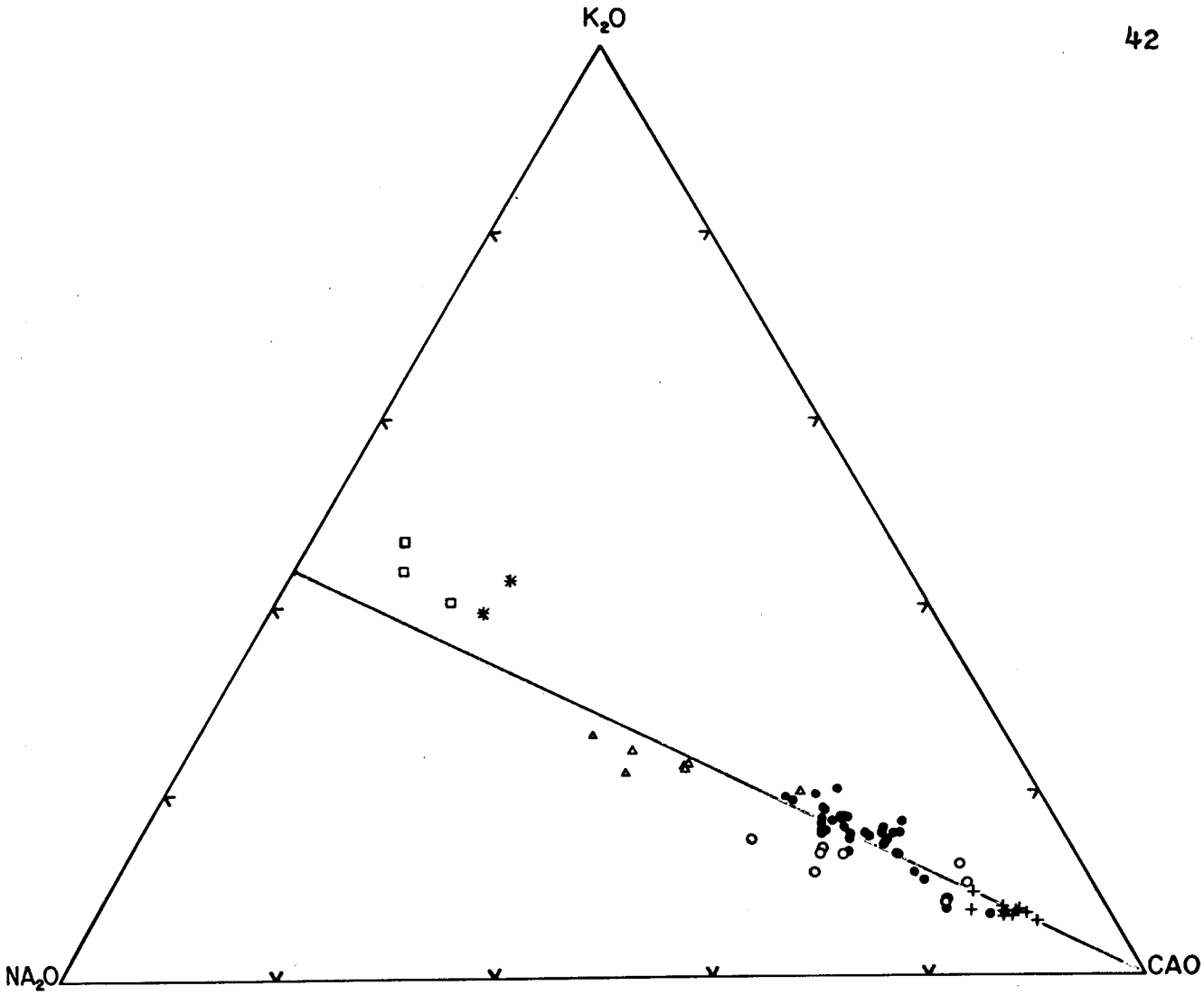

Figure 5. The Na_2O-K_2O-CaO ternary diagram for the whole rock composition indicates that the Na_2O/K_2O ratio of Jan Mayen rocks remain nearly constant as the lime content changes. The line for Na_2O/K_2O = 1.30 shown here corresponds to the average in Fig. 4B. Symbols are the same as in Fig. 2.

The character of the rocks of Jan Mayen, as plotted on the basalt tetrahedron implies that they belong to the straddle type alkalic association (Miyashiro, 1978). The ankaramites, alkali olivine basalts and trachyandesites are silica deficient and the latite andesites and trachytes are oversaturated with respect to silica (Fig. 6 and 7). Usually the undersaturated rocks contain normative nepheline and they lie in the Ne-Ol-Pl-Di subtetrahedron. Alkali olivine basalts SJ9B, NC27K and NJ17 are, however, hypersthene normative and lie in the Ol-Pl-Di-Hy subtetrahedron. Trachyandesites may contain normative nepheline, hypersthene or quartz. Silica oversaturated latite andesites and trachytes lie in the Qz-Hy-Pl-Di tetrahedron. Many of the rocks lie close to the Pl apex in projection on the basal face (Fig. 7B) and close to the Pl-Di join when projected to the back face (Fig. 7A). A somewhat linear trend from high Di ankaramites to the high Pl trachytes is observed on the critical plane (Fig. 7C), but three groups can be distinguished: 1) ankaramites, greater than 45 Di and less than 40 Pl, 2) alkali olivine basalts, 20-40 Di and 40-70 Pl, and 3) trachyandesites to trachytes, less than 20 Di and greater than 80 pl.

The variation of the major oxides (Fig. 8 and 9) are plotted against MgO. MgO is highest in the ankaramites and decreases continuously throughout the series. These diagrams closely resemble those described by Baxter (1975) for the Older Series Lavas of Mauritius Island in the Indian Ocean.

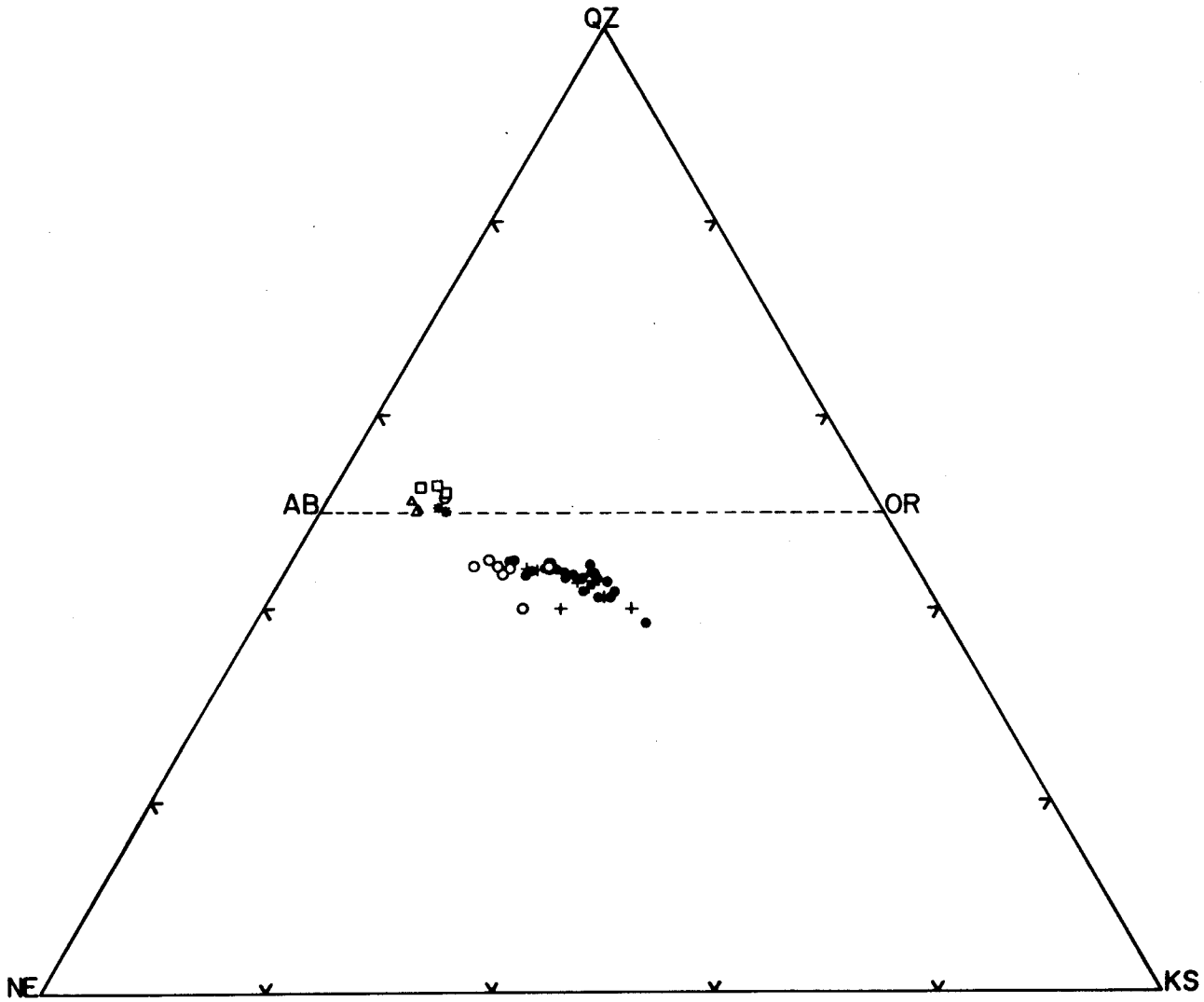

Figure 6. The Ne-Qz-Ks ternary diagram for the rocks of Jan Mayen (based on the normative mineralogy) demonstrates that the ankaramites, alkali olivine basalts, and trachyandesites are silica deficient and the latite andesites and trachytes are silica oversaturated. Symbols are the same as in Fig. 2.

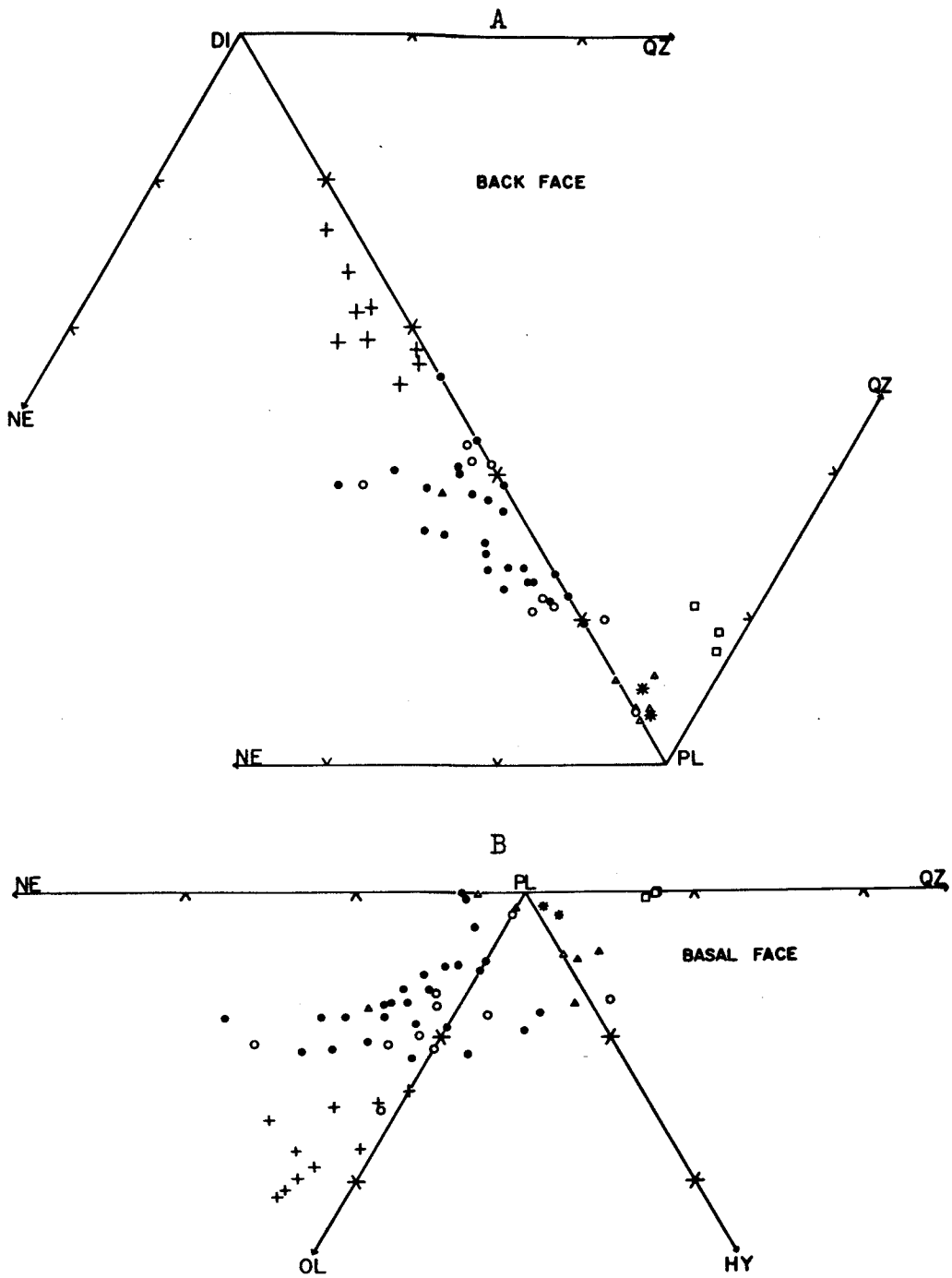

Figure 7. Basalt Tetrahedron. A. Back Face-all analyses lie close to the Di-Pl join. B. Basal Face-most alkali olivine basalts and ankaramites lie in the field of silica undersaturation. A few alkali olivine basalts, however, are hypersthene normative. Most trachyandesites, latite andesites, and trachytes lie in the field of silica saturation. Symbols are the same as in Fig. 2.

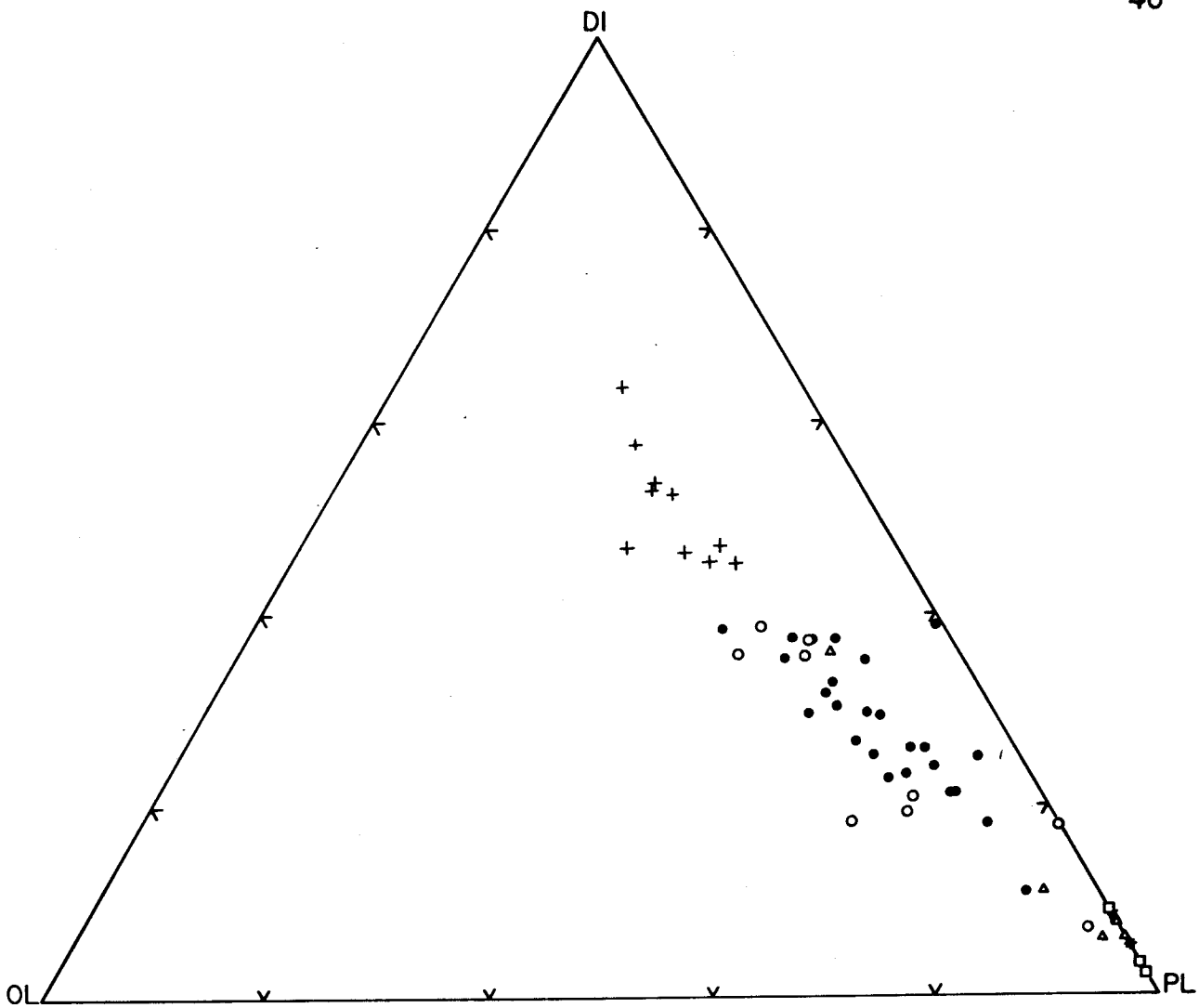

Figure 7. Basalt Tetrahedron continued. C. Critical Face-see text for description. Symbols are the same as in Fig. 2.

SiO_2. The ankaramites and alkali olivine basalts define a nearly horizontal trend at an average silica content of 47.27% as MgO decreases steadily, At about 3.3% MgO the silica content sharply increases, reflecting the degree to which the trachyandesites, latite andesites, and trachytes are silica saturated.

TiO_2 and FeO*. The content of FeO* (total iron as FeO) and TiO_2 increases from the ankaramites to a maximum in the alkali olivine basalts. They then decrease from the alkali olivine basalts to the trachytes as MgO continues to decrease. Titanium and total iron appear to be positively correlated to one another.

Al_2O_3. Alumina increases steadily from the ankaramites to a maximum in the trachyandesites and then decreases to the trachytes as MgO decreases.

MnO. There is no apparent correlation between MnO and MgO (the MgO variation diagram is not included).

CaO. Lime decreases continually with decreasing MgO through the whole series beginning with the ankaramites and ending with the trachytes. The rate of decrease, however, is lower from ankaramites to alkali olivine basalts than from the trachyandesites to the trachytes.

Na_2O and K_2O. The soda and potash contents of the Jan Mayen rocks increase with decreasing MgO from ankaramite to alkali olivine basalt (moderate rate of increase) to trachyandesite and finally to trachyte (higher rate of increase).

Figures 8 and 9. MgO variation diagrams for the major oxides. See text for explanation. FeO* represents total iron as FeO. + ankaramite, o Sor Jan alkali olivine basalt, • Nord Jan alkali olivine basalt, △ trachyandesite, ✳ latite andesite, □ trachyte.

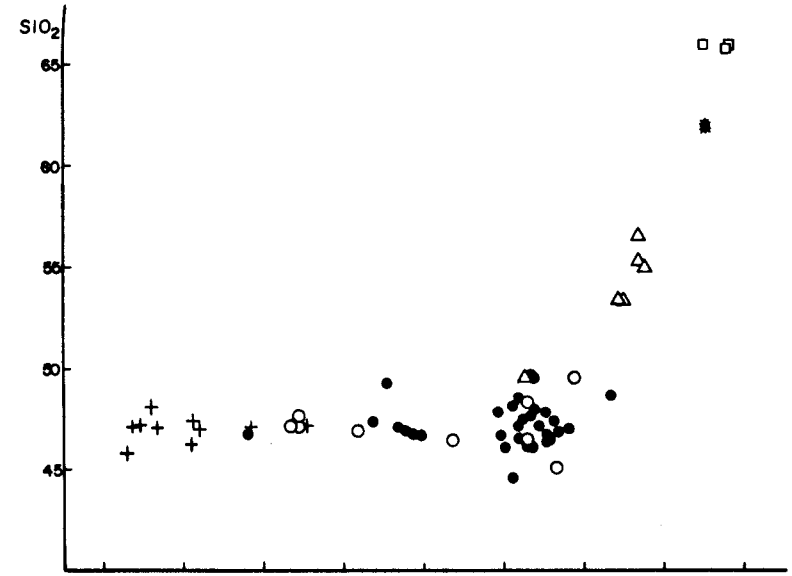
SIO2
65
60
55
50
45

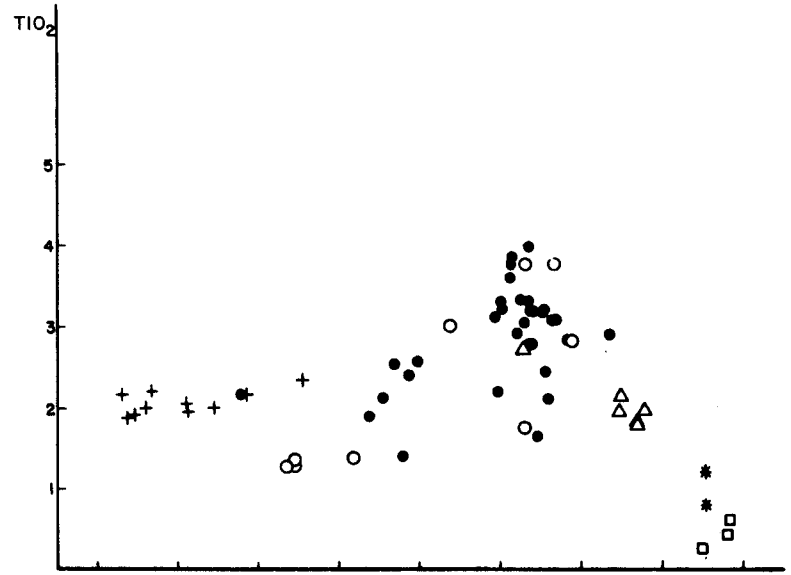
TIO2
5
4
3
2
1

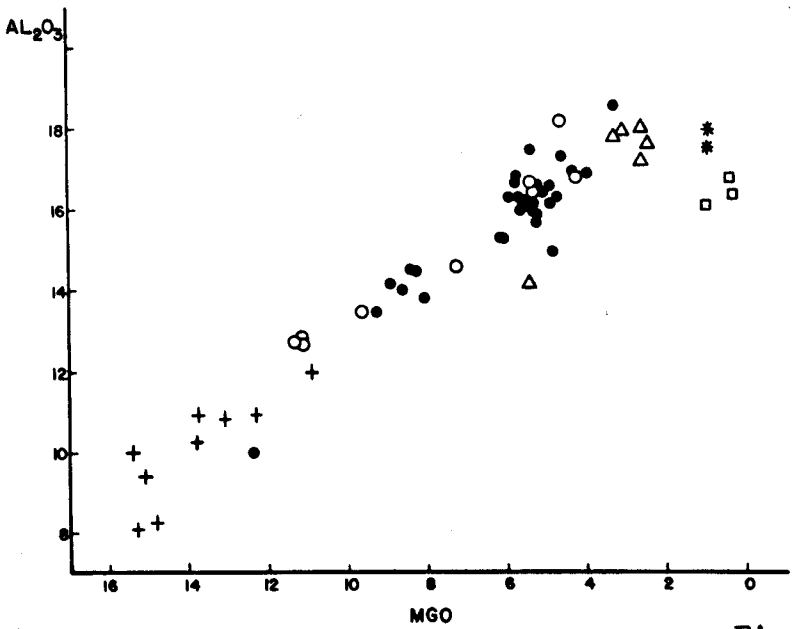
AL2O3
18
16
14
12
10
8
16
14
12
10
8
6
4
2
0
MGO

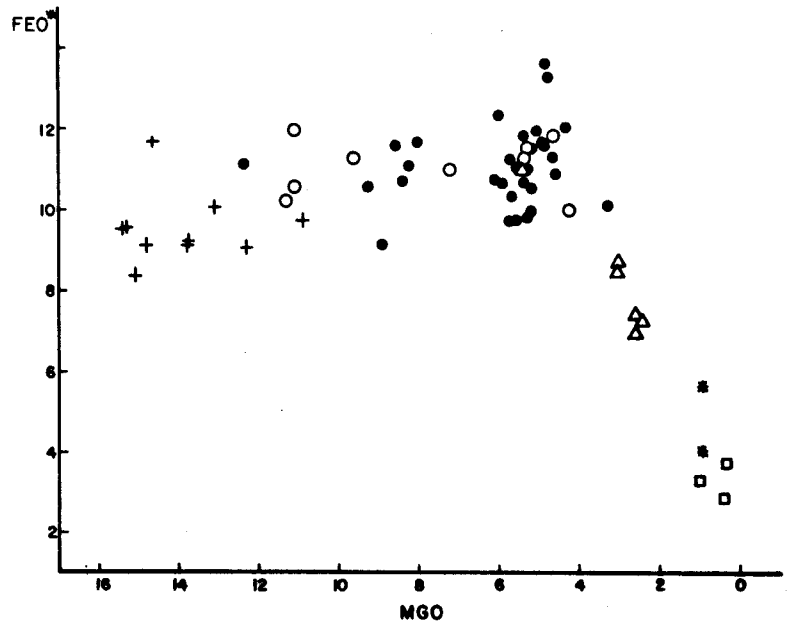
FEO
12
10
8
6
4
2
16
14
12
10
8
6
4
2
0
MGO

Figure 8.

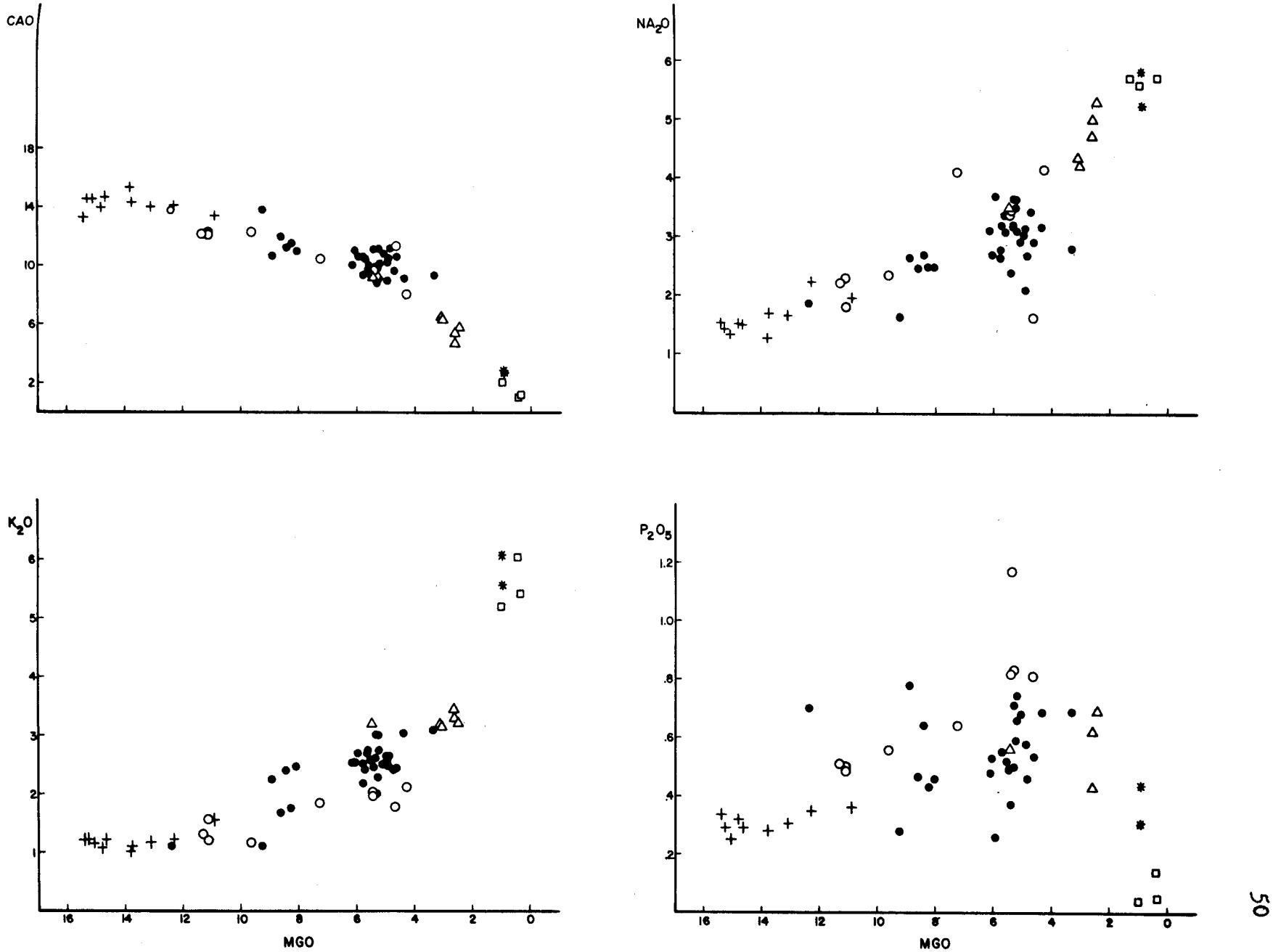
CAO
18
14
10
6
2
NA_2O
6
5
4
3
2
1
K_2O
6
5
4
3
2
1
16
14
12
10
8
6
4
2
0
MGO
P_2O_5
1.2
1.0
.8
.6
.4
.2
16
14
12
10
8
6
4
2
0
MGO

Figure 9.

TABLE 2[1]

MAJOR OXIDE ANALYSES FOR WHOLE ROCK AND MATRIX COMPOSITIONS

	Ankaramite (NC15, NC19)		Alkali Olivine Basalt (NC12C, NC13, NC22)	
	Whole Rock	Matrix	Whole Rock	Matrix
SiO_2	46.83	46.06	47.49	47.33
TiO_2	2.04	2.90	2.44	2.87
Al_2O_3	7.28	14.53	14.58	15.49
FeO*	10.57	11.00	11.43	11.04
MnO	.17	.16	.22	.18
MgO	14.64	6.75	6.55	5.00
CaO	14.54	12.70	10.59	10.40
Na_2O	1.54	2.48	2.88	3.57
K_2O	1.21	2.05	2.49	2.50
P_2O_5	.29	.59	.51	.69
H_2O^+	.42	.38	.34	.43
H_2O^-	.06	.05	.06	.06
Cr_2O_3	.22	.02	.05	.01

[1] Averages are calculated from the analyses of Hawkins and Roberts (1972).

P_2O_5. There is a tendency for P_2O_5 to increase with decreasing MgO from the ankaramites to alkali olivine basalts where it reaches a maximum and then decreases to the trachytes. There is, however, a considerable degree of variation.

Baxter (1975) suggests that the marked changes in the oxides may be correlated to the appearance of titanomagnetite (TiO_2 and FeO*) and plagioclase (CaO, Na_2O, K_2O, SiO_2 and Al_2O_3). Larger amounts of magnetite and plagioclase are observed to appear within the latite andesites and trachyte of the Jan Mayen volcanics.

Whole rock versus matrix analyses (Hawkins and Roberts, 1972) listed in Table 2 indicate that the ankaramites must have been primarily enriched with minerals high in MgO (matrix content is less than $\frac{1}{2}$ that of the whole rock), low in Al_2O_3 (matrix content is twice that of the whole rock) and high in Cr_2O_3 (the whole rock content of Cr_2O_3 is ten times greater than that of the matrix), such as olivine and clinopyroxene. Lesser variations indicate that TiO_2, FeO*, Na_2O, K_2O, and P_2O_5 are higher in the matrix and CaO is lower. Alkali olivine basalt matrix analyses more closely resemble their whole rock analyses, especially NC22, but the matrix is higher in TiO_2, Al_2O_3, Na_2O and P_2O_5 and lower in MgO, CaO and Cr_2O_3.

Whole Rock Trace Element Chemistry

Partial trace element analyses of 43 rocks include Rb, Sr, Ba, Ni and Cr (Appendix III). These rocks are divided into 6 major groups: 1) 9 ankaramites (DeLong and Long, unpub.; Lussiaa-Berdou-Polve and Vidal, 1973; Roberts and Hawkins, 1965), 2) 5 alkali olivine basalts of Sor Jan (DeLong and Long, unpub.; Carstens, 1961), 3) 23 alkali olivine basalts of Nord Jan (DeLong and Long, unpub.; Lussiaa-Berdou-Polve and Vidal, 1973; potash basalt from Hawkins and Roberts, 1972; trachybasalt from Roberts and Hawkins, 1965; Tyrrell, 1926; and Hawkins and Roberts, 1972), 4) 3 trachyandesites (Lussiaa-Berdou-Polve and Vidal, 1973; Roberts and Hawkins, 1965), 5) 2 latite andesites (DeLong and Long, unpub.) and 6) 1 trachyte (DeLong and Long, unpub.). The variation of the trace elements in the rocks of Jan Mayen is plotted against MgO.

Strontium isotope data were obtained from Long (unpub.). Cr, Sr and Ba contents, measured as oxides by Tyrrell (1926), Roberts and Hawkins (1965), Hawkins and Roberts (1972) and Carstens (1961), were recalculated to weight abundances in parts per million.

The distribution of Rb/Sr (Fig. 10) in the rocks of Jan Mayen indicates that the ratios for the alkali olivine basalts of Sor Jan (0.025-0.040), the ankaramites and alkali olivine basalts of Nord Jan (0.045-0.095), and the latite andesites and trachytes (greater than .100) of Sor Jan constitute three distinct groups. However, the ankaramites

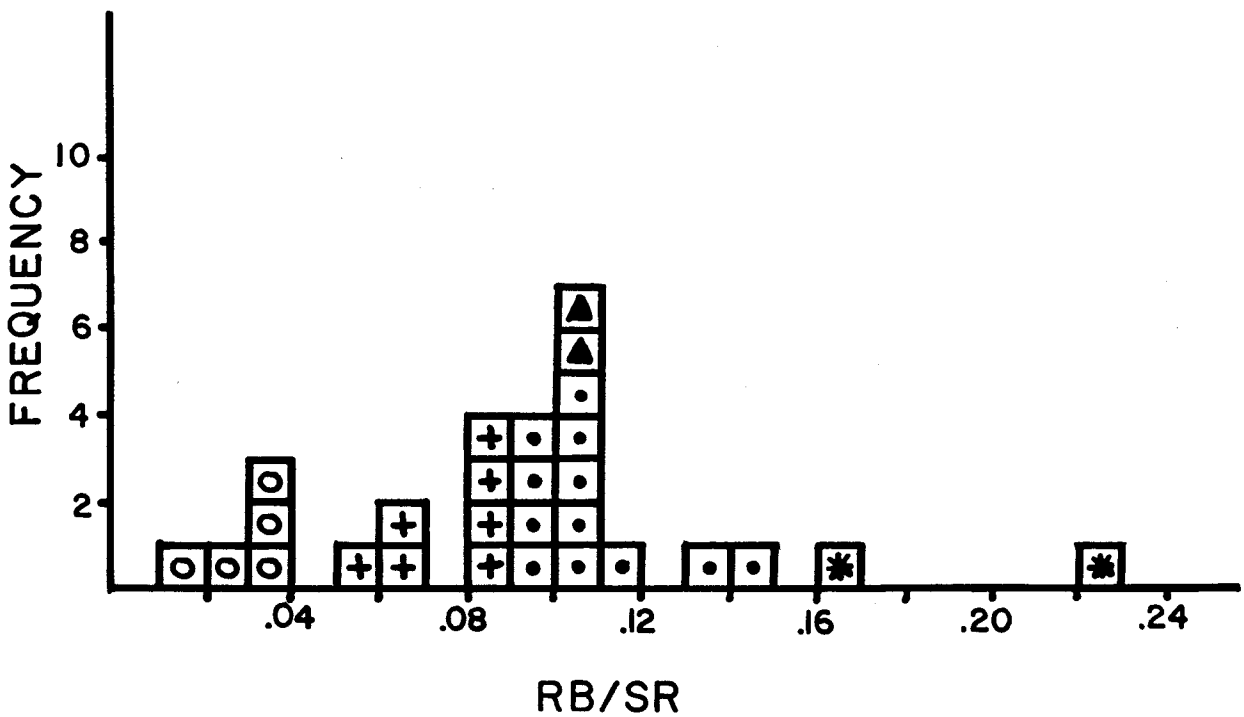

Figure 10. Rb/Sr frequency distribution histogram indicates that the alkali olivine basalts of Sor Jan, the alkali olivine basalts and ankaramites of Nord Jan, and the latite andesites and trachytes of Sor Jan constitute three distinct groups. + ankaramite, o Sor Jan alkali olivine basalt, o Nord Jan alkali olivine basalt, ▲ trachyandesite, * latite andesite. Trachyte has a Rb/Sr ratio of 1.000 and lies off of this graph.

have lower ratios than the alkali olivine basalts of Nord Jan, and the latite andesites have lower values than the trachyte.

The Sr^{87}/Sr^{86} ratio is nearly the same in all the rocks of Jan Mayen (.7035 to .7041) and is very close to the value of .7040 estimated for the mantle (Faure, 1977).

The variation of the trace elements Rb, Sr and Ni (Fig. 11) are plotted against MgO which decreases continuously from the ankaramites to the trachytes.

Ni. The nickel content of the Jan Mayen rocks decreases with decreasing MgO from the ankaramites to trachytes. SJ13A, SJ5A and SJ6 lie near the field of the ankaramites in these plots.

Rb and Sr. Two separate trends are observable in the variation diagrams for rubidium and strontium in the alkali olivine basalts. The Nord Jan trend consists of ankaramites and alkali olivine basalts and the Sor Jan trend is composed of alkali olivine basalts SJ1A, SJ13A, SJ5A and SJ6. The alkali olivine basalts of Sor Jan are generally separated by a large gap from the latite andesites and trachytes. The Nord Jan trend for rubidium is steeper than the Sor Jan trend; for strontium, both trends have nearly the same slope. Generally, Rb and Sr increase with decreasing MgO, but Sr in the latite andesites and trachyte is anomalously low.

The variation of Rb, Sr and K with respect to one another indicates that Rb, Sr and K are positively correlated to one another (Fig. 12). On the diagrams K:Sr and Rb:Sr

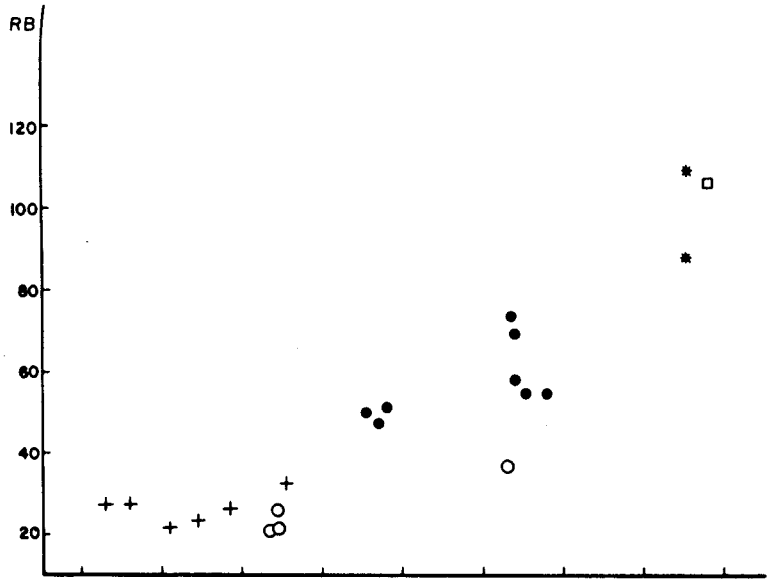

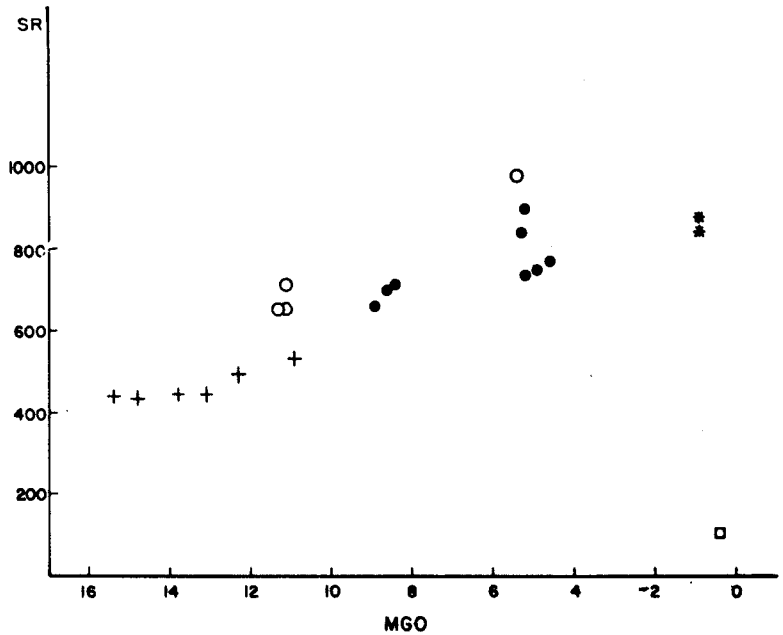

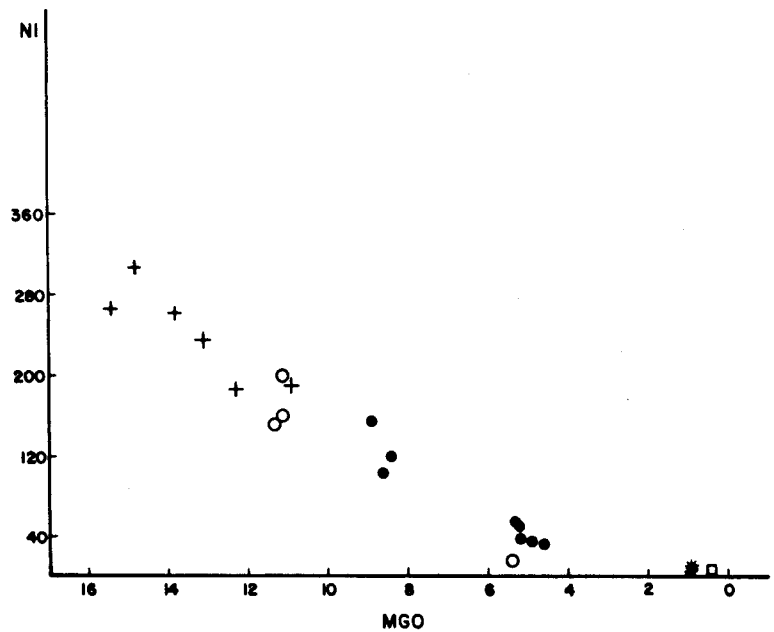

Figure 11. MgO variation diagrams for the trace elements Rb, Sr and Ni. See text for explanation. Same symbols as in Figures 8 and 9.

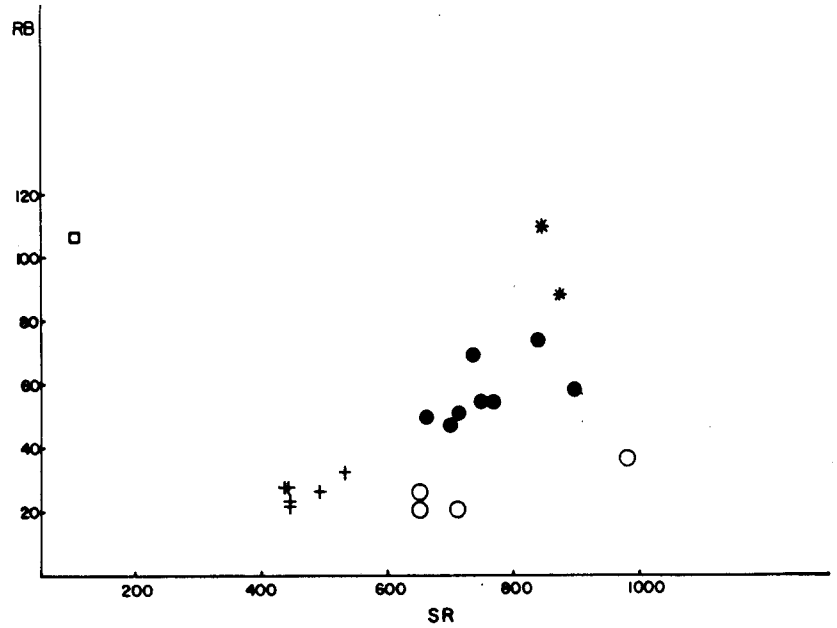

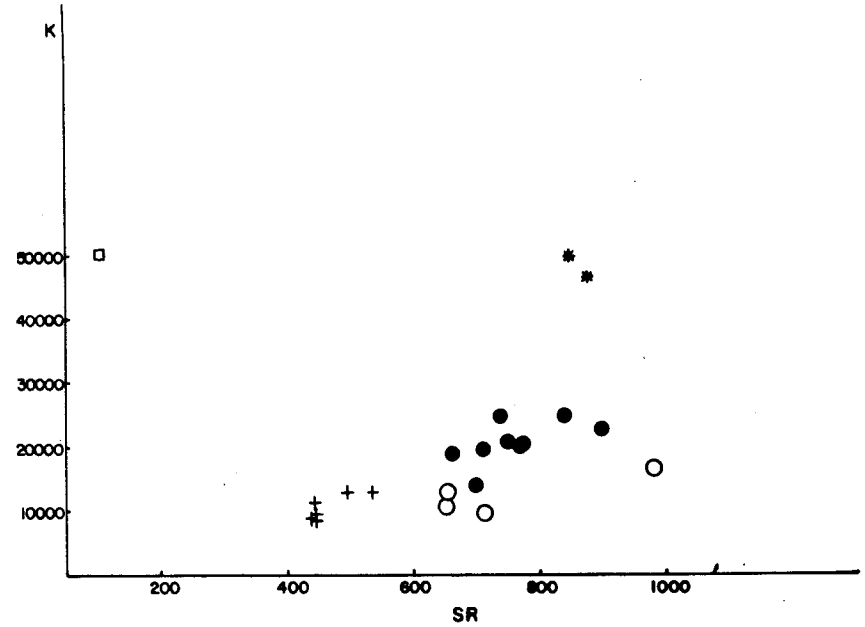

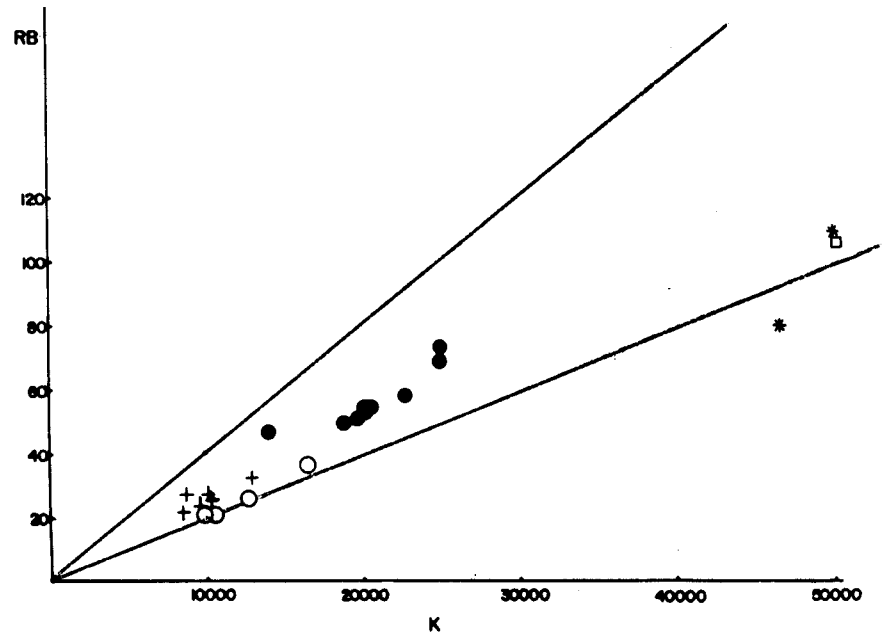

Figure 12. Trace element variation diagrams. See text for explanation. Same symbols as in Figures 8 and 9.

the alkali olivine basalts of Sor Jan appear to follow a different trend than the Nord Jan alkali olivine basalts which is similar to the separation observed in the trace element MgO variation diagrams. In general, the Sor Jan alkali olivine basalts contain less K and Sr. The trachyte is anomalous in its ratios of K:Sr and Rb:Sr having a very low Sr content with respect to the high K and Rb contents. The K/Rb ratio ranges between 250 and 500 for the volcanics of Jan Mayen and the trachyte and latite andesites are distinctly separated from the less differentiated rocks on this plot.

VI. MINERAL CHEMISTRY

Introduction

Chemical analyses of the major minerals in the rocks of Jan Mayen were determined on an ARL Model EMX-SM electron microprobe with an on line automation system at Harvard University. Polished thin sections of the rocks were carbon coated simultaneously and the analyses were performed on two separate occasions: Jan. 31 to Feb. 2, 1979 and March 12 to March 15, 1979. The analyses are estimated to be accurate to within $\pm$ 2 mole percent. Olivine analyses accepted in this study contain no aluminum, and weight percent totals are allowed to range from 97.8% to 101.5% for all minerals.

Determinations for zoning in the minerals proved difficult due to the pitted nature of the mineral surfaces. Probe points for the optically zoned minerals were strategically placed in different zones. Optically unzoned minerals were analyzed generally on the edges, in the interior and near the center of the crystal. These pitted surfaces are observed in olivine, clinopyroxene and plagioclase. Preferentially pitted surfaces in different plagioclase twin lamellae may be caused by different crystal orientations.

The opaques in the groundmass are so small and ill-defined that it was impossible to obtain analyses for them. It was equally difficult to obtain good analyses for the plagioclase, olivine and clinopyroxene in the groundmass.

The chemical analyses for the minerals (Appendix IV) are listed in weight percent and in molar proportions based on 4 oxygens for olivine, 6 oxygens for clinopyroxene, and 32 oxygens for plagioclase and opaques. The following components were also determined:

	Component(s)
Olivine	Fo
	Fe*/Fe*+Mg[1]
Clinopyroxene	Wo:En:Fs[2]
	Ti:NaM2:Al4
	OTHERS
	Fe*/Fe*+Mg
Plagioclase	Ca:Na:K

Mineral analyses in Appendix V are only complete analyses taken from Hawkins and Roberts (1972), Weigand (1972) and Carstens (1962).

---

[1] Fe* is total iron (Fe^{2+} + Fe^{3+}).
[2] Fs is based only on the calculated content of Fe^{2+}.

Olivine

Resorbed and polygonized olivine xenocrysts appear to have slightly different compositions in Nord Jan and Sor Jan rocks. Olivines in ankaramites and alkali olivine basalts of Sor Jan have an average composition of Fo_{83} (Fo_{78} to Fo_{88}), whereas those from Nord Jan have an average composition of Fo_{88} (Fo_{86} to Fo_{90}).

Alkali olivine basalts NC34B and JB202 contain phenocrysts of olivine with an average composition of Fo_{74} (Fo_{72} to Fo_{76}).

A groundmass olivine (forked needle) from NC17 has a composition of Fo_{58}. All olivine crystals observed in these rocks are chemically homogeneous.

Clinopyroxene

Two major types of xenocrystic clinopyroxenes are recognized in the Jan Mayen rocks (Fig. 15A). Each occurs as resorbed and as nearly euhedral crystals rimmed by a later growth of another clinopyroxene. Pale yellow green to colorless chromium diopside xenocrysts have an average composition of $Wo_{46}En_{49}Fs_5$. These xenocrysts are optically and chemically homogeneous, but all are distinctly rimmed by a purple brown titaniferous augite ($Wo_{48}En_{43}Fs_9$). They often exhibit features of polygonization or straining.

Xenocrysts of light purple brown to colorless titaniferous salite are both optically and chemically zoned with iron enriched cores ($Wo_{48}En_{42}Fs_{10}$) and Mg rich edges ($Wo_{48}En_{44}Fs_8$). Some are rimmed by a darker purple brown titaniferous augite with a composition of $Wo_{46}En_{43}Fs_{11}$ (those in SJ13A, NC17, NC12C, NC34B, JB202, NC30C and NC35B do not appear to have rims). Titaniferous salite crystals may also be sector zoned. Titaniferous salite is believed to be a xenocrystic mineral due to their resorbed appearance and to the presence of titaniferous augite rims. Hawkins and Roberts (1972) and Roberts and Hawkins (1965) list them as phenocrysts, but they do not account for their shapes and rims. Weigand (1972) does observe rims of titaniferous augite on the titaniferous salite crystals.

Green aegirine-augite phenocrysts are found as subhedral crystals only in trachyte SJ25B and they have an average composition of $Wo_{44}En_{34}Fs_{22}$.

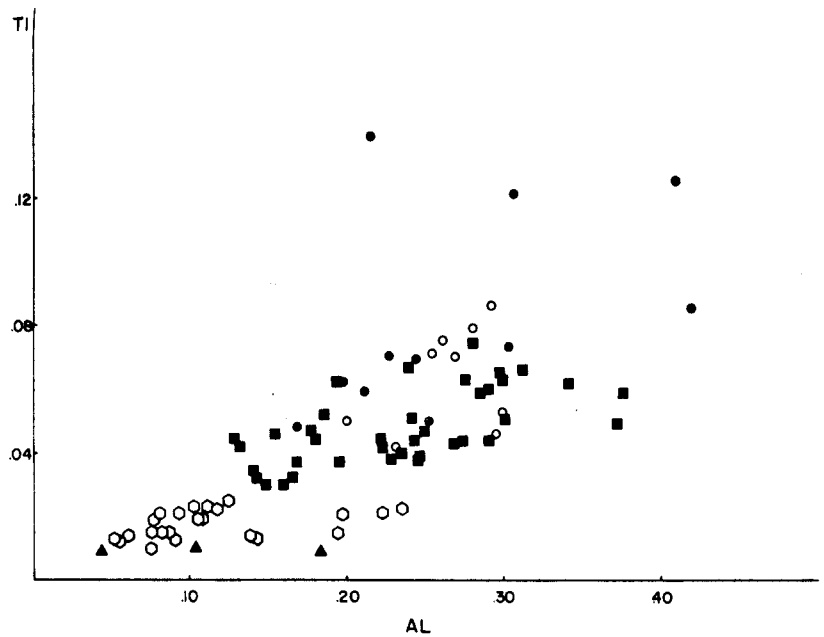

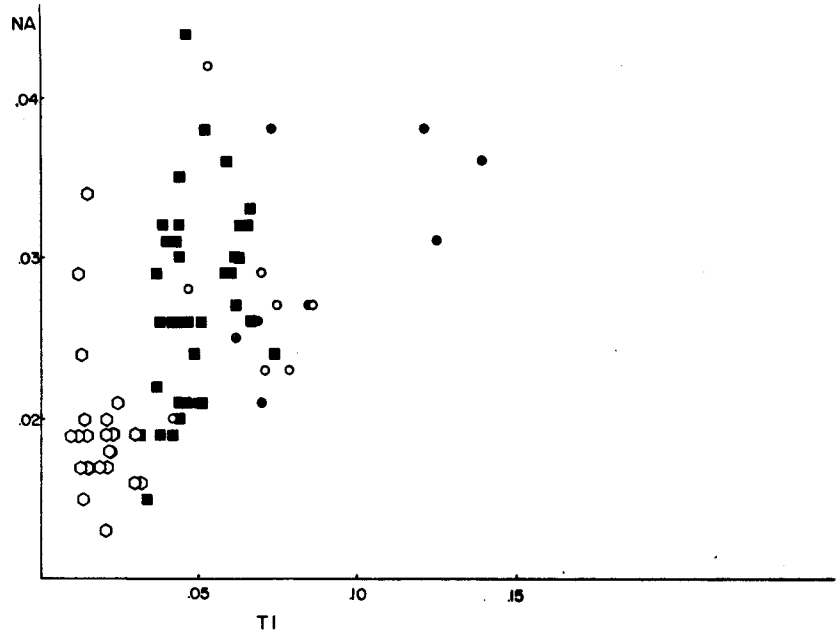

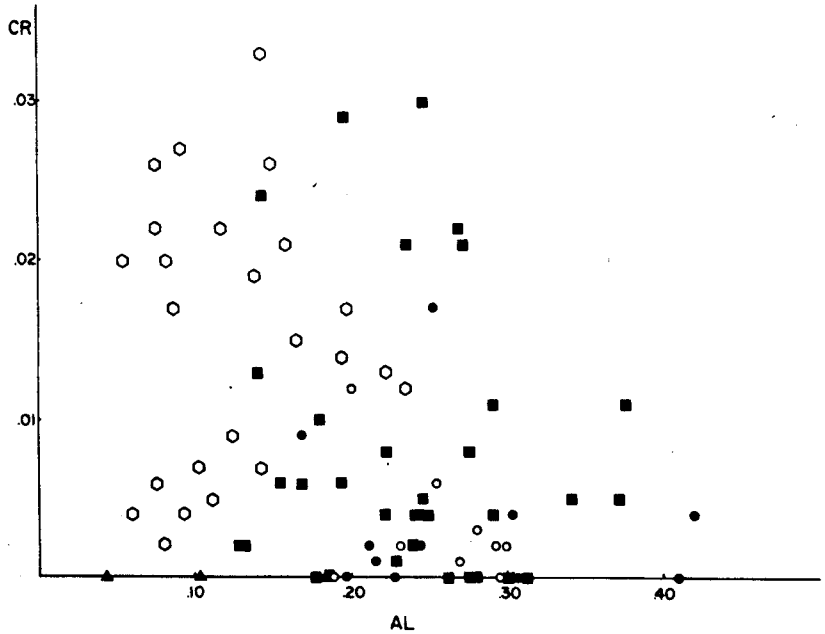

Figure 13. Minor element distribution in clinopyroxenes. See text for explanation. ○ chromium diopside, ■ titaniferous salite, o titaniferous augite rims on chromium diopside, ⊕ titaniferous augite in the groundmass, ▲ aegirine-augite.

Groundmass clinopyroxenes are titaniferous augites having an average composition of $Wo_{47}En_{41}Fs_{12}$.

Papike et al. (1974) suggest a method using Na (in the M2 site), Al (in the tetrahedral site), Ti and total OTHERS ($Al^{VI} + Fe^{3+VI} + Cr^{3+VI} + Ti^{4+VI} + Al^{IV} + NaM2$) to distinguish the different clinopyroxenes from one another (Fig. 15B). It is found that chromium diopside xenocrysts have a total OTHERS of 10.00% and an average composition of $Ti_{15}NaM2_{16}Al^{4}_{69}$. Rims on chromium diopside have total OTHERS (20.74%) and a composition ($Ti_{21}NaM2_{9}Al^{4}_{70}$) similar to that calculated for the groundmass titaniferous augite (23.28% total OTHERS, $Ti_{23}NaM2_{9}Al^{4}_{68}$). Titaniferous salite xenocrysts appear to be fairly homogeneous with respect to composition ($Ti_{19}NaM2_{11}Al^{4}_{70}$), but the total OTHERS appears to decrease from the core (20.68%) to near the rim (17.32%). The rims on titaniferous salite have a total OTHERS of 12.30%, almost half of that of groundmass clinopyroxenes. However, the composition of the rim ($Ti_{25}NaM2_{11}Al^{4}_{64}$) is fairly close to the groundmass titaniferous augite. The major differences between the clinopyroxenes occur in the Ti and NaM2 contents: chromium diopside is relatively more sodic than the titanium enriched titaniferous salites and augites.

Minor element distributions in the clinopyroxenes are shown in Fig. 13. Total Al was used in order to plot the groundmass clinopyroxenes because Al does not go into preferential lattice sites of the clinopyroxenes that are

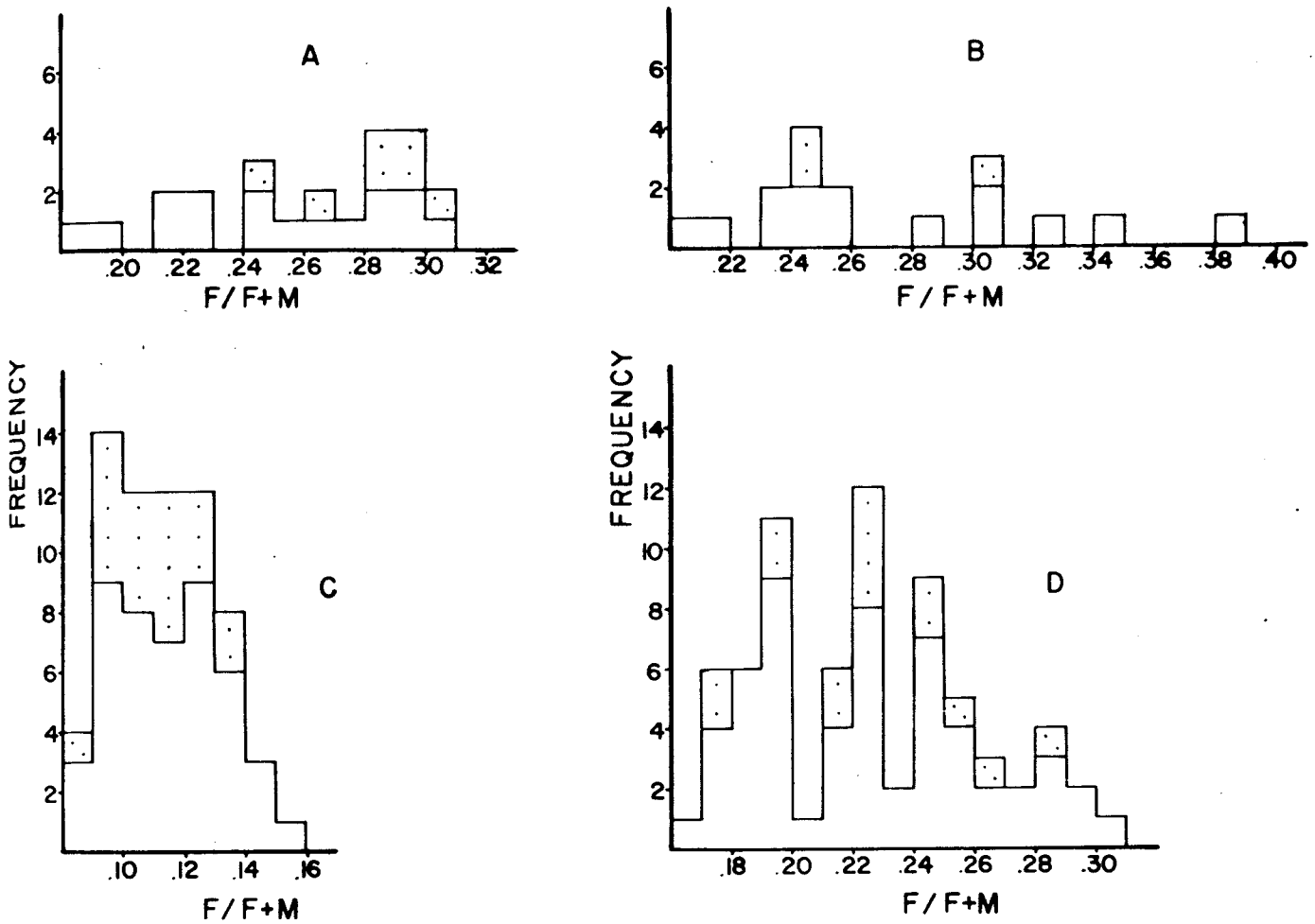

Figure 14. Fe*/Fe*+Mg (molar) frequency distribution histograms for A. titaniferous augite rims. B. titaniferous augite groundmass. C. chromium diopside. D. titaniferous salite. See text for explanation. Fe* represents total iron (Fe^{3+} + Fe^{2+}). Stippled areas represent Jan Mayen clinopyroxenes from the literature, and unmarked areas represent clinopyroxenes from this study.

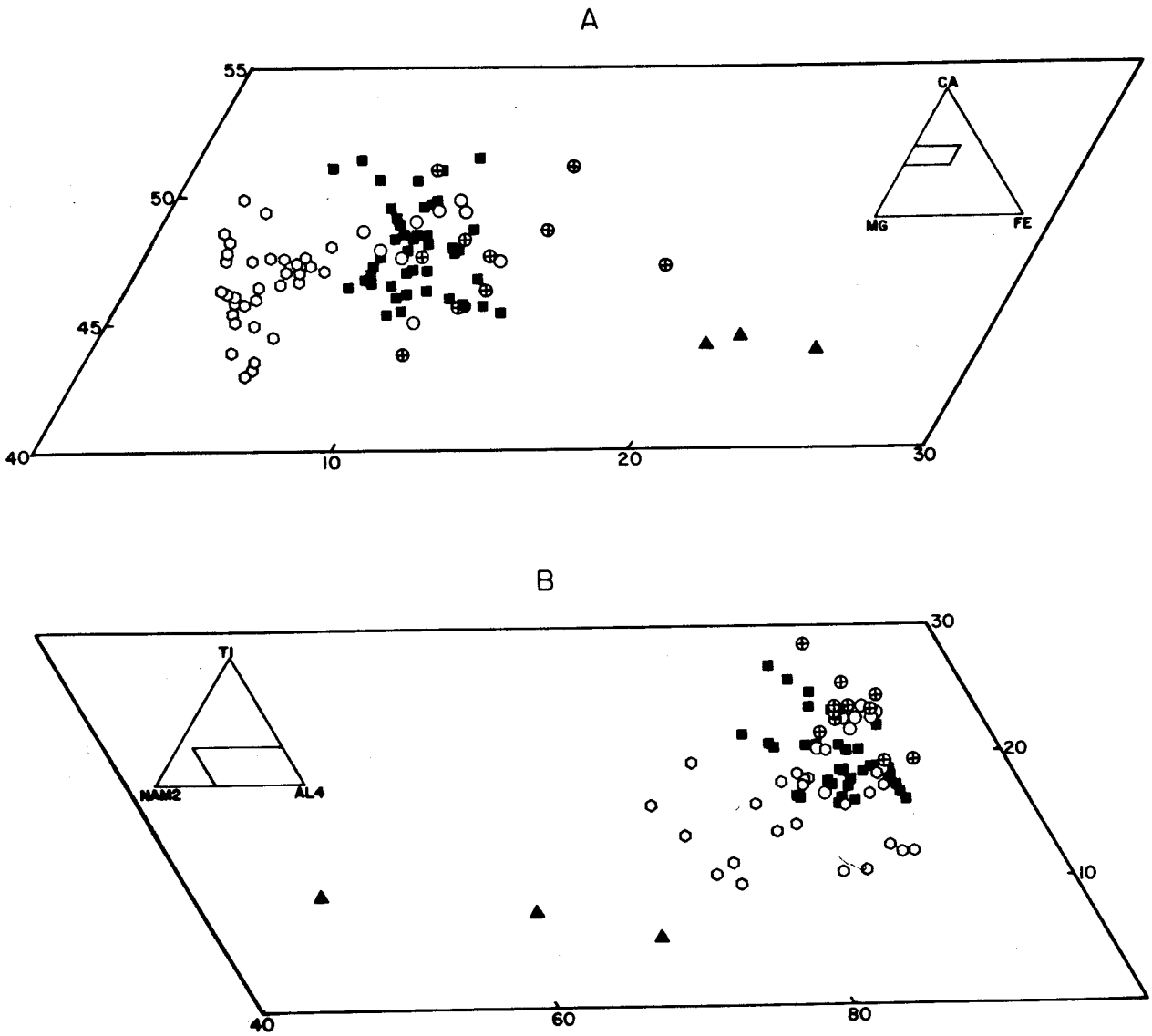

Figure 15. A. Ca-Mg-Fe (molar) ternary diagram for the clinopyroxenes where Fe is the ferrous ion. B. Ti-NaM2-Al4 (molar) ternary diagram for the clinopyroxenes (adapted from Papike et al., 1974). See text for explanation. Symbols are the same as in Fig. 13.

rapidly quenched out of a magma. Al is later distributed between the sites. Chromium diopside xenocrysts of Jan Mayen are moderately enriched in Cr and Al, but some from Sor Jan have anomalously high contents of Na. In contrast, titaniferous salite xenocrysts are Ti and Al rich clinopyroxenes. Titaniferous augite rims on the chromium diopside xenocrysts and groundmass titaniferous augite have compositions similar to titaniferous salite, but are even more enriched in Ti. Aegirine-augite is very sodic with essentially neither Ti nor Cr.

The clinopyroxene Fe*/Fe*+Mg frequency diagram (Fig. 14) indicates that the chromium diopsides form a distinct group from titaniferous salite, and titaniferous augite rims and groundmass. The ratio of Fe*/Fe*+Mg increases in the following manner: chromium diopside, titaniferous salite, titaniferous augite rims, titaniferous augite groundmass. The diagram also includes data calculated from analyses published by Hawkins and Roberts (1972), Roberts and Hawkins (1965) and Carstens (1962).

Feldspar

Xenocrystic bytownite crystals ($Ca_{88}Na_{11}K_1$ to $Ca_{73}Na_{25}K_2$) are resorbed and rimmed by labradorite ($Ca_{61}Na_{37}K_2$ to $Ca_{51}Na_{45}K_4$) in most alkali olivine basalts and ankaramites (Fig. 16). Resorbed and rounded xenocrystic glomerocrysts of labradorite have a much more sodic composition ($Ca_{69}Na_{30}K_1$ and $Ca_{74}Na_{24}K_2$) than the xenocrysts.

Phenocrysts of plagioclase in NC34B and JB202 are very abundant. They are normally zoned bytownites ($Ca_{81}Na_{18}K_2$ to $Ca_{83}Na_{16}K_2$) that are abruptly rimmed by labradorite ($Ca_{60}Na_{37}K_3$ to $Ca_{62}Na_{34}K_4$). Phenocrysts of labradorite ($Ca_{69}Na_{29}K_2$) in NC12C are the most sodic plagioclases observed in the alkali olivine basalts.

Groundmass plagioclase laths in the ankaramites and alkali olivine basalts have a labradorite composition ($Ca_{72}Na_{26}K_2$ to $Ca_{54}Na_{43}K_3$).

Plagioclase phenocrysts in the latite andesites are zoned from andesine to oligoclase in the core ($Ca_{50}Na_{46}K_4$ to $Ca_{18}Na_{69}K_{13}$) and are rimmed by alkali feldspar ($Ca_3Na_{61}K_{36}$) The trachyte contains xenocrysts of andesine ($Ca_{32}Na_{62}K_6$) which are resorbed and rimmed by alkali feldspar ($Ca_0Na_{56}K_{44}$), and phenocrysts of anorthoclase ($Ca_2Na_{67}K_{31}$). Groundmass feldspars in the latite andesites and trachyte consist of andesine ($Ca_{34}Na_{60}K_6$) and alkali feldspar ($Ca_3Na_{58}K_{39}$) which have compositions similar to the rims found on the phenocrysts.

The feldspars of Jan Mayen lie within the range of solid solution (Fig. 16) defined at 900°C and P_{H_2O} = 1 kb

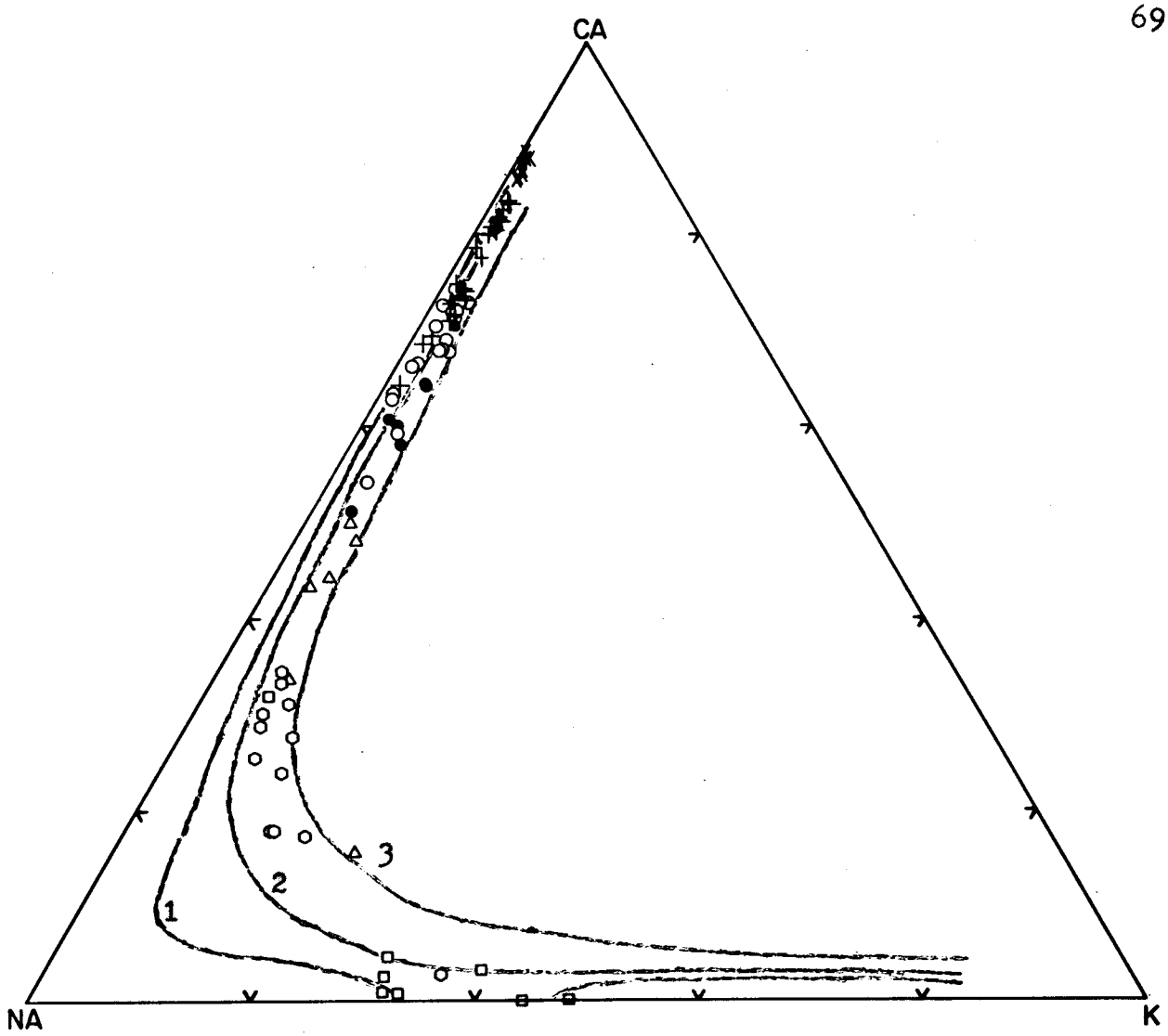

Figure 16. Ca-Na-K (molar) ternary diagram for the feldspars indicates that the feldspars of Jan Mayen are volcanic in origin. The curves represent the feldspar solid solution for the plagioclase and alkali feldspars at 650°C (1), 750°C (2) and 900°C (3) at a water pressure of 1 kb (Ribbe, 1975). See text for explanation. x xenocryst, + phenocryst, o groundmass, • rims, Δ feldspars from JB1I, ⬡ feldspars from SJ2B, □ feldspars from SJ25B.

(Ribbe, 1975). However, due to the presence of hydrous phases in the volcanics of Jan Mayen (biotite and kaersutite) the vapor pressure may actually have been greater, thus the solid solution curves would move toward the Na rich apex reducing the field of solid solution. Therefore, the temperature at which the feldspars of Jan Mayen are in solid solution could have been at higher temperatures and higher P_{H_2O} than observed on this graph.

Opaques

A total of 6 opaque minerals were analyzed and their compositions indicate that they are: 1) titanomagnetite (12NC17, 7NC12C and 10SJ25B), 2) ilmenite (7SJ25B and 9SJ25B) and 3) hematite (8SJ25B) according to Weigand (1972). Opaques in the other alkali olivine basalts and ankaramites of Jan Mayen probably include titanomagnetites as both groundmass and microphenocryst phases (Weigand, 1972). Hematite, ilmenite and titanomagnetite appear to form glomerocrysts with aegirine-augite in the trachyte.

Comparison of the Analyses in this Study with Previously Published Analyses from Jan Mayen

Hawkins and Roberts (1972), Weigand (1972) and Carstens (1962) have reported analyses for olivine, chromium diopside and titaniferous salite. The data (listed in Appendix V) appear to correlate quite well with the data obtained in this study. Weigand (1972), however, reports only partial olivine analyses which are considerably more iron rich than those analyzed in this study. He also reports analyses for groundmass (higher iron content than in this study) and rim titaniferous augite. Hawkins and Roberts (1972) have reported mineral analyses from a few of the same rocks in this study (NC15, NC22 and NC12C), and they are surprisingly well correlated with one another.

VII. LEAST SQUARES MAGMA MIXING AND FRACTIONATION MODELS

Introduction

The results from least squares magma mixing models and Rayleigh fractionation curves indicate that the alkali olivine basalts and ankaramites of Jan Mayen formed by the accumulation of clinopyroxene, olivine and plagioclase in a parental magma. Olivine and plagioclase equilibrium curves also support this conclusion.

Least Squares Magma Mixing

Introduction. The least squares method for magma mixing is used here to determine possible original liquid compositions from which the rocks of Sor Jan and Nord Jan are derived. It is hypothesized that alkali olivine basalts (based on geologic location and age) NC22 and SJ1A may represent possible parental liquids for the rocks of Nord Jan and Sor Jan, respectively. NC22 and SJ1A are chosen on the basis that they are the most fine grained, equigranular and xenocryst free rocks from Nord Jan and Sor Jan. The chemical composition of the matrix of NC22 is essentially the same as the whole rock chemistry (Hawkins and Roberts, 1972). A few xenocrysts (olivine, chromium, titaniferous salite and plagioclase) are present in NC22 and a few phenocrysts of plagioclase are present in SJ1A. The presence of

xenocrysts or phenocrysts in these two rocks chosen as parental liquids may affect the results of the mixing calculation. For example: an ankaramite or alkali olivine basalt derived from NC22 may have chromium diopside, but in just the same amount as in NC22 whose composition already accounts for the presence of the chromium diopside. Thus, an ankaramite such as NC20 may simply be derived by the addition of plagioclase, olivine and titaniferous salite to NC22 even though chromium diopside xenocrysts are present in NC20 (petrographically NC20 is composed of mostly titaniferous salite with very little chromium diopside).

The mixing calculations were done in the following manner (Bryan et al., 1969): a given rock composition is estimated by adding different proportions of olivine, plagioclase, titaniferous salite and chromium diopside to a hypothetical parental magma (NC22 or SJ1A). Mathematically,

$$ROCK = aLIQ + bOL + cPL + dTISAL + eCRDI$$

where a, b, c, d and e are the estimated weight percentages of liquid (hypothetical parental magma), olivine, plagioclase, titaniferous salite and chromium diopside, respectively. These estimated rock compositions are compared to the observed rock compositions and their differences are described in terms of the sum of the squares of the residuals (Σ residual^2). The residuals are the differences between the observed and estimated compositions for each oxide. Only those calculations for which the sum

of the squares of residuals is equal to or less than 5.500 and for which minerals must be added to the parental liquid are used.

The results of least squares magma mixing for eight ankaramites and alkali olivine basalts are given in Appendix VI. The observed and estimated whole rock compositions are listed along with the estimated weight percentages of the parental liquid and the minerals needed to obtain the estimated whole rock composition. The minerals are listed by number and refer to the analyses in Appendix IV.

Results. It is observed that if more and more phases (minerals) are added to a parental liquid the estimated composition of the rock begins to resemble the observed composition very quickly (increasing the number of variables allows more flexibility in the computations resulting in very similar extimated and observed rock compositions). Thus, the number of minerals added to the parental liquid is kept to a minimum.

The xenocrystic nature of the alkali olivine basalts and ankaramites, as observed in thin section, suggests that all of the alkali olivine basalts and ankaramites may be accounted for by the mixing of different proportions of olivine, titaniferous salite, chromium diopside and plagioclase to a hypothetical parental magma (NC22 or SJ1A). For example: ankaramite NC15 is derived by adding OL:CRDI:TISAL in the proportions of 1.86:1.00:5.44 to 39.54% of parental liquid NC22.

The amount of parental liquid required to form the estimated rock compositions appears to be roughly proportional to the modal content of matrix in the rocks. Generally, the ankaramites contain less matrix (quenched parental liquid) than do the alkali olivine basalts.

It appears that the mixing calculations define the relative amounts of xenocrysts present in each rock with respect to the composition and petrography of the hypothetical parental liquid. The effect of the addition of olivine to the parental liquids is small for alkali olivine basalts, but is higher for the ankaramites. It is observed that the alkali olivine basalts contain fewer olivine xenocrysts than do the ankaramites. Xenocrystic plagioclase has a negligible effect on the estimated rock compositions, and petrographically, there are only minor amounts of plagioclase xenocrysts in these rocks. When both titaniferous salite and chromium diopside are added to the parental liquids, titaniferous salite appears to have a much greater effect (by a factor of 6 to 18) on the estimated ankaramite compositions, such as NC15 and SJ20B, than the chromium diopside. These two rocks are petrographically more enriched in titaniferous salite than chromium diopside. Chromium diopside, however, appears to have a marginally greater effect than titaniferous salite (by a factor of 3) on the estimated alkali olivine basalt compositions. Alkali olivine basalt NC23 appears in thin section to contain approximately equal quantities of chromium diopside and titaniferous salite.

Calculations appear to be relatively accurate for the Nord Jan samples since no chromium diopside is observed petrographically or in the mixing calculation for NC12C which contains titaniferous salite as the only clinopyroxene.

Rayleigh Fractionation

Introduction. Rayleigh fractionation curves were calculated for Rb, Sr, Ni, $K/Sr/(K/Sr)_o$;K/K_o and $Rb/Sr/(Rb/Sr)_o$;Rb/Rb_o (Fig. 17 to 19). The curves are calculated from the estimated weight percentages of the minerals from the least squares magma mixing results, average values for $D_K^{xl/liq}$, $D_{Sr}^{xl/liq}$, and $D_{Rb}^{xl/liq}$ from Arth (1976) and average $D_{Ni}^{xl/liq}$ values from Schilling et al. (1978).

The equation for the curves in Figure 17 is:

$$C_A^x = C_A^o F^{D_A - 1}$$

where C_A^x = concentration of trace element A in rock x, C_A^o = concentration of trace element A in the parental liquid (NC22 or SJ1A), F = percent of parental liquid left after an interval of fractional crystallization, and D_A = bulk rock distribution coefficient for trace element A where A = Rb, Sr or Ni. C_A^x is calculated from this equation with values of F varying from 1 to 0 to obtain the curves. The observed values of C_A^x (in ppm) from Appendix III are plotted against the estimated weight percent of parental liquid (F) obtained from the least squares magma mixing results in Appendix VI.

The curves in Figures 18 and 19 are obtained from the equations:

$$\frac{A}{A_o} = \frac{C_A^x}{C_A^o} = F^{D_A - 1}$$

$$\frac{A/B}{(A/B)_o} = \frac{C_A^x/C_B^x}{C_A^o/C_B^o} = F^{D_A - D_B}$$

TABLE 3.

CRYSTAL/LIQUID DISTRIBUTION COEFFICIENTS (D)[1]

	Sr	Rb	K	Ni
CrDi	0.12	0.015	0.011	5
TiSal	0.12	0.031	0.038	5
Ol	0.014	0.0098	0.0068	15
Plag	1.83	0.071	0.71	0.1

TABLE 4.

BULK ROCK CRYSTAL/LIQUID DISTRIBUTION COEFFICIENTS (D)

	Sr	Rb	K	Ni
NC15	0.096	0.024	0.028	7.24
NC20	0.149	0.027	0.034	7.49
NC27L	0.174	0.016	0.017	6.75
NC12C	0.196	0.030	0.041	6.07
NC23	0.478	0.029	0.050	6.55
SJ15A	0.273	0.020	0.026	6.26
SJ20B	0.105	0.027	0.032	6.42
SJ6	0.232	0.070	0.023	7.21

[1] Data from Arth (1976) and Schilling et al. (1978).

where A = K or Rb, B = Sr, D_A = bulk rock distribution coefficient for trace element A, D_B = bulk rock distribution coefficient for trace element B, and the other variables are the same as in the preceding description. In these diagrams the curves are obtained by plotting A/A_o and $A/B/(A/B)_o$ at the same value of F which varies from 1 to 0. Observed values of A/A_o and $A/B/(A/B)_o$ calculated from values in Appendix III) for each rock are plotted as points on the graph.

Results: Rayleigh Fractionation Curves for Sr, Rb and Ni. The limiting Rayleigh fractionation curves for Sor Jan and Nord Jan (Fig. 17) indicate that Rb and Sr should be concentrated in and Ni depleted in the remaining liquid with increasing fractionation (decreasing F). This behavior is directly related to the values of the bulk rock crystal/liquid distribution coefficients: for values less than 1.000 the element is preferentially concentrated into the liquid and for values greater than 1.000 the element is preferentially incorporated into the crystallizing phases (Table 4).

The observed values for Rb and Sr in the alkali olivine basalts and ankaramites are much smaller than that predicted by Rayleigh fractionation. Ni contents of the rocks are enormously higher than expected, with the ankaramites containing the highest Ni contents at the lowest values of F.

Rb, Sr and Ni concentrations in the alkali olivine basalts and ankaramites follow trends that are exactly

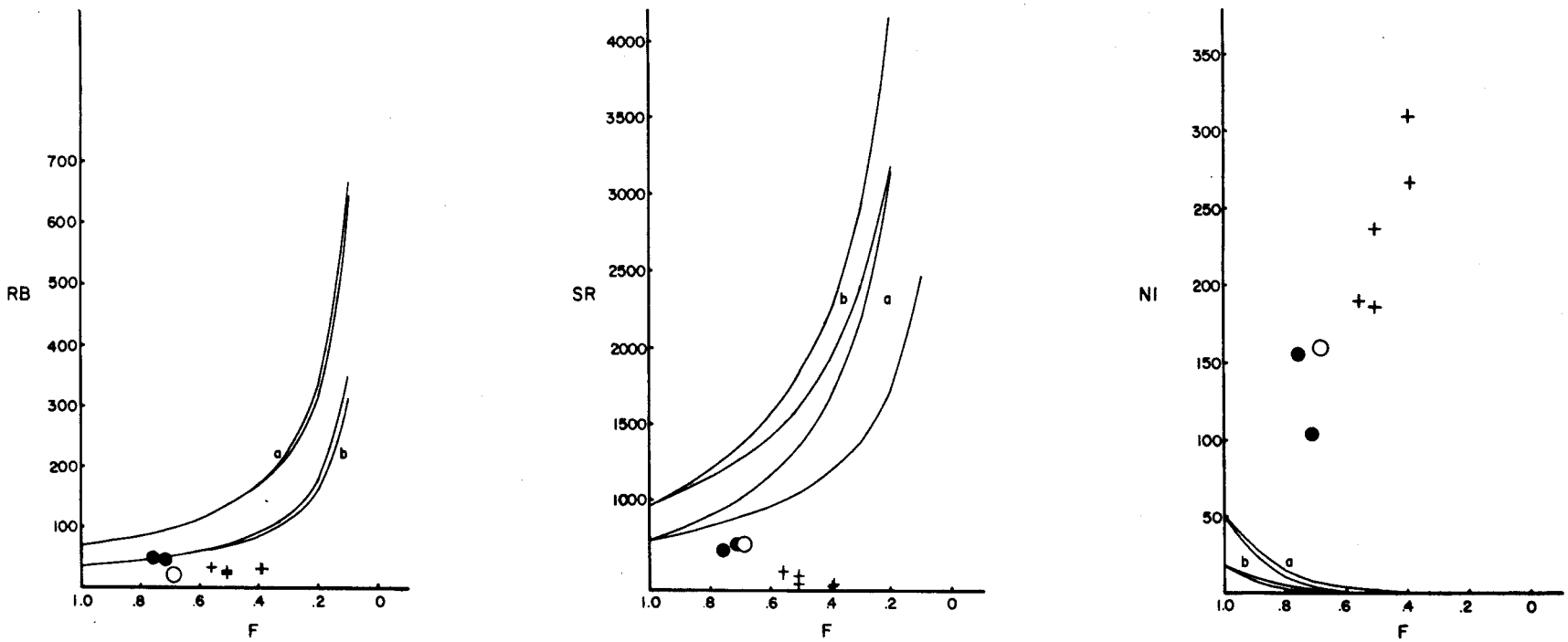

Figure 17. Simple Rayleigh fractionation curves for Rb, Sr and Ni. See text for explanation. a = calculated curves for Nord Jan, b = calculated curves for Sor Jan, o = Sor Jan alkali olivine basalt, ● = Nord Jan alkali olivine basalt, + = ankaramite.

opposite to the trend of concentration calculated for a magma undergoing Rayleigh fractionation. It is believed that this phenomenon is due to the accumulation of crystals high in Ni and low in Rb and Sr, such as olivine and perhaps clinopyroxene. The value of F, or percent of parental liquid left over as measured by the least squares magma mixing model, for each rock appears to represent the amount of interstitial unfractionated magma in which the accumulative phases were suspended. Therefore, the rocks containing greater quantities of cumulate phases have lower values of F and higher Ni and lower Rb and Sr contents, such as the ankaramites.

Results: Rayleigh Fractionation Curves for $K/Sr/(K/Sr)_o$: K/K_o and $Rb/Sr/(Rb/Sr)_o$:Rb/Rb_o.

The alkali olivine basalts and ankaramites of Nord lie in the lower left corner in the direction opposite to a typical fractionation scheme. The hypothetical parental liquid for Nord Jan, NC22, has the highest values of K, Rb and Sr of the Nord Jan rocks probably because it is the least contaminated by xenocrysts. Therefore, the rocks may be derived from the accumulation of olivine and clinopyroxene, as discussed in the previous section. The concentrations of K, Rb and Sr in the liquid (matrix of the rocks) are thus diluted by the xenocrysts.

The ankaramites and alkali olivine basalt SJ13A of Sor Jan have anomalously high values of normalized K/Sr and Rb/Sr ratios for their low normalized K and Rb contents,

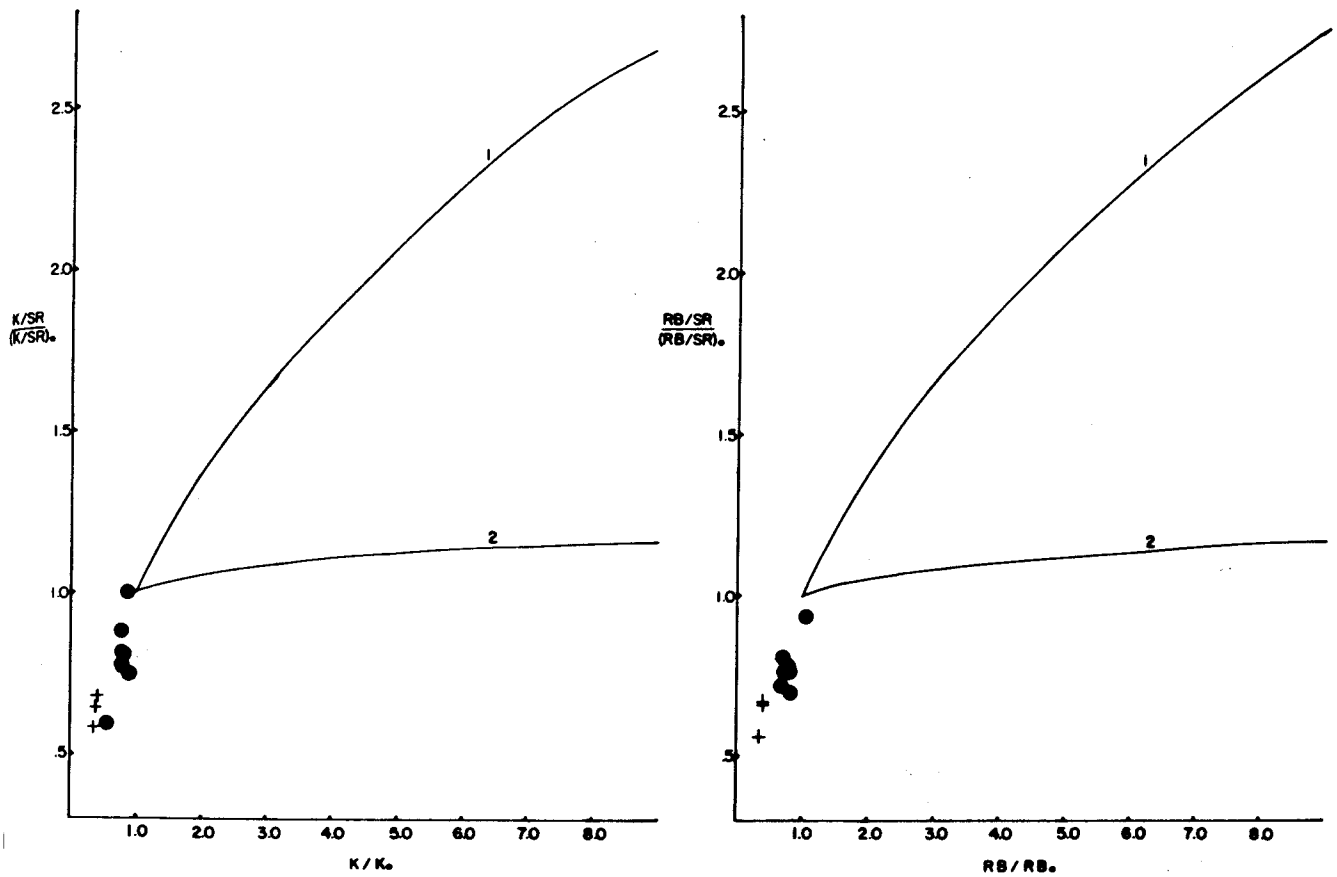

Figure 18. Rayleigh fractionation curves for Nord Jan. See text for explanation. 1 = 1.70:2.68:1.00:1.56 (olivine:chromium diopside:titaniferous salite:plagioclase) for NC23, 2 = 1.86:1.00:5.44 (olivine:chromium diopside:titaniferous salite) for NC15, • = alkali olivine basalt, + = ankaramite. (Adapted from DeLong, 1974.)

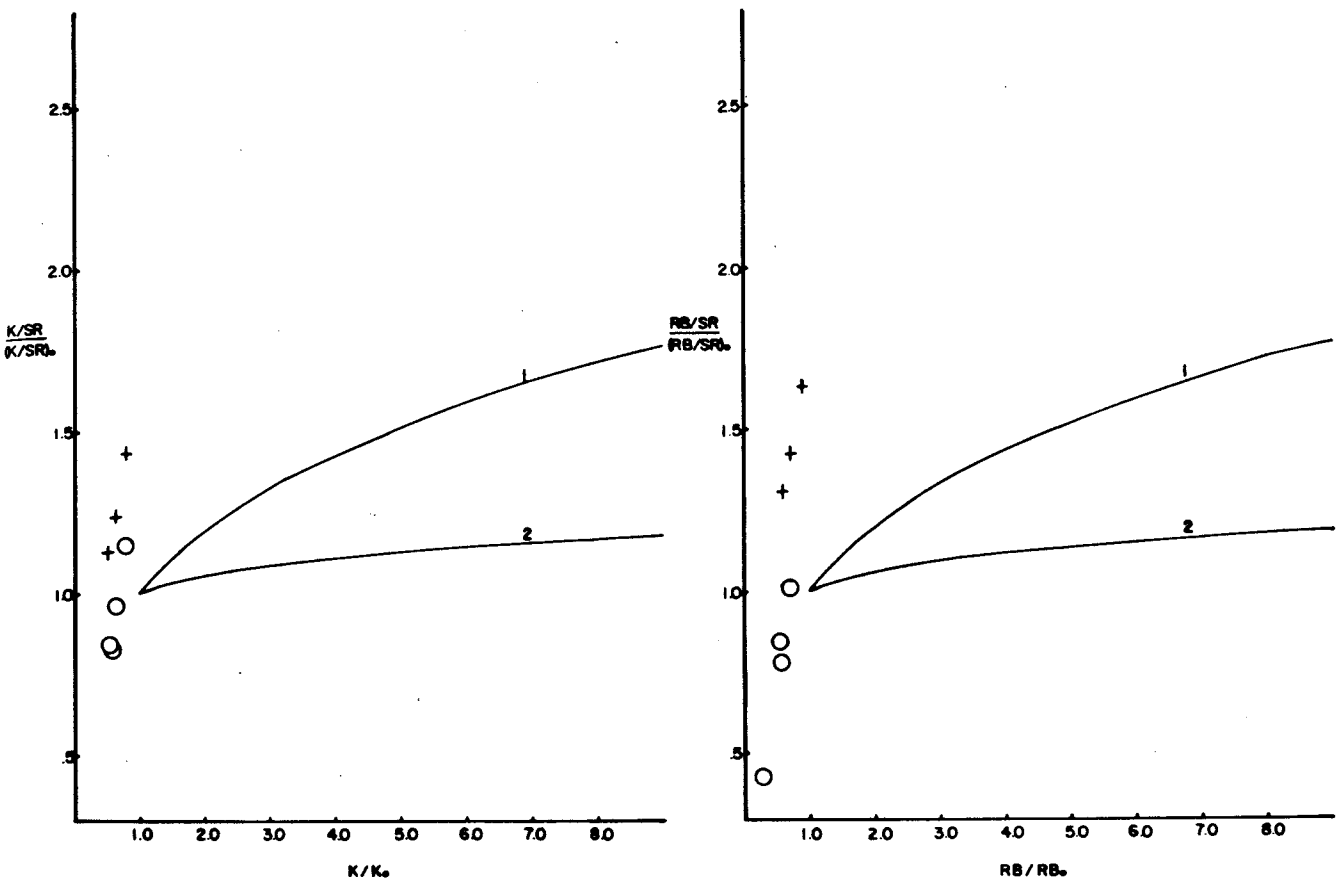

Figure 19. Rayleigh fractionation for Sor Jan. See text for explanation. 1 = 1.74:7.22:1.00 (olivine: chromium diopside:plagioclase) for SJ15A, 2 = 3.50:1.00: 20.11 (olivine:chromium diopside:titaniferous salite) for SJ20B, o = alkali olivine basalt, + = ankaramite. (Adapted from DeLong, 1974.)

respectively. This may be an effect of choosing SJ1A as a parental liquid, because it has an anomalously high Sr content. The ratios $(K/Sr)_o$ and $(Rb/Sr)_o$ are very low in SJ1A so that the normalized ratios of K/Sr and Rb/Sr become very large when the K/Sr ratio of each rock exceeds that of SJ1A. Thus, SJ1A is not an acceptable parental magma for the rocks of Sor Jan. The other choices available in this study, however, are also unacceptable as parental magmas due to their highly xenocrystic nature.

An alternative explanation for the behavior of the ankaramites of Sor Jan based on the above data may be that they are more highly xenocrystic with respect to plagioclase than the rocks of Nord Jan. However in thin section, the Nord Jan volcanics are definitely more enriched in plagioclase xenocrysts than the Sor Jan rocks.

Olivine Equilibrium. The ankaramites and alkali olivine basalts (Fig. 20A) tend to fall above and below the curve for $K_{MgO/FeO}^{liq/ol} = 0.3$, respectively. Most of the points, however, lie fairly close to the curve. Petrographically, the alkali olivine basalts contain less olivine than the ankaramites and it is found that the Fo content of olivine in alkali olivine basalts NC17, NC22 and NC23 is greater than expected for the bulk rock Fo composition (determined from molar proportions for the rock-$Mg/Mg+Fe^{2+}$). The olivine in these three rocks are thus clearly xenocrysts. Olivine xenocrysts of a similar composition in very large amounts, as in the ankaramites, increase the bulk rock

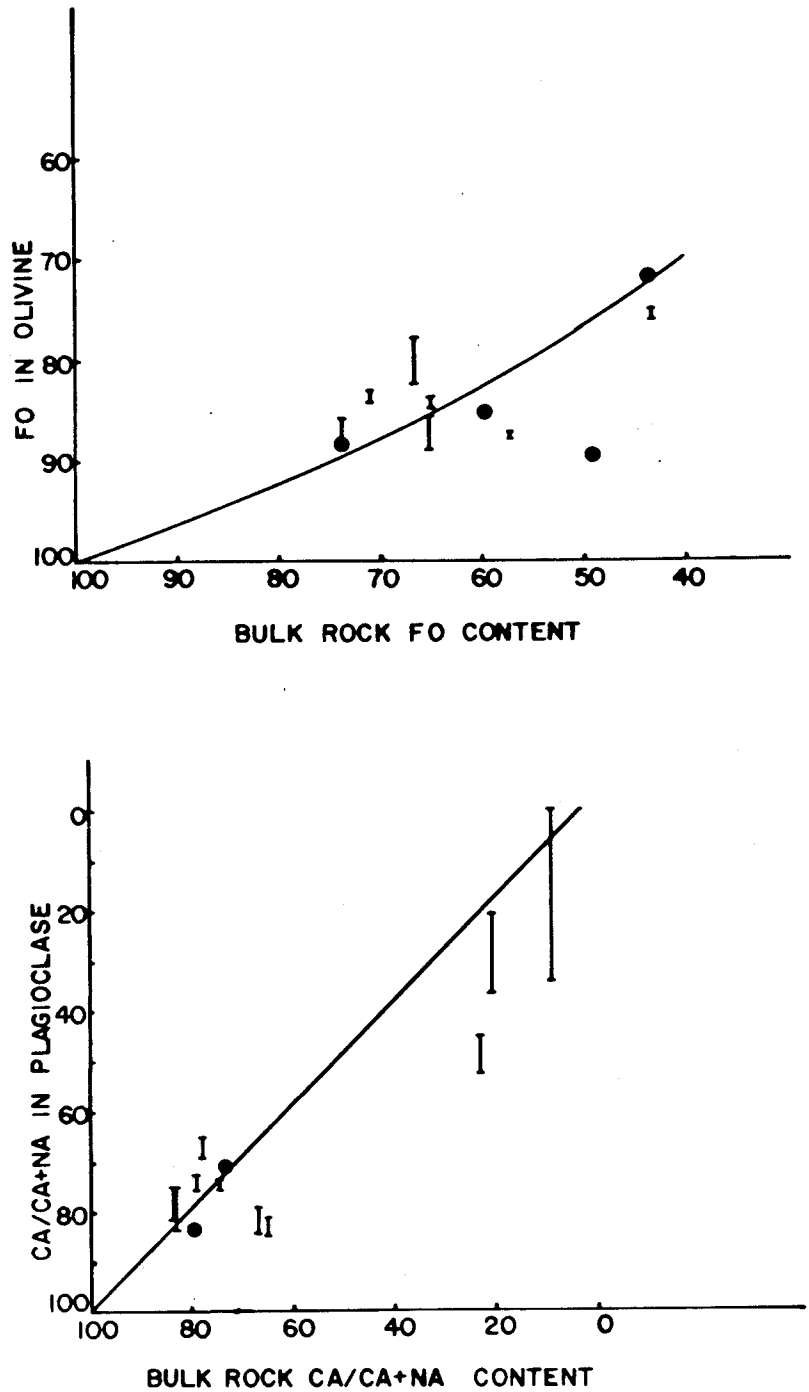

Figure 20. A. Olivine equilibrium. $K^{liq/ol}_{MgO/FeO} = 0.30$ equilibrium curve is plotted from Shibata, DeLong and Walker (1979). B. Plagioclase equilibrium. Curve approximated from above source. Compositional ranges for several analyses in a single rock are represented by a vertical bar. Filled circles represent the composition of a rock represented by a single analysis. See text for explanation.

magnesia content, thus displacing the bulk rock Fo content to higher values than that with which the olivine is presumed to be in equilibrium. Olivine in alkali olivine basalts SJ6, SJ13A and NC12C appear to be in equilibrium with the bulk rock composition, but the presence of resorbtion cavities indicates that they are not in equilibrium. Olivine in NC34B and JB202 appear to be in equilibrium with the bulk rock composition, petrographically and according to Figure 20A. These olivine phenocrysts are the most ferrous in the rocks of Jan Mayen.

Plagioclase Equilibrium. The ankaramites and most alkali olivine basalts lie above the estimated curve for equilibrium between Ca/Ca+Na in plagioclase phenocrysts and the bulk rock composition (Fig. 20B). This indicates that the bulk rock Ca/Ca+Na content is much higher than expected. This effect is probably due to the presence of large amounts of calcic clinopyroxene xenocrysts in the rocks, thus increasing the Ca portion of the ratio Ca/Ca+Na. Plagioclase from the relatively clinopyroxene-free alkali olivine basalts NC34B and JB202 have higher Ca/Ca+Na ratios than expected for their bulk rock compositions indicating that they are most probably xenocrysts. The presence of sodic rims on the plagioclase in these rocks also tends to support an origin from a different source than that represented by the bulk rock composition.

VIII. DISCUSSION AND CONCLUSIONS

Crystal-Liquid Disequilibrium upon Eruption of the Lavas

The ankaramites and alkali olivine basalts of Jan Mayen contain crystals which are apparently in disequilibrium with the magma in which they were erupted. Evidence for disequilibrium includes rounded and embayed edges and discontinuous to continuous rims on chromium diopside, titaniferous salite and plagioclase. Olivines typically are only resorbed. The discontinuity of rims on chromium diopside crystals indicates that even the rims are not in equilibrium with the erupting lava. This suggests that they may be more closely related to the titaniferous salite crystals (which are also resorbed) than the groundmass titaniferous augite. Rims of sodic plagioclase around plagioclase xenocrysts and discontinuous iron-rich rims on titaniferous salites have compositions close to groundmass plagioclase and titaniferous augite, respectively. This suggests that there was probably a very short period of additional crystal growth as the magma was quenched forming the groundmass.

Olivine and plagioclase equilibrium curves indicate that olivine and plagioclase crystals of the ankaramites and alkali olivine basalts should have crystallized from a magma with higher Mg and Ca contents. Other evidence

suggesting that the crystals did not originate from the magma in which they were erupted come from comparison with least squares magma mixing models and Rayleigh fractionation curve behavior. The results show that the ankaramites and alkali olivine basalts may be derived by accumulation of crystals high in Ni and low in Rb and Sr contents - namely, olivine, chromium diopside and titaniferous salite in a hypothetical parental magma. The least squares magma mixing model also suggests a small degree of plagioclase accumulation.

Crystal-Liquid Disequilibrium Prior to Lava Eruption

Disequilibrium between the magma and crystals even before eruption, is indicated by the presence of glass or melt inclusions in titaniferous salite and plagioclase, and reverse zonation of the titaniferous salite. Chromium diopside crystals appear to be free of this type of reaction. Neither the titaniferous augite rims nor the chromium diopside itself contain glass inclusions.

Melt inclusions in plagioclase are rounded, but often have semi-rectangular shapes and are oriented parallel to the twin lamellae. Some are even bounded by the faces of the twin lamellae. The melt was probably entrapped after the formation of the twin lamellae during a short period of resorption, since the orientation of the melt inclusions appears to be controlled by them. This short period of plagioclase resorption was probably followed by continued crystal growth which separated small patches of melt in the plagioclase from the main magma.

Melt inclusions form a spongy texture in the cores or rims of titaniferous salite crystals. The melt inclusions are often devitrified or may have tiny quench crystals. A few samples contain unaltered clear red-brown rounded patches of glass.

The formation of these melt inclusions in the crystals may be the result of: 1) immersion of the crystals in a liquid whose composition was different than that in which they had formed or 2) a sudden change in crystal-magma

compositions due to changing physical conditions (Dungan and Rhodes, 1978). In order to make definite conclusions as to which of these two processes occurred, the composition of the melt inclusions must be determined. The first process is preferred in this study based primarily upon petrographic evidence of disequilibrium between the crystals and magma even though no melt inclusion compositions are known.

Titaniferous salite cores are normally zoned and are mantled by a Mg rich zone which may itself be rimmed by an iron rich titaniferous clinopyroxene. This Mg rich mantle may be due to: 1) mixing of a more Mg rich magma with the alkali basalt magma in which the titaniferous salite was growing, 2) a change in temperature or pressure in the magma or 3) a change in oxygen fugacity causing iron oxides to precipitate out of the melt thus relatively enriching the melt in Mg (Wilkinson, 1975). The first explanation is preferred for the same reason as the explanation for the melt inclusions.

Possible Origins for the Xenocrysts

The xenocrysts occurring in the Jan Mayen alkali olivine basalts and ankaramites may have originated by the following processes: 1) as fractional crystallization products of the original magma (followed by gravitational accumulation or flotation), 2) as unmelted upper mantle residue that is brought to the surface by mantle derived magmas or 3) as ultramafic or mafic rock fragments accidentally captured by a magma as it ascended through the oceanic crust.

Titaniferous salites are typically formed by differentiation of alkali basalt magmas (volcanic islands: Aoki and Kushiro, 1968; Wilkinson, 1956; LeMaitre, 1962; Baker, 1969; Hughes and Brown, 1972; Ridley, 1970; transform faults: Shibata et al., in press). The presence of titaniferous salite glomerocrysts (± olivine, ± plagioclase) indicates that they formed by gravitational accumulation or some type of flow mechanism. The absence of strain features suggests, however, that accumulation of these phases was not far advanced and that they were still suspended in a relatively large amount of melt when they were erupted. Concentric zonation in titaniferous salite and plagioclase indicate a continual change in the compositional equilibrium of the magma due to fractionation. The composition of this magma was probably high in Fe, Al and Ti, according to the composition of the titaniferous salite.

Some alkali olivine basalts are choked with plagioclase glomerocrysts (NC34B and JB202). These may have formed by flotation and accumulation from the same but slightly more fractionated alkali basalt magma that had formed the titaniferous salite glomerocrysts.

Kaersutite(?) inclusions in titaniferous salite are typically rounded and are oriented parallel to the host clinopyroxene cleavage. The boundary between the kaersutite(?) and host clinopyroxene is usually filled with tiny opaques. These opaques may represent some type of reaction of the inclusion with the titaniferous salite host. This same type of phenomenon has been observed by Binns (1969) and Ridley (1970). It appears that kaersutite(?) was probably incorporated as inclusions into the titaniferous salite as it was growing.

Aegirine-augite phenocrysts in the trachytes develop from differentiation of a highly fractionated (peraikaline) liquid (LeMaitre, 1962; Hughes and Brown, 1972; Ridley, 1970).

Chromium diopsides from Jan Mayen have compositions that are similar to both mafic (gabbros) and ultramafic (peridotites) diopsides (Table 5). The lack of exsolution, (suggesting relatively high temperatures), the sometimes nearly euhedral shapes and the scarcity of glomerocrysts of chromium diopside indicate that they may have been in the process of accumulation ($\pm$ olivine, $\pm$ plagioclase) when they were incorporated into the magma. However, the presence of polygonization in chromium diopside (also

TABLE 5.

ANALYSES OF CHROMIUM DIOPSIDES FROM MAFIC AND ULTRAMAFIC ROCKS

	Xenocrysts	Gabbros[1]			Peridotite[2]	
	Jan Mayen (24)	La Palma (1)	Lanzarote (11)	East Island (1)	Lanzarote (1)	Lanzarote (3)
SiO_2	52.13 (1.18)[1]	51.10	50.91	51.6	52.15	52.32
TiO_2	0.72 (0.22)	0.87	0.30	0.9	0.18	0.15
Al_2O_3	2.89 (1.16)	3.49	3.65	3.8	3.85	3.97
FeO*	3.98 (0.56)	4.74	5.82	4.5	2.88	2.83
MnO	0.11 (0.02)	0.15	0.13	0.07	0.08	0.08
MgO	16.92 (0.86)	15.87	18.03	15.6	16.80	17.27
CaO	22.08 (0.66)	22.38	20.40	22.8	21.28	21.35
Na_2O	0.28 (0.07)	0.91	0.33	0.4	0.78	0.76
Cr_2O_3	0.57 (0.29)		0.23		1.40	1.05

* Total iron as FeO.
1 ( ) represents the standard deviation.
2 Analyses from Fuster, Paez and Sagredo (1969) and Gunn et al., (1970).
3 Analyses from Munoz and Sagredo (1974).

recognized by Roberts and Hawkins, 1965), deformation lamellae in olivine, and deformed Carlsbad-albite twins in plagioclase indicates that some of these xenocryst inclusions were derived from a solid deformed mafic or ultramafic rock.

The uniform composition of the unzoned chromium diopsides and olivines also suggests that they formed under equilibrium conditions in a nonfractionating magma. The magma composition from which the chromium diopside, olivine and plagioclase precipitated, based on their chemistries, was enriched in Mg, Ca, Ni and Cr. The presence of a titaniferous clinopyroxene rim about the chromium diopsides suggests that they acted as crystallization surfaces for titaniferous salite precipitating from the alkali basalt magma that had captured the chromium diopside. It is believed that these xenocrysts probably were derived from the mafic or ultramafic rocks of the oceanic crust.

Thus, it appears that the "xenocrysts" in the Jan Mayen volcanics originated as fractional crystallization products of an alkali basalt magma (titaniferous salite glomerocrysts) and as accidental ultramafic or mafic rock fragments captured by the alkali basalt magma as it rose to the surface (chromium diopside glomerocrysts).

Evolution of the Jan Mayen Volcanics

Chemical and temporal evidence suggest the possible existence of two separate regions of magma generation in the mantle from which the rocks of Jan Mayen were derived. Rb/Sr ratios indicate that there are distinct differences between the otherwise similar basic rocks of Sor Jan and Nord Jan. Rb and Sr variation diagrams also support the apparent existence of two separate fractionation trend for the rocks of Nord Jan and Sor Jan at different levels of Rb and Sr enrichment. The highly differentiated rocks of Sor Jan, the trachytes, have anomalously high Rb/Sr ratios which are consistent with observations from other volcanic islands (Baker, 1969; LeMaitre, 1962).

There is also a significant difference between the ages of the volcanics of Nord Jan and Sor Jan. The volcanics of Sor Jan are the oldest known on the island. The youngest lavas there are 30,000 years old and there is no volcanic activity on Sor Jan at the present, (these dates are probably not very accurate since the development of the K-Ar method was in its infancy at this time: Fitch, Grasty and Miller, 1965). The oldest age estimates for the lavas of Nord Jan are at least 12,000 years old (Fitch, Nairn and Talbot, 1965) and volcanism and hydrothermal activity continues to the present. Topographic features of Sor Jan (highly eroded flat tableland) and Nord Jan (dominated by the active Beerenberg volcano) also indicate an age difference between the two regions. Despite these differences, the two

volcanic series appear to have formed by the same mechanism.

The closeness of Jan Mayen to the Jan Mayen Fracture Zone and the similarity of compositions of the whole rocks (Table 6) with alkali basalts from other fracture zones suggest that the Jan Mayen volcanics are related to transform volcanism in an extensional regime (Shibata et al., in press; Batiza et al., 1977; Melson et al., 1967; Aumento, 1968).

The parental alkali basalt magma was probably derived by melting of the mantle (Sr^{87}/Sr^{86} = .7035 to .7041 for the volcanics of Jan Mayen) at pressures greater than 10 kb (straddle type volcanics). LeMaitre (1969), Baker (1969), Hughes and Brown (1972) and Flower (1969) emphasize the possible role of phlogopite in the genesis of alkali basalt magmas. Partial melting of phlogopite and other mantle phases at 100 to 130 km depths (Oxburgh and Turcotte, 1968; Hughes and Brown, 1972) produces melts with low K/Rb contents (less than 500) and high Ti as observed in the alkali basalt volcanics of Jan Mayen. The absence or presence of xenocrystic phlogopite indicates complete or incomplete assimilation of phlogopite into the melt, respectively. Flower (1969) reports the presence of a large "xenocrystic" phlogopite and he suggests that the magma forming the volcanics of Jan Mayen did not assimilate phlogopite completely.

Differentiation of the alkali basalt magma began with the crystallization of titaniferous salite at relatively high pressures. High pressure experiments by Thompson (1974)

TABLE 6.

COMPOSITION OF VOLCANICS FROM FRACTURE ZONES AS COMPARED WITH THOSE FROM JAN MAYEN

	45°N Atlantis[1] (1)	St. Paul's Rocks[2] (1)	Siqueiros Transform Fault[3] (4)	Nord Jan (34)
SiO_2	46.80	43.15	48.3	46.98
TiO_2	1.71	2.70	2.48	2.73
Al_2O_3	15.9	13.46	16.00	15.48
FeO*	9.69	12.29	10.00	10.97
MnO	0.23	0.11	0.15	0.20
MgO	7.20	10.80	6.89	6.13
CaO	7.7	9.8	9.55	10.45
Na_2O	4.8	3.47	3.83	2.93
K_2O	1.90	1.63	1.09	2.36
P_2O_5	0.37	0.75		0.59

---

* Total iron as FeO.
1 Analysis from Aumento, 1968.
2 Analysis from Nelson et al., 1967.
3 Analysis from Batiza et al., 1977.

suggests that titaniferous clinopyroxenes form at pressures equal to or greater than 10 kb (at 1225°C) which corresponds to a depth of 33 km. This depth coincides with: 1) the depth of seismicity measured on Jan Mayen (28 to 33 km, as reported by Sylvester in 1974 and Zobin in 1972), and 2) the lower crust-upper mantle boundary in this region (based on the age of the oceanic crust under Jan Mayen). Plagioclase glomerocrysts comprising the bulk of some rocks suggest that crystal flotation may have also occurred within this magma. Walker and Hays (1977) and Shibata et al. (1979) have shown that plagioclase does float in primitive liquids.

The alkali basalt magma and its related mineral phases appear to have been: 1) intruded through and fragmented the oceanic crust "capturing" xenocrysts from mafic and/or ultramafic rocks and 2) intruded through a zone of partial accumulation of these same rocks.

Mixing of the alkali basalt magma and the magma in the zone of partial accumulation of the mafic or ultramafic rocks resulted in resorption of all crystals in question due to the changed crystal-melt equilibrium. Titaniferous salite and its associated plagioclase were resorbed and then continued crystallizing leaving melt inclusions in the crystals. A Mg rich mantle containing poikilitic melt inclusions in titaniferous salite appear to have also formed at this time. This may be due to an increase of Mg from the magma from which the mafic or ultramafic rock was in the process of precipitating. Chromium diopside crystals

were resorbed without the development of melt inclusions that are so characteristic of the titaniferous salites. However, the chromium diopsides were subsequently rimmed by a titaniferous clinopyroxene that is close in composition to the Mg rich mantle on titaniferous salites.

Upon eruption of the magma all crystals were again in disequilibrium resulting in resorption of the rims about titaniferous salite and chromium diopside. Rims of a more sodic plagioclase equivalent in composition to the groundmass plagioclase and similar, but rare, rims of more Fe rich titaniferous augite formed about plagioclase and titaniferous salite, respectively. The presence of reversely rimmed euhedral microphenocrysts of titaniferous salite suggest a sudden change in the oxygen fugacity resulting in the precipitation of iron oxides (the groundmass is choked with tiny opaques) and subsequent enrichment of Mg in the magma. All olivine crystals appear to have reacted with the magma by only being resorbed, but some were later altered by local deuteric action to iddingsite and/or a magnetite reaction rim.

Highly differentiated liquids giving rise to the trachytes on Jan Mayen probably originated by strong fractionation of the magma combined with the transfer of alkalies and silica in a vapor phase, probably near the top of the magma chamber (Ridley, 1970; Arana et al., 1973; Baker, 1969).

Further Considerations

In order to fully understand the petrogenesis of the volcanics of Jan Mayen it would be useful and interesting to determine the compositions of: 1) melt inclusions in titaniferous salite and plagioclase, 2) opaque phases and 3) amphiboles and micas. Trace element geochemistries of the groundmass of these rocks and of the individual mineral phases would more rigorously constrain the possible origins of the xenocrystic crystals.

BIBLIOGRAPHY

Aoki, K. and Kushiro, I., 1968, Some Clinopyroxenes from Ultramafic Inclusions in Dreiser Weiher, Eifel, Contrib. Mineral. Petrol., v.18, p.326-337.

Arana, V., Badiola, E.R. and Hernan, F., 1973, Peralkaline Acid Tendencies in Gran Canaria (Canary Islands), Contrib. Mineral. Petrol., v.40, p.53 62.

Arth, J.G., 1976, Behavior of Trace Elements During Magmatic Processes - A Summary of Theoretical Models and Their Applications, Jour. Research U. S. Geol. Surv., v.4, no.1, p.41-47.

Aumento, F., 1968, The Mid-Atlantic Ridge Near 45° N II. Basalts from the Area of Confederation Peak, Can. Jour. Earth Sci., v.5, no.1, p.1-21.

Baker, I., 1969, Petrology of the Volcanic Rocks of Saint Helena Island, South Atlantic, Geol. Soc. Am. Bull., v.80, p.1283-1310.

Baxter, A.N., 1975, Petrology of the Older Series Lavas from Mauritius, Indian Ocean, Geol. Soc. Am. Bull., v.86, p.1449-1458.

Batiza, R., Rosendahl, B.R. and Fisher, R.L., 1977, Evolution of Oceanic Crust 3. Petrology and Chemistry of Basalts from the East Pacific Rise and the Siqueiros Transform Fault, Jour. Geophys. Res., v.82, no.2, p.265-276.

Binns, R.A., 1969, High Pressure Megacrysts in Basanitic Lavas Near Armidale, New South Wales, Am. Jour. Sci., v.267A, p.33-49.

Birkenmajer, K., 1972, Geotectonic Aspects of the Beerenberg Volcano Eruption 1970, Jan Mayen Island, Acta Geologica Polonica, v.22, no.1, p.1-15.

Bryan, W.B., Finger, L.W. and Chayes, F., 1969, Estimating Proportions in Petrographic Mixing Equations by Least Squares Approximation, Science, v.163, p.926-927.

Carstens, Harald, 1961, Cristobalite-Trachytes of Jan Mayen, Oslo Norsk Polarinst. Skrifter, nr.121, 10pp.

Carstens, H., 1962, Leucite- and Sodalite-Bearing Trachybasalts of Jan Mayen, Oslo Norsk Polarinst. Arbok, v.1962, p.185-186.

DeLong, S.E., 1974, Distribution of Rb, Sr and Ni in Igneous Rocks, Central and Western Aleutian Islands, Alaska, Geochim. Cosmochim. Acta, v.38, p.245-266.

DeLong, S.E., Unpublished normative mineralogies recalculated from the literature for Jan Mayen.

DeLong, S.E. and Long, Unpublished Ni, Rb and Sr analyses for the rocks of Jan Mayen.

Dollar, A.T.J., 1966, Genetic Aspects of the Jan Mayen Fissure Volcano Group on the Mid-Ocean Submarine Mohns Ridge, Norwegian Sea, Bull. Volcanol. Abstr., v.29, p.25-26.

Dungan, M.A. and Rhodes, J.M., 1978, Residual Glasses and Melt Inclusions in Basalts from DSDP Legs 45 and 46: Evidence for Magma Mixing, Contrib. Mineral. Petrol., v.67, p.417-431.

Faure, G., 1977, Principles of Isotope Geology, John Wiley and Sons, Inc., New York, p.112.

Fitch, F.J., 1962, The University of London 1961 Beerenberg Expedition, Nature, v.194, p.624-626.

Fitch, F.J., written commun., unpublished chemical analyses from Jan Mayen.

Fitch, F.J., Grasty, R.L. and Miller, J.A., 1965, Potassium-Argon Ages of Rocks from Jan Mayen and an Outline of Its Volcanic History, Nature, v.207, no.5004, p.1349-1351

Fitch, F.J., Nairn, A.E.M. and Talbot, C.J., 1965, Palaeomagnetic Studies on Rocks from North Jan Mayen, Oslo Norsk Polarinst. Arbok, v.1963, p.49-60.

Flower, M.F.J., 1969, Phlogopite from Jan Mayen Island (North Atlantic), Earth Planet. Sci. Letters, v.6, p.467-478.

Fuster, J.M., Paez, A. and Sagredo, J., 1969, Significance of Basic and Ultramafic Rock Inclusions in the Basalts of Canary Islands, Bull. Volcanol., V.33, p.665-693.

Gunn, B.M., Coy-Yll, R., Watkins, N.D., Abranson, C.E. and Nougier, J., 1970, Geochemistry of an Oceanite-Ankaramite-Basalt Suite from East Island, Crozet Archipelago, Contrib. Mineral. Petrol., v.28, p.319-339.

Hawkins, T.R.W. and Roberts, B., 1972, The Petrology of the Volcanic and Intrusive Rocks of Nord-Jan, Jan Mayen, Oslo Norsk Polarinst. Arbok, v.1970, p.19-41.

Hughes, E.J. and Brown, G.C., 1972, Basalts from Madeira: A Petrochemical Contribution to the Genesis of Oceanic Alkali Rock Series, Contrib. Mineral. Petrol., v.37, p.91-109.

Irvine, T.N. and Baragar, W.R.A., 1971, A Guide to the Chemical Classification of the Common Volcanic Rocks, Can. Jour. Earth Sci., v.8, p.523-548.

Jennings, J.N., 1948, Glacier Retreat in Jan Mayen, Jour. Glac., v.1, no.4, p.167-181.

King, A., 1939, The Imperial College Expedition to Jan Mayen Island, Geogr. Jour., v.94, p.115-134.

Kinsman, D.J.J. and Sheard, J.W., 1972, The Glaciers of Jan Mayen, Jour. Glac., v.4, p.439-448.

Kinsman, D.J.J., Sheard, J.W. and Fitch, F.J., 1962, Glacial History of Beerenberg, Jan Mayen Island, Nature, v.195, no.4844, p.897-898.

Lamb, H.H., Probert-Jones, J.R. and Sheard, J.W., 1962, A New Advance of the Jan Mayen Glaciers and A Remarkable Increase of Precipitation, Jour. Glac., v.4, no.33, p.355-366.

LeMaitre, R.W., 1962, Petrology of Volcanic Rocks, Gough Island, South Atlantic, Geol. Soc. Am. Bull., v.73 p.1309-1340.

LeMaitre, R.W., 1969, Kaersutite-Bearing Plutonic Xenoliths from Tristan da cunha, South Atlantic, Mineral. Mag., v.37, p.185-197.

Lussiaa-Berdou-Polve, M. and Vidal, P., 1973, Initial Strontium Isotopic Composition of Volcanic Rocks from Jan Mayen and Spitsbergen, Earth Planet. Sci. Letters, v.18, p.333-338.

MacDonald, G.A. and Katsura, T., 1964, Chemical Composition of Hawaiin Lavas, Jour. Petrol., v.5, no.1, p.82-133.

Melson, W.G., Jarosewich, E., Cifelli, R. and Thompson, G., 1967, Alkali Olivine Basalt Dredged Near St. Paul's Rocks, Mid-Atlantic Ridge, Nature, v.215, p.381-382.

Miyashiro, A., 1978, Nature of Alkalic Volcanic Rock Series, Contrib. Mineral. Petrol., v.66, p.91-104.

Munoz, M. and Sagredo, J., 1974, Clinopyroxenes as Geobarometric Indicators, in Mafic and Ultramafic Rocks from Canary Islands, Contrib. Mineral. Petrol., v.44, p.139-147.

Nicholls, G.D., 1955, The Geology of North-East Jan Mayen, Geol Mag., v.92, p.127-140.

Oxburgh, E.R. and Turcotte, D.L., 1968, Problem of High Heat Flow and Volcanism Associated with Zones of Descending Mantle Convective Flow, Nature, v.128, no.5146, p.1041-1043.

Papike, J.J., Cameron, K.L. and Baldwin, K., 1974, Amphiboles and Pyroxenes: Characterization of OTHER than Quadrilateral Components and Estimates of Ferric Iron from Microprobe Data, Geol. Soc. Am. Abstr. Prog., v.6, no.7, p.1033-1054.

Ribbe, P.H., 1975, The Chemistry, Structure and Nomenclature of Feldspars, in Min. Soc. Am. Short Course Notes, Feldspar Min., v.2, p.R-2.

Ridley, W.I., 1970, The Petrology of the Las Canadas Volcanoes, Tenerife, Canary Islands, Contrib. Mineral. Petrol., v.26, p.124-160.

Roberts, B. and Hawkins, T.R.W., 1965, The Geology of the Area Around Nordkapp, Jan Mayen, Oslo Norsk Polarinst. Arbok, v.1963, p.25-48.

Schilling, J.G., Sigurdsson, H. and Kingsley, R.H., 1978, Skagi and Western Neovolcanic Zones in Iceland: 2. Geochemical Variations, Jour. Geophys. Research, v.83, no.B8.

Shibata, T., DeLong, S.E. and Walker, D., 1979, Abyssal Tholeiites from the Oceanographer Fracture Zone I. Petrology and Fractionation, Contrib. Mineral. Petrol., v.70, p.89-102.

Shibata, T. and Fox, P.J., 1975, Fractionation of Abyssal Tholeiites: Samples from the Oceanographer Fracture Zone (35°N, 35°W), Earth Planet. Sci. Letters, v.27, p.62-72.

Shibata, T., Thompson, G. and Frey, F.A., (in press), Tholeiitic and Alkali Basalts from the Mid-Atlantic Ridge at 43°N.

Siggerud, T., 1972, The Volcanic Eruption on Jan Mayen 1970, Oslo Norsk Polarinst. Arbok, v.1970, p.5-18.

Sylvester, A.G., 1974, Surface Faulting and Fumarolic Activity Since the 1970 Beerenberg Eruption, Jan Mayen, Norsk Geologisk Tidsskrift, v.54, p.385-393.

Sylvester, A.G., 1975, History and Surveillance of Volcanic Activity on Jan Mayen Island, Bull. Volcanol., v.39, p.311-335.

Talwani, M. and Eldholm, O., 1977, Evolution of the Norwegian-Greenland Sea, Geol. Soc. Am. Bull., v.88, p.969-999.

Thompson, R.N., 1974, Some High-Pressure Pyroxenes, Min. Mag., v.39, p.768-787.

Tyrrell, G.W., 1926, The Petrography of Jan Mayen, Roy. Soc. Edin. Trans., v.54, pt.3, p.747-765.

Upton, B.G.J., Wadsworth, W.J. and Neuman, T.C., 1967, The Petrology of Rodriguez Island, Indian Ocean, Geol. Soc. Am. Bull., v.78, p.1495-1506.

Walker, D. and Hays, J.F., 1977, Plagioclase Flotation and Lunar Crust Formation, Geology, v.5, p.425-428.

Weigand, P.W., 1972, Bulk-Rock and Mineral Chemistry of Recent Jan Mayen Basalts, Oslo Norsk Polarinst. Arbok, v.1970, p.42-52.

Wilkinson, J.F.G., 1975, Ultramafic Inclusions and High Pressure Megacrysts from a Nephelinite Sill, Nandewar Mountains, Northeastern New South Wales, and Their Bearing on the Origin of Certain Ultramafic Inclusions in Alkaline Volcanic Rocks, Contrib. Mineral. Petrol, v.51, p.235-262.

Zobin, V.M., 1972, Focal Mechanism of Volcanic Earthquakes, Bull. Volcanol., v.36, p.561-571.

APPENDIX I

Micrographs of Olivine, Clinopyroxene and Plagioclase

EXPLANATION
(all photos taken with polarized light)

Olivine

A. Anhedral crystal 1A-B of SJ15A has a rounded shape and is resorbed (magnification 40x).

B. A strongly polygonized crystal of olivine from NC15 (magnification 40x).

C. Arrows point to diamond shaped and elongate, forked groundmass olivine of SJ1A (magnification 100x).

Clinopyroxene

A. Chromium diopside 10A-D of SJ15A is nearly euhedral, simply twinned, and rimmed by purple brown titaniferous augite. It also encloses a rounded crystal of olivine. (magnification 40x).

B. Chromium diopside 5A-B of NC22 is an anhedral crystal also rimmed by purple brown titaniferous augite (magnification 40x).

C. Titaniferous salite 9A-F of SJ13A is an euhedral, reversely zoned crystal with sector zones (magnification 40x).

D. Titaniferous salite 9A-B of SJ20B is anhedral, reversely zoned and rimmed by titaniferous augite (magnification 40x).

E. Titaniferous salite 8A-C of SJ20B is an euhedral, reversely rimmed (Mg rich rim) crystal (magnification 100x).

F. Titaniferous salites of NC12C are sector zoned and form glomerocrysts (magnification 40x).

Feldspar

A. Bytownite xenocryst 2A-B of NC22 is anhedral and rimmed by labradorite (magnification 40x).

B. Bytownite glomerocryst of NC15 is anhedral and resorbed (magnification 40x).

C. Bytownite glomerocryst of JB202 is composed of normally zoned and multiply twinned crystals (magnification 40x).

D. Andesine glomerocryst 11A-B of SJ25B is rimmed by a highly potassic alkali feldspar (magnification 40x).

E. Oligoclase 2A-B of SJ2B is a strongly zoned euhedral groundmass feldspar (magnification 100x).

F. A highly potassic alkali feldspar glomerocryst of SJ25B also includes green aegirine-augite and magnetite (magnification 40x).

OLIVINE

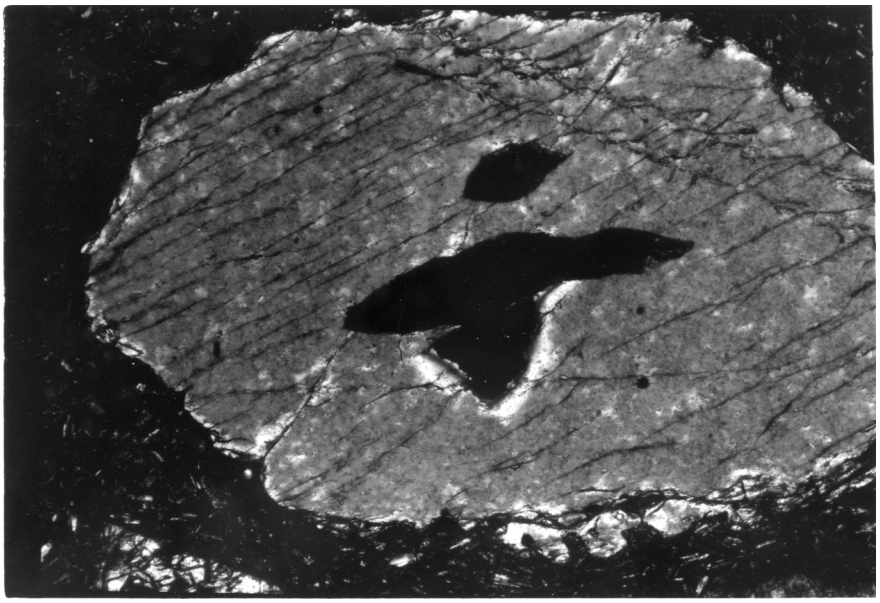

A

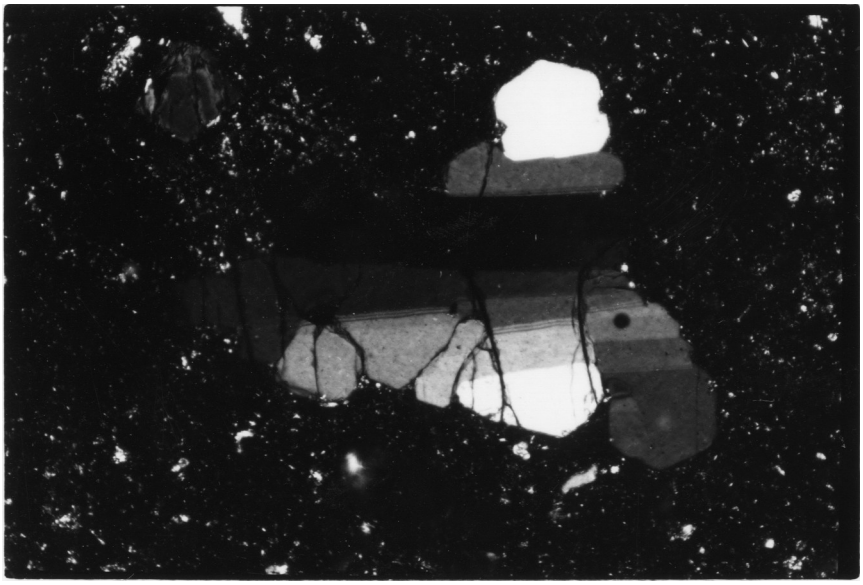

B

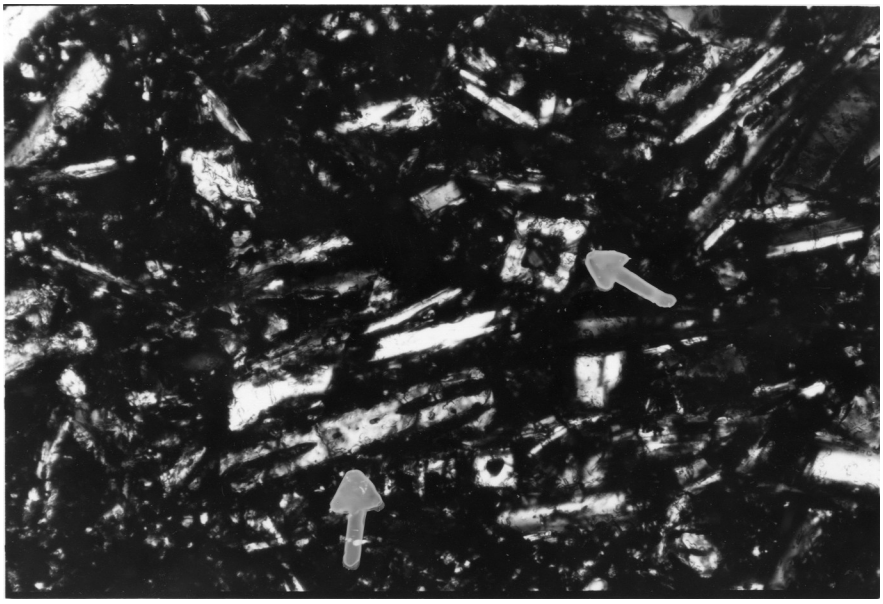

C

CLINOPYROXENE

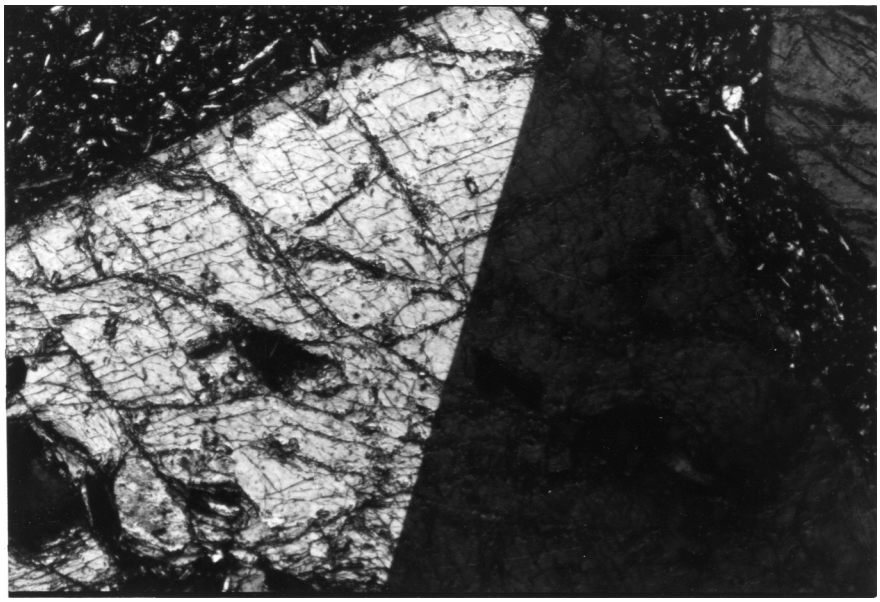

A

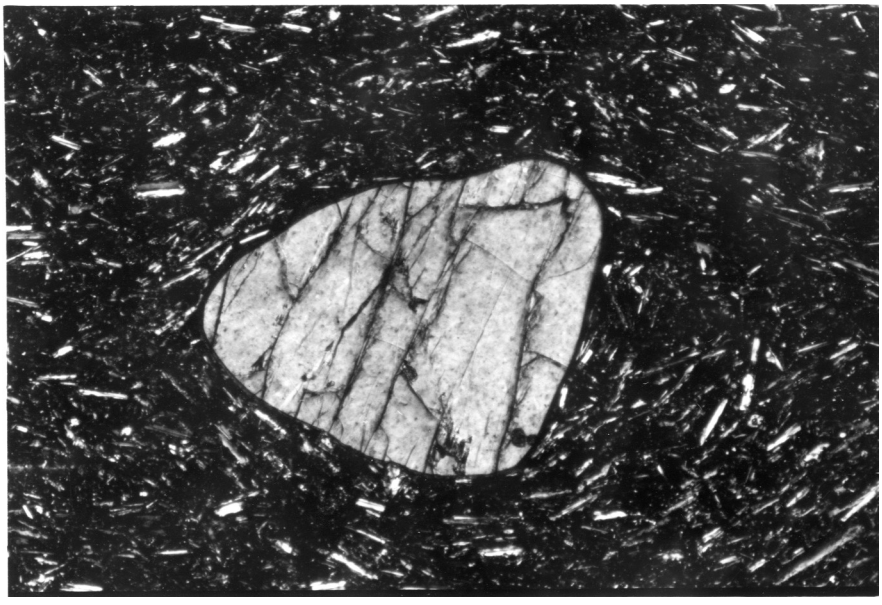

B

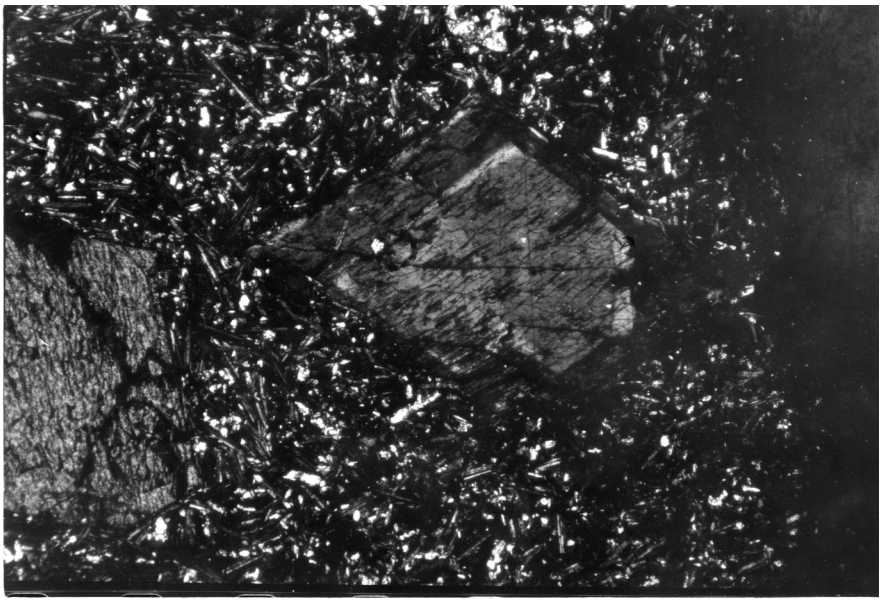

C

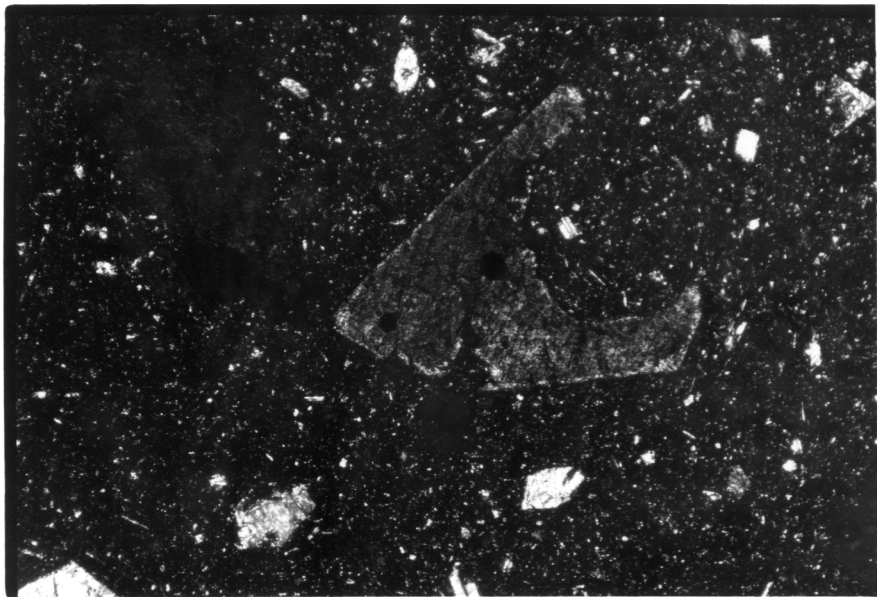

D

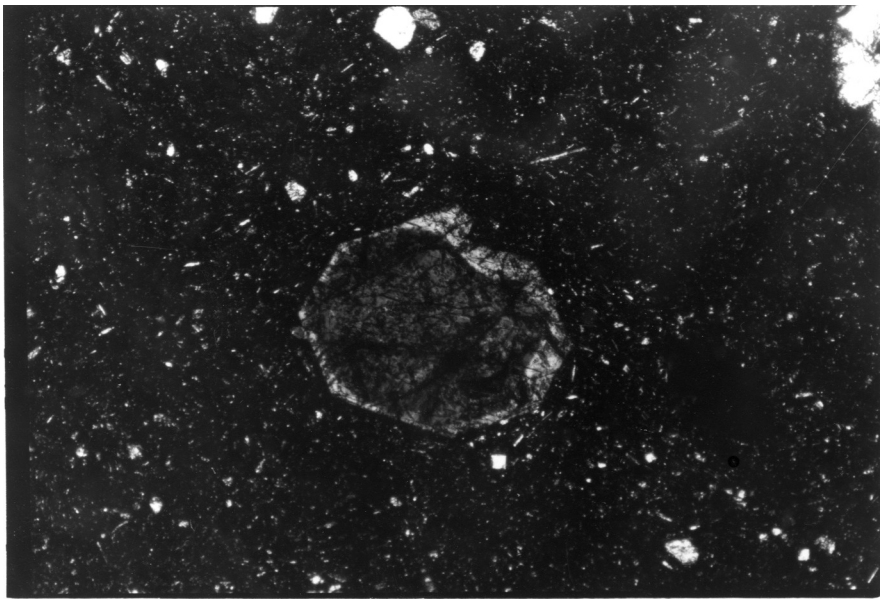

E

F

FELDSPAR

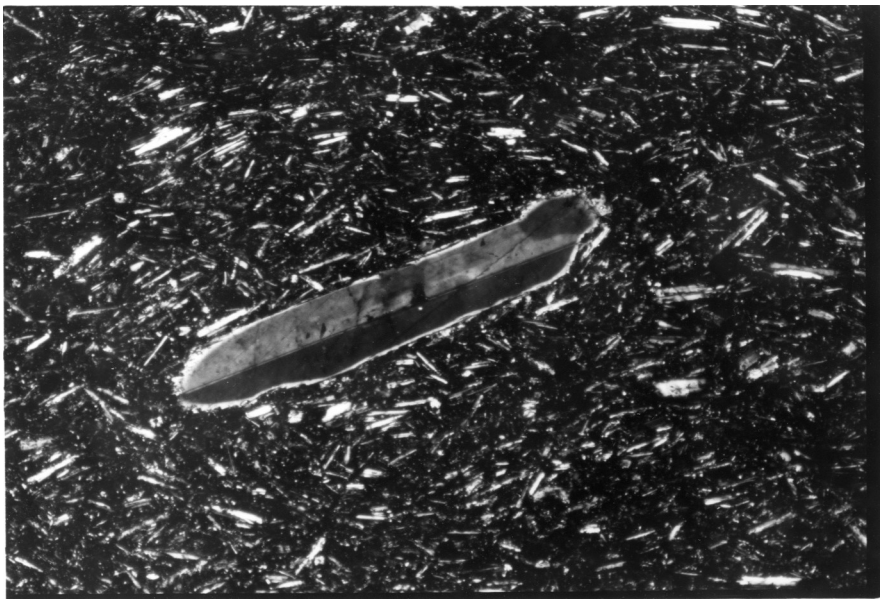

A

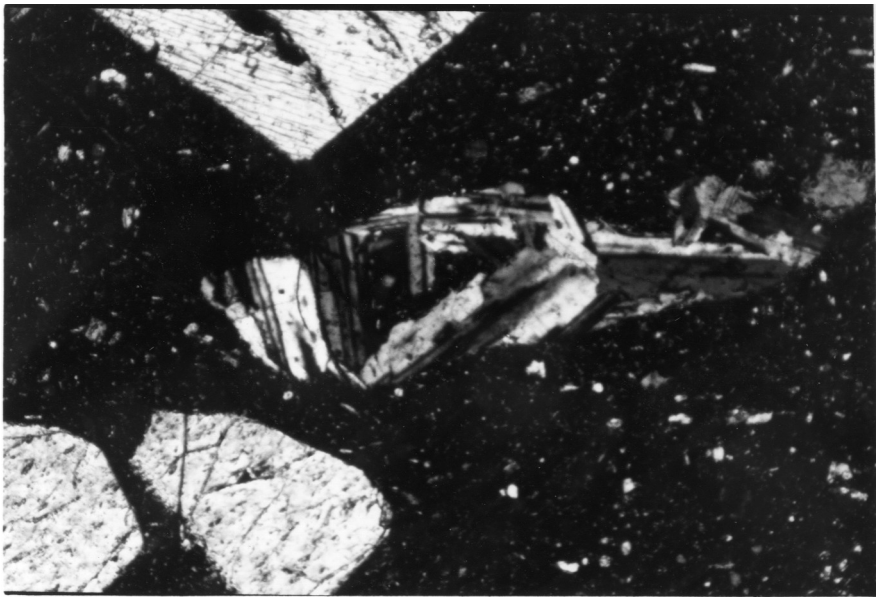

B

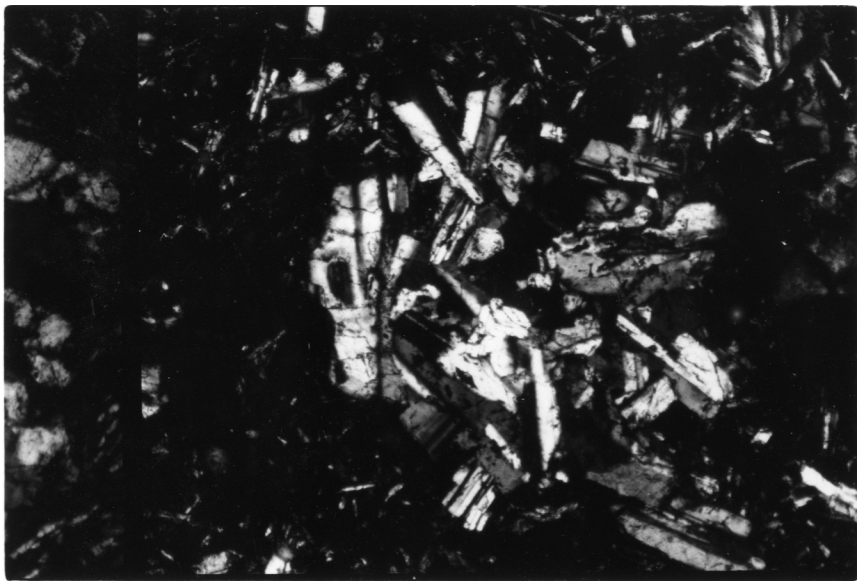

C

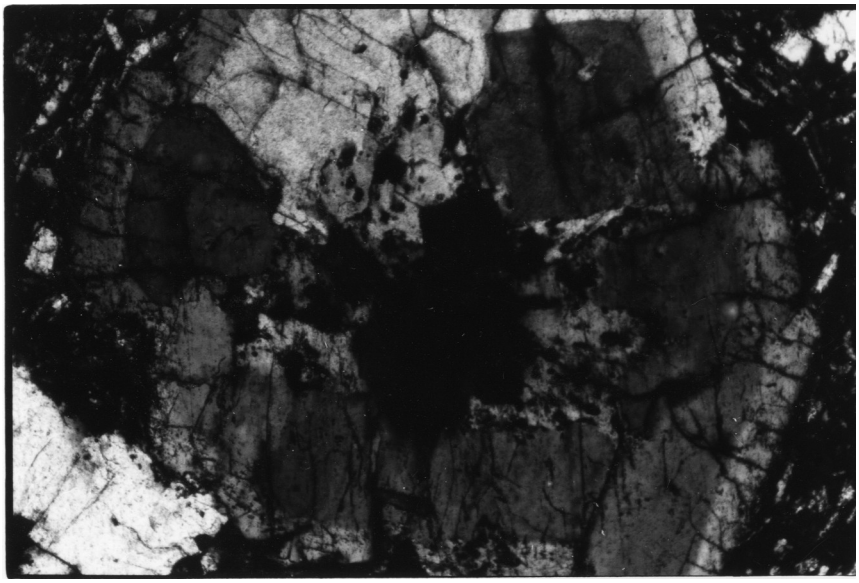

D

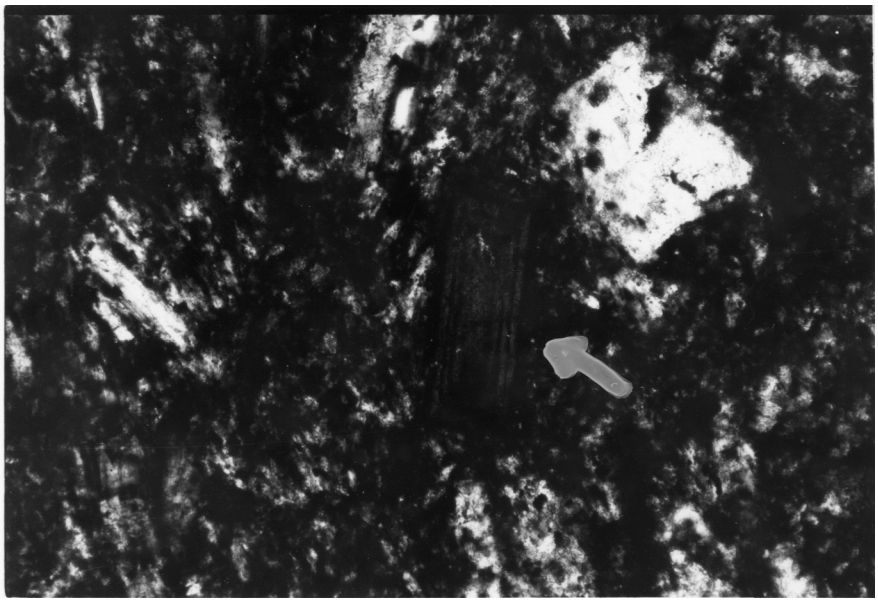

E

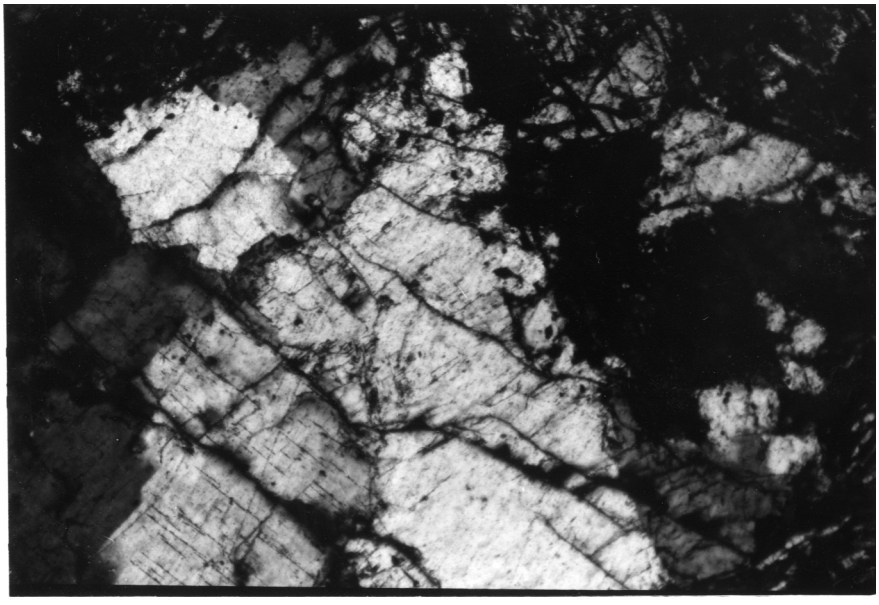

F

APPENDIX II

WHOLE ROCK MAJOR OXIDE CHEMISTRY

AND

NORMATIVE MINERALOGY

	Ankaramite								
	SJ14B	SJ15A	SJ20B	NC20	NC15	NC27L	NC19	NC15*	7^T
SiO_2	46.40	47.40	47.20	46.30	46.80	46.70	46.84	46.81	46.73
TiO_2	2.07	2.18	2.35	2.21	1.96	1.99	2.21	1.87	1.90
Al_2O_3	10.30	11.00	12.00	10.10	8.02	10.70	6.54	8.02	9.30
Fe_2O_3	2.66	2.19	2.18	3.18	3.68	4.29	4.76	4.42	3.25
FeO	6.87	7.13	7.89	6.98	5.76	5.05	7.37	5.51	5.37
MnO	0.19	0.19	0.14	0.14	0.14	0.18	0.18	0.17	0.29
MgO	13.89	12.39	10.99	15.54	14.39	12.95	14.09	15.18	14.93
CaO	15.42	14.19	13.43	13.44	13.60	13.85	14.59	14.48	14.50
Na_2O	1.27	2.24	1.95	1.54	1.47	1.63	1.48	1.41	1.32
K_2O	1.02	1.24	1.55	1.22	1.05	1.16	1.21	1.21	1.14
P_2O_5	0.28	0.35	0.36	0.34	0.31	0.30	0.29	0.29	0.25
H_2O^+							0.38	0.45	0.50
H_2O^-							0.03	0.08	0.45
	100.37	100.50	100.04	100.99	97.18	98.80	99.97	99.90	99.93
Q	0	0	0	0	0	0	0	0	0
Or	6.03	7.33	9.16	7.21	6.21	6.86	7.15	6.21	6.74
Ab	3.76	7.47	9.58	6.17	11.12	11.12	8.17	11.12	6.82
An	19.30	16.30	19.59	16.95	17.00	18.68	7.63	17.00	16.08
Ne	3.88	6.22	3.57	3.81	0.76	1.22	2.36	0.76	2.36
Di	43.96	41.30	35.79	37.59	38.20	37.84	49.79	38.20	42.73
Wo	0	0	0	0	0	0	0	0	0
Hy	0	0	0	0	0	0	0	0	0
Ol	14.96	13.75	13.80	19.53	15.94	12.76	12.70	15.94	15.36
Mt	3.80	3.18	3.13	4.48	5.36	7.05	6.90	5.36	4.71
Il	3.93	4.14	4.46	4.20	3.72	3.78	4.20	3.72	3.61
Hm	0	0	0	0	0	0	0	0	0
Tn	0	0	0	0	0	0	0	0	0
Pf	0	0	0	0	0	0	0	0	0
Ap	0.66	0.83	0.85	0.81	0.73	0.71	0.69	0.73	0.59
DI	13.66	21.02	22.31	17.19	18.09	19.19	17.68	18.09	15.91
I.B.*	ank	ank	ank	ank	ank	ank	ank	ank	ank

* Irvine and Baragars (1971) classification of rock types: ank=ankaramite, ab=alkali basalt, trb=trachybasalt, tri=tristanite, tr=trachyte.

Alkali Olivine Basalts - Sor Jan

	C9	SJ1A	SJ13A	SJ5A	SJ6	SJ9B	3^T	5^T	5^C
SiO_2	46.59	47.30	46.50	46.30	45.60	45.20	46.04	46.30	46.25
TiO_2	1.92	1.70	1.31	1.25	1.25	1.32	3.96	3.85	3.75
Al_2O_3	10.26	16.30	12.40	12.50	12.40	13.00	16.39	16.25	16.07
Fe_2O_3	10.07	4.59	3.69	6.75	7.44	7.20	4.01	1.94	1.88
FeO		6.92	7.03	4.23	3.62	4.05	7.89	8.54	10.08
MnO	0.17	0.19	0.18	0.21	0.15	0.17	0.30	0.43	0.19
MgO	13.51	5.29	10.86	11.11	10.71	9.27	5.29	5.67	5.37
CaO	14.01	9.26	11.96	11.92	11.81	11.85	9.75	10.45	9.33
Na_2O	1.65	3.32	1.75	2.17	2.20	2.17	3.18	3.18	3.45
K_2O	1.09	1.99	1.53	1.28	1.18	1.12	1.97	2.40	1.97
P_2O_5		0.80	0.47	0.50	0.48	0.54	0.83	0.55	1.17
H_2O^+	0						0.36	0.10	0.18
H_2O^-	0.09						0.17	0.09	0.02
	99.34	97.66	97.68	98.22	96.84	95.89	100.14	99.75	99.71
Q	0	0	0	0	0	0	0	0	0
Or	6.44	11.76	9.04	7.56	6.97	6.62	11.64	14.18	11.64
Ab	13.96	25.99	14.26	18.45	18.16	19.12	23.20	14.55	22.98
An	17.37	23.29	20.83	20.54	19.44	22.02	24.63	22.98	22.55
Ne	0	1.55	0.94	0	1.30	0	2.01	6.69	3.37
Di	35.90	14.11	28.33	27.55	28.03	25.88	14.74	20.57	13.24
Wo	0	0	0	0	0	0	0	0	0
Hy	0	0	0	0.03	0	1.93	0	0	0
Ol	11.92	9.41	15.58	10.77	9.59	6.42	8.13	9.19	13.18
Mt	9.06	6.80	5.45	9.73	10.43	10.20	5.81	2.81	2.73
Il	0.36	3.23	2.49	2.37	2.37	2.51	7.52	7.31	7.12
Hm	0	0	0	0	1.46	0.40	0	0	0
Tn	1.00	0	0	0	0	0	0	0	0
Pf	2.31	0	0	0	0	0	0	0	0
Ap	0	1.89	1.11	1.18	1.14	1.28	1.97	1.30	2.77
DI	20.40	39.30	24.24	26.01	26.44	25.74	36.85	35.43	37.99
I.B.	ank	ab	ank	ank	ank	ank	ab	ab	ab

Alkali Olivine Basalts - Nord Jan

	NC12C	NC12C*	NC17	NC17*	NJ17	NJ17*	NC27K	NC27K*	JB202
SiO_2	47.20	46.59	46.10	46.53	46.20	46.42	46.12	47.05	46.20
TiO_2	2.56	2.41	1.38	2.56	1.62	2.41	2.17	1.88	3.05
Al_2O_3	14.10	14.41	14.30	13.77	16.10	16.04	10.00	13.38	17.10
Fe_2O_3	5.44	4.93	4.64	4.77	4.77	5.32	2.60	3.68	8.79
FeO	5.50	6.61	6.72	7.33	6.99	8.77	8.76	7.18	2.40
MnO	0.12	0.21	0.23	0.22	0.21	0.23	0.16	0.18	0.14
MgO	8.64	8.22	8.21	8.01	4.96	4.86	12.30	9.18	4.54
CaO	12.06	11.43	11.08	10.96	10.63	10.17	13.70	13.69	10.44
Na_2O	2.47	2.47	2.64	2.47	2.83	2.08	1.85	1.62	2.86
K_2O	1.69	1.76	2.37	2.46	2.45	2.46	1.10	1.12	2.43
P_2O_5	0.47	0.43	0.63	0.46	0.67	0.58	0.70	0.28	0.53
H_2O^+		0.42		0.36		0.58	0.57	0.52	
H_2O^-		0.07		0.13		0.17	0.05	0.22	
	100.25	99.96	98.30	100.03	97.43	100.03	100.08	99.98	99.48
Q	0	0	0	0	0	0	0	0	0
Or	9.99	10.40	14.01	14.54	14.48	14.54	6.67	6.62	14.36
Ab	17.19	17.39	11.35	13.83	16.93	17.60	9.43	13.71	20.72
An	21.45	23.04	18.78	19.22	23.86	27.17	15.57	25.93	26.60
Ne	2.97	1.90	7.37	3.83	3.94	0	3.41	0	1.93
Di	27.78	24.52	25.68	25.67	19.90	15.93	38.73	32.16	16.73
Wo	0	0	0	0	0	0	0	0	0
Hy	0	0	0	0	0	5.08	0	2.15	0
Ol	7.59	9.50	10.54	9.60	6.99	5.40	16.18	9.12	2.49
Mt	8.82	7.15	6.61	6.92	7.18	7.71	3.94	5.34	8.39
Il	4.86	4.58	2.62	4.86	3.08	4.58	4.26	3.57	5.66
Hm	0	0	0	0	0	0	0	0	0
Tn	0	0	0	0	0	0	0	0	0
Pf	0	0	0	0	0	0	0	0	0.12
Ap	1.11	1.02	1.49	1.09	1.59	1.37	1.68	0.66	1.26
DI	30.15	26.69	32.73	32.20	35.35	32.14	19.51	20.33	37.01
I.B.	ank	ank	ab	ank	ab	ank	ank	ank	ab

	JB202*	NC22	NC23	NC34B	NC35B	NC30C	NC3	NC13	SJ48
SiO_2	46.36	49.60	49.30	46.10	47.80	49.50	46.78	46.49	48.71
TiO_2	2.11	2.78	2.13	3.20	3.19	2.78	2.82	2.20	2.90
Al_2O_3	14.95	15.90	14.20	16.50	16.60	16.10	16.77	15.21	18.61
Fe_2O_3	11.27	2.26	2.96	2.33	3.63	2.71	4.04	3.03	1.80
FeO	3.13	7.55	5.88	9.43	6.28	6.85	8.33	9.58	8.48
MnO	0.21	0.19	0.17	0.18	0.15	0.23	0.22	0.22	0.19
MgO	4.81	5.17	8.99	4.94	5.21	5.31	4.33	6.01	3.30
CaO	11.21	9.15	10.72	10.50	10.10	8.81	9.08	11.08	9.35
Na_2O	2.68	3.64	2.64	3.13	3.10	3.64	3.14	2.68	2.81
K_2O	2.66	3.01	2.27	2.49	2.74	3.01	3.02	2.54	3.09
P_2O_5	0.46	0.66	0.78	0.57	0.74	0.71	0.68	0.53	0.69
H_2O^+	0.15						0.36	0.36	0.13
H_2O^-	0						0.34	0.05	0.05
	100.00	99.91	100.04	99.37	99.54	99.65	99.91	99.98	100.11
Q	0	0	0	0	0	0	0	0	0
Or	15.72	17.79	13.41	14.72	16.19	17.79	17.85	15.01	18.35
Ab	17.67	21.86	20.96	13.01	20.37	23.04	18.63	11.63	21.48
An	20.91	18.65	19.83	22.90	23.24	18.12	22.75	21.97	28.91
Ne	2.72	4.34	1.11	8.03	3.22	4.80	4.30	5.98	1.14
Di	24.68	18.34	22.52	20.96	17.61	16.97	14.61	24.25	11.23
Wo	0	0	0	0	0	0	0	0	0
Hy	0	0	0	0	0	0	0	0	0
Ol	0.38	9.39	12.46	9.19	6.07	8.53	8.28	10.92	9.02
Mt	4.66	3.61	4.60	3.41	5.48	4.16	5.86	4.39	2.70
Il	4.01	5.28	4.05	6.08	6.06	5.28	5.36	4.18	5.47
Hm	8.06	0	0	0	0	0	0	0	0
Tn	0	0	0	0	0	0	0	0	0
Pf	0	0	0	0	0	0	0	0	0
Ap	1.09	1.56	1.85	1.35	1.75	1.68	1.61	1.26	1.68
DI	36.10	43.99	35.49	35.76	39.78	45.63	40.78	32.63	40.97
I.B.	ab	ab	ab	ab	ab	ab	ab	ank	ab

	SJ53	JM5	JM6	JM7	JM3	4T	6T	C15	C10
SiO_2	45.93	47.40	46.80	47.90	47.50	46.15	45.08	48.27	46.40
TiO_2	3.18	3.32	3.28	3.12	3.29	3.05	2.93	3.76	3.00
Al_2O_3	15.60	16.20	15.90	15.30	15.90	17.44	14.15	16.70	15.90
Fe_2O_3	3.05	2.91	3.63	3.24	3.24	4.94	2.28	10.82	12.22
FeO	8.77	8.35	7.68	7.81	8.03	6.19	8.59		
MnO	0.20	0.20	0.20	0.20	0.20	0.33	0.22	0.18	0.20
MgO	5.20	5.48	5.55	6.12	5.27	5.40	7.01	5.75	4.57
CaO	11.15	9.53	9.67	10.06	9.79	11.05	10.20	9.36	9.39
Na_2O	3.48	3.37	3.34	3.11	3.18	2.37	3.99	2.77	3.33
K_2O	2.28	2.58	2.67	2.54	2.61	2.45	1.79	2.52	2.37
P_2O_5	0.59	0.49	0.52	0.48	0.50	0.37	0.62		
H_2O+	0.33	0.11	0.15	0.09	0.44	0.16	0.75	0	0
H_2O-	0.09					0.14	0.15	0.38	0.12
	99.85	99.94	99.39	99.97	99.95	100.04	97.76	100.51	97.50
Q	0	0	0	0	0	0	0	0	0
Or	13.34	15.39	16.02	15.14	15.66	14.48	10.58	14.89	14.01
Ab	12.05	19.92	18.65	20.26	20.76	15.96	13.89	23.44	28.18
An	20.29	21.68	20.85	20.48	21.75	29.71	15.41	25.69	21.44
Ne	9.17	6.38	7.09	4.75	4.95	2.22	10.76	0	0
Di	26.40	18.26	19.55	21.37	19.41	18.02	25.27	6.51	12.05
Wo	0	0	0	0	0	0	0	0	0
Hy	0	0	0	0	0	0	0	5.83	0
Ol	6.64	9.60	8.24	9.17	8.31	5.54	10.64	3.84	4.06
Mt	4.41	3.07	3.85	3.42	3.44	7.16	3.31	9.74	10.99
Il	6.08	4.67	4.64	4.39	4.66	5.79	5.56	0.39	0.43
Hm	0	0	0	0	0	0	0	0	0
Tn	0	0	0	0	0	0	0	8.73	0.90
Pf	0	0	0	0	0	0	0	0	4.22
Ap	1.34	1.03	1.10	1.01	1.06	0.88	1.47	0	0
DI	34.56	41.69	41.76	40.15	41.37	32.66	35.23	38.33	42.18
I.B.	ab	ab	ab	ab	ab	ank	ab	ab	ab

					Trachyandesite				
	C11	C12	1^s	2^s	NC22	3^c	2^H	2^T	C13
SiO_2	48.03	44.07	48.40	45.79	49.39	56.71	54.83	54.45	52.10
TiO_2	2.88	3.54	3.20	3.19	2.72	1.80	1.96	1.78	1.92
Al_2O_3	15.84	16.65	17.10	16.21	14.13	17.06	17.58	17.77	17.50
Fe_2O_3	10.68	12.33	4.33	2.22	3.17	3.55	3.22	2.05	9.17
FeO			7.89	8.59	8.07	3.68	4.32	5.46	
MnO	0.17	0.19	0.23	0.23	0.22	0.17	0.23	0.44	0.23
MgO	5.51	5.67	4.99	5.89	5.43	2.57	2.43	2.57	3.01
CaO	9.92	11.44	9.10	10.57	9.26	4.67	5.84	5.35	6.31
Na_2O	3.03	2.63	3.07	3.66	3.48	4.94	5.29	4.65	4.25
K_2O	2.72	2.17	2.69	2.68	3.18	3.43	3.21	3.25	3.10
P_2O_5				0.26	0.56	0.43	0.69	0.61	
H_2O+	0.25	0.39		0.38	0.25	0.70	0.25	0.50	0
H_2O-	0.12	0.07			0.05	0.04	0.02	0.59	0.17
	99.15	99.15	101.00	99.67	99.91	99.75	99.87	99.47	97.76
Q	0	0	0	0	0	3.01	0	0	0.05
Or	16.07	12.82	15.90	15.84	18.79	20.27	18.97	19.21	18.32
Ab	25.64	19.34	21.24	7.39	20.54	41.80	44.51	39.35	35.96
An	21.59	27.22	24.94	19.89	13.54	14.25	14.74	18.02	19.52
Ne	0	1.58	2.57	12.77	4.82	0	0.14	0	0
Di	14.22	13.98	16.35	25.14	23.39	4.84	7.83	3.75	4.67
Wo	0	0	0	0	0	0	0	0	0
Hy	0	0	0	0	0	5.28	0	9.01	5.33
Ol	5.00	5.36	7.65	8.38	7.46	0	3.43	1.29	0
Mt	9.61	11.09	6.28	3.22	4.60	5.15	4.67	2.97	8.25
Il	0.36	0.41	6.08	6.06	5.17	3.42	3.72	3.38	0.49
Hm	0	0	0	0	0	0	0	0	0
Tn	2.10	0	0	0	0	0	0	0	4.08
Pf	3.21	5.38	0	0	0	0	0	0	0
Ap	0	0	0	0.62	1.33	1.02	1.63	1.44	0
DI	41.71	33.74	39.70	36.00	44.16	65.08	63.62	58.55	54.33
I.B.	ab	ab	ab	ab	ab	trb	trb	trb	trb

		Latite Andesite		Trachyte		
	C14	SJ2B	JB1I	SJ25B	1^{c}	1^{T}
SiO_2	53.07	62.20	59.30	65.70	64.88	65.85
TiO_2	2.13	0.80	1.18	0.43	0.60	0.25
Al_2O_3	17.70	17.60	17.80	16.80	16.10	16.10
Fe_2O_3	9.64	1.80	3.91	2.60	3.35	3.17
FeO		2.24	1.01	0.72	0.70	0.42
MnO	0.23	0.19	0.22	0.23	0.18	0.20
MgO	3.01	0.95	0.95	0.41	0.32	0.98
CaO	6.31	2.76	2.84	1.09	1.23	2.05
Na_2O	4.21	5.84	5.20	5.71	5.61	5.58
K_2O	3.13	5.60	6.01	6.04	5.33	5.20
P_2O_5		0.31	0.43	0.14	0.05	0.04
H_2O^+	0				1.13	0.27
H_2O^-	0.24				0.06	0.06
	99.67	100.29	98.85	99.87	99.54	100.17
Q	1.00	1.39	0.63	8.10	9.47	9.13
Or	18.50	33.09	35.52	35.69	31.50	30.73
Ab	35.62	48.57	43.92	46.88	47.47	47.22
An	20.16	5.72	7.52	3.13	3.01	3.53
Ne	0	0	0	0	0	0
Di	3.61	4.88	2.92	1.06	1.72	4.97
Wo	0	0	0	0	0.23	0
Hy	5.82	1.77	1.01	0.53	0	0.14
Ol	0	0	0	0	0	0
Mt	8.77	2.75	1.39	1.70	1.10	1.28
Il	0.49	1.52	2.24	0.82	1.14	0.47
Hm	0	0	3.94	1.28	2.59	2.29
Tn	4.59	0	0	0	0	0
Pf	0	0	0	0	0	0
Ap	0	0.73	1.02	0.33	0.12	0.09
DI	55.12	83.05	80.06	90.67	88.44	87.07
I.B.	trb	tri	tri	tr	tr	tr

APPENDIX III

WHOLE ROCK TRACE ELEMENT CHEMISTRY

(in ppm)

Ankaramite

	Cr	Ni	Rb	Sr	Ba	Rb/Sr	87/86
SJ14B		262	21.8	446		0.049	
SJ15A		186	26.3	494		0.053	
SJ20B		190	32.5	533		0.061	
NC20		266	27.3	442		0.062	.7035
NC15		309	27.3	436		0.063	
NC27L		236	23.3	444		0.052	
NC19	1300				896		
NC15	1711				537		
C9			27.5	452		0.061	.7039 & .7039

Alkali Olivine Basalt - Sor Jan

	Cr	Ni	Rb	Sr	Ba	Rb/Sr	87/86
SJ1A		17.5	36.7	981		0.037	.7036
SJ13A		199	26.0	654		0.039	
SJ5A		152	20.7	653		0.032	.7041
SJ6		160	21.0	714		0.029	
SJ9B		199	10.6	656		0.016	

Alkali Olivine Basalt - Nord Jan

	Cr	Ni	Rb	Sr	Ba	Rb/Sr	87/86
NC12C		104	47.1	701		0.067	.7036
NC12C*	342				537		
NC17		121	51.3	713		0.072	.7036
NC17*	410				537		
NJ17		34.8	53.2	774		0.069	
NJ17*	0				537		
NC27K	479						
NC27K*	547				537		
JB202		34.5	54.8	771		0.071	
NC22		50.4	69.2	738		0.094	.7036
NC23		156	49.9	663		0.075	
NC34B		37.7	54.8	750		0.073	
NC35B		38.2	58.3	899		0.065	
NC30C		55.2	73.8	842		0.088	
NC3	0				1075		
NC13	274				1433		
SJ48	547				1702		
SJ53	137				1164		
6T	684			423	537		
C15			56.7	803		0.071	.7035
C10			54.1	826		0.065	.7037 & .7036
C11			58.8	849		0.069	.7037 & .7036
C12			50.7	762		0.071	.7038 & .7038

Trachyandesite	Cr	Ni	Rb	Sr	Ba	Rb/Sr	87/86
NC22	479				1433		
C13			75.3	1026		0.073	.7035
C14			75.5	1026		0.074	.7035

Latite Andesite	Cr	Ni	Rb	Sr	Ba	Rb/Sr	87/86
SJ2B		7.0	88.0	876		0.100	.7038
JB1I		9.6	109	847		0.129	

Trachyte	Cr	Ni	Rb	Sr	Ba	Rb/Sr	87/86
SJ25B		9.4	106	106		1.000	.7035

APPENDIX IV

MINERAL CHEMISTRY

(THIS STUDY)

OLIVINE ANALYSES

	1ASJ15A	1BSJ15A	2SJ15A	1SJ20B	2ASJ20B	2BSJ20B	2CSJ20B	2DSJ20B	3SJ20B
SiO_2	39.49	39.50	38.95	38.59	39.39	38.23	38.28	38.61	38.75
Al_2O_3	0	0	0	0	0	0	0	0	0
FeO*	16.11	15.69	15.43	15.10	16.40	20.31	20.18	20.78	19.70
MnO	.25	.25	.27	.21	.27	.33	.34	.36	.33
MgO	44.86	45.53	45.44	44.88	43.16	40.14	40.19	41.35	40.54
CaO	.31	.32	.35	.37	.32	.24	.24	.25	.26
NiO	.13	.14	.18	.17	.17	.17	.19	.12	.14
Cr_2O_3	.04	.02	.04	.02	.02	0	.02	.01	.03
	101.19	101.45	100.64	99.34	99.74	99.43	99.44	101.46	99.76
	Number of ions in the formula on the basis of 4 oxygens								
Si	.986	.982	.977	.980	1.000	.993	.993	.983	.999
Al	0	0	0	0	0	0	0	0	0
Fe*	.336	.326	.323	.320	.348	.440	.438	.442	.424
Mn	.005	.005	.005	.003	.005	.007	.007	.007	.006
Mg	1.669	1.688	1.701	1.699	1.633	1.555	1.556	1.571	1.559
Ca	.008	.008	.009	.009	.008	.006	.006	.006	.006
Ni	.002	.002	.003	.003	.003	.003	.003	.002	.002
Cr	0	0	0	0	0	0	0	0	0
	3.006	3.012	3.018	3.015	2.996	3.003	3.003	3.012	2.996
Fo	83.24	83.81	84.04	84.15	82.43	77.94	78.03	78.04	78.62
F/F+M	.168	.162	.160	.159	.176	.221	.220	.220	.214
	x	x	x	x	x	x	x	x	x

	1NC20	2NC20	11NC20	2NC15	3NC15	1ANC15	1BNC15	1ASJ13A	1BSJ13A
SiO_2	40.48	40.11	40.51	40.47	40.46	39.93	39.78	40.34	40.19
Al_2O_3	0	0	0	0	0	0	0	0	0
FeO*	10.95	11.76	11.00	10.93	11.32	13.14	13.62	11.71	11.71
MnO	.18	.23	.16	.16	.22	.23	.23	.19	.15
MgO	49.09	48.16	49.30	49.20	48.15	46.76	46.27	47.70	47.38
CaO	.35	.40	.33	.43	.40	.42	.38	.30	.31
NiO	.20	.20	.24	.20	.20	.14	.20	.21	.23
Cr_2O_3	.03	.04	.02	.04	.01	0	0	.01	.02
	101.28	100.89	101.56	101.42	100.77	100.62	100.47	100.44	100.00

Number of ions in the formula on the basis of 4 oxygens

Si	.986	.986	.985	.985	.993	.990	.989	.994	.995
Al	0	0	0	0	0	0	0	0	0
Fe*	.223	.241	.223	.222	.231	.272	.283	.241	.242
Mn	.003	.004	.002	.002	.004	.004	.004	.003	.002
Mg	1.784	1.765	1.789	1.786	1.761	1.729	1.716	1.753	1.749
Ca	.008	.010	.008	.010	.010	.011	.009	.007	.008
Ni	.003	.003	.004	.003	.003	.002	.003	.003	.004
Cr	0	0	0	0	0	0	0	0	0
	3.009	3.009	3.012	3.009	3.002	3.007	3.005	3.001	3.000
Fo	88.91	87.99	88.93	88.96	88.40	86.41	85.84	87.91	87.85
F/F+M	.111	.120	.111	.111	.116	.136	.142	.121	.122
	x	x	x	x	x	x	x	x	x

	2SJ13A	3SJ13A	1SJ6	2SJ6	1ANC17	1BNC17	1NC22	1ANC23	1BNC23
SiO_2	40.17	39.85	39.47	39.36	39.50	40.08	39.63	40.51	40.48
Al_2O_3	0	0	0	0	0	0	0	0	0
FeO*	11.18	13.20	14.61	15.29	12.23	12.12	10.14	11.09	11.39
MnO	.15	.22	.23	.25	.18	.19	.16	.16	.18
MgO	47.88	44.30	44.92	44.06	48.59	47.43	48.39	48.57	48.64
CaO	.31	.30	.26	.25	.41	.39	.34	.34	.34
NiO	.26	.27	.15	.17	.20	.19	.25	.21	.20
Cr_2O_3	.04	.04	.02	.04	0	.02	.04	.07	.08
	100.00	98.67	99.66	99.42	101.13	100.42	98.96	100.95	101.31

Number of ions in the formula on the basis of 4 oxygens

Si	.993	1.007	.994	.996	.972	.991	.986	.991	.988
Al	0	0	0	0	0	0	0	0	0
Fe*	.230	.279	.307	.323	.251	.250	.210	.227	.232
Mn	.002	.004	.004	.005	.003	.003	.002	.002	.003
Mg	1.764	1.688	1.687	1.663	1.783	1.748	1.797	1.772	1.770
Ca	.008	.007	.006	.006	.011	.010	.008	.008	.008
Ni	.005	.005	.003	.003	.003	.003	.004	.003	.003
Cr	0	0	0	0	0	0	0	0	.001
	3.002	2.991	3.002	2.997	3.024	3.005	3.009	3.004	3.006
Fo	88.47	85.82	84.60	83.74	87.66	87.49	89.54	88.66	88.43
F/F+M	.115	.142	.154	.163	.123	.125	.105	.114	.116
	x	x	x	x	x	x	x	x	x

	1NC12C	1NC34B	2NC34B	3NC34B	4NC34B	1JB202	2NC17
SiO_2	39.49	38.25	38.05	37.90	38.38	37.90	37.24
Al_2O_3	0	0	0	0	0	0	0
FeO*	14.08	22.07	22.42	22.41	22.09	25.61	34.66
MnO	.20	.35	.35	.38	.40	.39	.86
MgO	45.65	39.37	38.39	38.36	39.41	36.48	26.74
CaO	.26	.34	.37	.36	.32	.30	.50
NiO	.13	.13	.17	.14	.18	.16	.12
Cr_2O_3	.04	.01	0	.02	.01	.02	.05
	99.86	100.52	99.76	99.56	100.80	100.87	100.24

Number of ions in the formula on the basis of 4 oxygens

Si	.990	.990	.994	.993	.991	.994	1.027
Al	0	0	0	0	0	0	0
Fe*	.295	.477	.490	.491	.476	.562	.799
Mn	.003	.007	.007	.007	.008	.008	.019
Mg	1.706	1.520	1.497	1.500	1.517	1.427	1.100
Ca	.006	.009	.010	.009	.008	.007	.014
Ni	.002	.002	.003	.002	.003	.003	.002
Cr	0	0	0	0	0	0	0
	3.003	3.005	3.001	3.001	3.004	3.001	2.963
Fo	85.26	76.11	75.34	75.34	76.12	71.74	57.93
F/F+M	.147	.239	.247	.247	.239	.283	.410
	x	p	p	p	p	p	g

CLINOPYROXENE ANALYSES

	10BSJ15A	10CSJ15A	10DSJ15A	12BSJ15A	8BNC20	8ANC15
SiO_2	52.23	52.07	51.92	52.69	52.58	53.34
TiO_2	.87	.96	.89	.72	.55	.79
Al_2O_3	2.40	2.91	2.60	1.80	2.04	1.91
FeO*	4.53	4.71	4.61	4.09	3.55	4.58
MnO	.13	.12	.11	.11	.12	.15
MgO	16.62	16.46	16.38	17.21	17.46	18.09
CaO	22.69	22.43	22.58	22.59	22.14	21.59
Na_2O	.27	.31	.27	.25	.28	.18
Cr_2O_3	.28	.35	.22	.23	.60	.10
	100.03	100.33	99.57	99.69	99.32	100.73
	Number of ions in the formula on the basis of 6 oxygens					
Si	1.916	1.903	1.912	1.934	1.930	1.934
Ti	.023	.025	.023	.019	.015	.021
Al	.103	.125	.112	.077	.087	.081
Fe*	.139	.144	.142	.125	.108	.138
Mn	.003	.003	.003	.003	.003	.004
Mg	.908	.897	.899	.941	.955	.977
Ca	.891	.878	.891	.888	.870	.838
Na	.019	.021	.018	.017	.019	.013
Cr	.007	.009	.005	.006	.017	.002
	4.009	4.006	4.006	4.010	4.004	4.007
Ca	47.00	46.68	47.03	46.40	45.79	43.56
Mg	47.88	47.64	47.45	49.16	50.23	50.76
Fe	5.11	5.68	5.53	4.44	3.98	5.68
Ti	17.84	17.58	17.96	17.87	13.83	20.24
NaM2	14.28	14.64	14.05	16.00	18.15	11.89
Al4	67.88	67.78	67.99	66.13	68.03	67.87
Other	9.10	10.15	9.30	7.33	7.93	7.20
F/F+M	.132	.138	.136	.117	.101	.123
	CrDi	CrDi	CrDi	CrDi	CrDi	CrDi

	8BNC15	8CNC15	8DNC15	9BNC15	10ANC15	10BNC15
SiO_2	53.21	53.00	53.74	52.12	50.69	52.37
TiO_2	.55	.55	.45	.53	1.18	.78
Al_2O_3	1.77	1.95	1.31	3.25	3.81	2.15
FeO*	3.10	3.28	3.09	3.34	4.53	4.20
MnO	.09	.09	.05	.12	.10	.08
MgO	17.80	17.60	17.96	17.29	15.95	16.86
CaO	22.20	22.54	22.30	22.11	22.32	22.60
Na_2O	.25	.25	.29	.30	.23	.24
Cr_2O_3	.80	.73	.73	.70	.52	.16
	99.77	100.00	99.93	99.74	99.32	99.43

Number of ions in the formula on the basis of 6 oxygens

Si	1.939	1.932	1.954	1.903	1.873	1.927
Ti	.015	.015	.012	.014	.032	.021
Al	.076	.083	.055	.139	.166	.093
Fe*	.094	.099	.094	.102	.140	.128
Mn	.002	.002	.001	.003	.002	.002
Mg	.967	.957	.973	.941	.878	.924
Ca	.866	.879	.869	.865	.883	.891
Na	.017	.017	.019	.020	.016	.017
Cr	.022	.020	.020	.019	.015	.004
	3.998	4.004	3.997	4.005	4.005	4.006
Ca	45.24	46.12	45.16	46.22	47.26	46.61
Mg	50.45	50.09	50.59	50.27	46.98	48.36
Fe	4.30	3.79	4.25	3.50	5.76	5.03
Ti	15.95	14.33	15.49	10.55	18.16	18.42
NaM2	18.69	16.80	25.73	15.39	9.13	14.61
Al4	65.37	68.87	58.79	74.06	72.71	66.97
Other	6.44	7.49	5.48	10.86	13.10	7.83
F/F+M	.088	.093	.088	.097	.137	.121
	CrDi	CrDi	CrDi	CrDi	CrDi	CrDi

	11NC15	1BNC27L	1CNC27L	2BNC27L	3NC27L	4NC27L
SiO_2	50.86	50.83	51.64	52.00	50.55	50.03
TiO_2	1.11	1.11	.83	.48	.78	.86
Al_2O_3	3.45	3.68	2.73	3.33	5.13	5.43
FeO*	4.91	4.84	4.09	3.48	3.93	4.13
MnO	.12	.12	.09	.12	.09	.13
MgO	15.93	15.57	16.43	17.19	15.63	15.73
CaO	22.46	22.72	22.68	21.93	21.96	21.86
Na_2O	.27	.23	.26	.24	.27	.27
Cr_2O_3	.90	.77	.81	.29	.48	.42
	100.02	99.87	99.57	99.04	98.83	98.85
	Number of ions in the formula on the basis of 6 oxygens					
Si	1.873	1.874	1.901	1.910	1.868	1.850
Ti	.030	.030	.022	.013	.021	.023
Al	.149	.159	.118	.143	.223	.235
Fe*	.151	.148	.125	.106	.121	.126
Mn	.003	.003	.002	.003	.002	.003
Mg	.875	.856	.902	.940	.861	.867
Ca	.886	.897	.895	.862	.870	.866
Na	.019	.016	.018	.017	.019	.019
Cr	.026	.021	.022	.007	.013	.012
	4.011	4.004	4.005	4.001	3.998	4.001
Ca	47.61	48.04	47.48	45.78	47.05	47.30
Mg	46.97	45.79	47.84	49.91	46.57	47.34
Fe	5.42	6.16	4.67	4.31	6.38	5.36
Ti	16.68	17.29	15.83	10.68	12.49	12.15
NaM2	10.46	9.24	12.78	13.76	11.15	9.84
Al4	72.86	73.48	71.39	75.56	76.37	78.01
Other	13.38	13.05	10.34	9.75	13.25	15.33
F/F+M	.147	.147	.121	.101	.123	.126
	CrDi	CrDi	CrDi	CrDi	CrDi	CrDi

	5NC27L	8SJ13A	10BSJ6	10CSJ6	10DSJ6	5BNC22
SiO_2	50.39	51.96	53.81	53.35	51.38	54.32
TiO_2	.79	.46	.41	.47	.55	.54
Al_2O_3	4.54	3.29	1.82	2.18	4.50	1.46
FeO*	4.15	3.50	3.57	3.88	3.73	3.58
MnO	.09	.13	.11	.11	.09	.08
MgO	15.96	17.13	18.16	17.98	16.59	18.04
CaO	22.13	20.20	21.15	21.39	20.64	22.56
Na_2O	.27	.41	.29	.36	.50	.23
Cr_2O_3	.59	1.15	.94	1.00	.52	.15
	98.92	98.23	100.25	100.71	98.50	100.96

Number of ions in the formula on the basis of 6 oxygens

Si	1.866	1.918	1.949	1.929	1.895	1.957
Ti	.021	.012	.010	.013	.015	.014
Al	.198	.143	.076	.092	.195	.061
Fe*	.128	.107	.107	.117	.114	.106
Mn	.002	.003	.003	.003	.002	.002
Mg	.880	.942	.980	.969	.911	.968
Ca	.878	.798	.820	.829	.815	.870
Na	.020	.029	.019	.024	.034	.015
Cr	.017	.033	.026	.027	.014	.004
	4.010	3.984	3.991	4.002	3.995	3.996
Ca	47.56	43.20	42.99	43.89	44.43	44.96
Mg	47.70	50.96	51.34	51.32	49.67	50.00
Fe	4.74	5.84	5.66	4.79	5.90	5.04
Ti	12.09	10.44	13.53	11.37	9.71	19.36
NaM2	10.66	23.98	24.67	22.45	22.75	21.26
Al4	77.25	65.58	61.81	66.18	67.54	59.39
Other	14.01	10.93	6.48	8.67	12.66	4.63
F/F+M	.127	.102	.098	.107	.111	.098
	CrDi	CrDi	CrDi	CrDi	CrDi	CrDi

	1ASJ14B	1BSJ14B	11ASJ15A	11BSJ15A	11CSJ15A	11DSJ15A
SiO_2	46.49	47.52	50.94	49.40	49.04	49.32
TiO_2	2.20	2.16	1.54	1.74	1.85	1.63
Al_2O_3	7.72	6.61	3.03	5.77	5.55	5.09
FeO*	7.14	7.11	6.18	6.38	6.51	6.39
MnO	.12	.14	.13	.13	.13	.19
MgO	13.43	13.71	14.79	14.38	13.96	14.73
CaO	21.16	21.71	21.83	22.16	21.95	22.38
Na_2O	.42	.42	.27	.37	.37	.30
Cr_2O_3	.20	.17	.11	.15	.18	.16
	98.87	99.55	98.80	100.49	99.58	100.18

Number of ions in the formula on the basis of 6 oxygens

Si	1.750	1.777	1.901	1.820	1.826	1.826
Ti	.062	.060	.042	.047	.051	.044
Al	.342	.291	.132	.250	.242	.222
Fe*	.224	.222	.192	.195	.202	.198
Mn	.003	.004	.003	.003	.003	.005
Mg	.753	.764	.822	.789	.773	.813
Ca	.853	.869	.873	.875	.874	.888
Na	.030	.029	.019	.026	.026	.021
Cr	.005	.004	.002	.004	.004	.004
	4.022	4.020	3.987	4.008	4.001	4.020
Ca	48.85	49.08	46.23	48.30	48.06	48.72
Mg	43.12	43.11	43.56	43.59	42.51	44.60
Fe	8.03	7.81	10.21	8.11	9.42	6.68
Ti	17.47	18.58	26.97	18.40	20.16	17.94
NaM2	8.60	9.32	12.19	10.09	10.40	8.51
Al4	73.93	72.10	60.84	71.51	69.44	73.55
Other	26.17	23.42	9.76	18.66	17.79	18.50
F/F+M	.229	.225	.189	.198	.207	.195
	TiSal	TiSal	TiSal	TiSal	TiSal	TiSal

	11ESJ15A	8ASJ20B	8BSJ20B	8CSJ20B	9ASJ20B	9BSJ20B
SiO_2	50.68	46.97	50.07	47.97	49.43	47.20
TiO_2	1.63	2.36	1.35	2.11	1.57	2.21
Al_2O_3	2.97	7.11	4.47	6.51	4.07	6.16
FeO*	6.70	7.76	5.13	7.91	6.24	7.59
MnO	.20	.14	.11	.15	.16	.12
MgO	15.23	13.17	13.91	13.30	14.60	13.14
CaO	21.74	21.66	21.91	21.20	21.14	20.99
Na_2O	.27	.46	.31	.51	.45	.45
Cr_2O_3	.11	.02	1.03	.32	.36	.02
	99.53	99.66	98.29	99.98	98.03	97.89
	Number of ions in the formula on the basis of 6 oxygens					
Si	1.884	1.760	1.875	1.789	1.864	1.797
Ti	.044	.066	.037	.059	.044	.063
Al	.129	.313	.196	.286	.180	.276
Fe*	.208	.243	.160	.246	.196	.241
Mn	.005	.004	.003	.004	.004	.003
Mg	.844	.735	.777	.740	.821	.745
Ca	.866	.870	.879	.847	.854	.856
Na	.020	.033	.022	.036	.032	.032
Cr	.002	0	.029	.008	.010	0
	4.003	4.024	3.978	4.014	4.005	4.013
Ca	45.96	49.55	48.41	47.87	46.48	47.84
Mg	44.78	41.90	42.75	41.77	44.65	41.65
Fe	9.27	8.55	8.85	10.36	8.87	10.51
Ti	24.71	18.81	20.54	18.71	20.40	20.51
NaM2	10.55	9.45	12.16	11.66	15.07	10.77
Al4	64.73	71.74	67.30	69.63	64.53	68.72
Other	11.92	25.19	14.13	21.93	14.05	21.10
F/F+M	.197	.248	.170	.249	.192	.244
	TiSal	TiSal	TiSal	TiSal	TiSal	TiSal

	10SJ20B	11SJ20B	7ANC20	7BNC20	7CNC20	7DNC20
SiO_2	49.07	50.51	49.11	51.13	47.21	46.65
TiO_2	1.56	1.36	1.82	1.26	2.34	2.25
Al_2O_3	5.53	3.84	4.27	3.25	6.78	6.75
FeO*	6.30	5.77	8.04	5.62	8.20	8.09
MnO	.12	.09	.19	.12	.14	.14
MgO	14.11	14.96	13.85	15.84	13.17	13.04
CaO	21.39	21.10	20.95	22.11	21.85	22.04
Na_2O	.37	.41	.30	.23	.44	.41
Cr_2O_3	.18	.25	.02	.48	0	.02
	98.64	98.29	98.55	100.03	100.14	99.39

Number of ions in the formula on the basis of 6 oxygens

Si	1.837	1.890	1.854	1.884	1.765	1.761
Ti	.044	.037	.051	.034	.065	.063
Al	.244	.169	.189	.141	.298	.300
Fe*	.196	.180	.253	.173	.255	.254
Mn	.003	.002	.005	.003	.004	.004
Mg	.788	.834	.779	.871	.734	.733
Ca	.858	.846	.847	.873	.875	.890
Na	.026	.029	.021	.015	.032	.030
Cr	.004	.006	0	.013	0	0
	4.001	3.994	4.000	4.006	4.029	4.035
Ca	47.06	45.46	45.67	46.38	49.66	50.64
Mg	43.17	44.83	41.99	46.21	41.63	41.67
Fe	9.77	9.70	12.34	7.41	8.71	7.69
Ti	18.65	21.49	23.27	20.25	18.88	18.08
NaM2	11.40	16.70	9.89	9.53	9.15	8.49
Al4	69.96	61.81	66.84	70.23	71.96	73.43
Other	16.46	11.01	14.83	12.08	24.88	25.68
F/F+M	.199	.177	.245	.165	.257	.257
	TiSal	TiSal	TiSal	TiSal	TiSal	TiSal

	7ENC20	12NC15	9ASJ13A	9BSJ13A	9CSJ13A	9DSJ13A
SiO_2	51.33	47.46	49.76	48.31	48.20	48.80
TiO_2	1.19	2.66	1.46	2.41	1.85	2.20
Al_2O_3	3.29	6.42	5.47	5.44	6.88	4.38
FeO*	4.83	7.37	5.85	7.46	8.89	6.99
MnO	.09	.16	.11	.15	.22	.16
MgO	15.54	13.33	14.75	13.27	13.39	13.65
CaO	22.24	22.29	21.64	22.05	19.97	21.29
Na_2O	.29	.34	.44	.38	.67	.38
Cr_2O_3	.87	0	.77	.08	0	.23
	99.66	100.04	100.25	99.38	100.07	98.07
	Number of ions in the formula on the basis of 6 oxygens					
Si	1.892	1.771	1.832	1.808	1.795	1.847
Ti	.032	.074	.040	.067	.051	.062
Al	.143	.281	.236	.240	.301	.194
Fe*	.148	.229	.179	.233	.276	.221
Mn	.002	.004	.003	.004	.006	.004
Mg	.854	.742	.809	.743	.743	.770
Ca	.878	.891	.854	.887	.796	.863
Na	.019	.024	.031	.026	.048	.027
Cr	.024	0	.021	.002	0	.006
	3.992	4.016	4.005	4.011	4.018	3.994
Ca	46.70	49.75	47.26	48.69	45.72	46.70
Mg	45.39	41.38	44.81	40.76	42.63	41.65
Fe	7.91	8.87	7.93	10.55	11.65	11.65
Ti	20.54	22.06	16.50	23.26	16.41	25.74
NaM2	12.91	7.27	12.82	9.46	15.32	11.46
Al4	66.55	70.67	70.67	67.28	68.27	62.80
Other	10.69	23.79	17.27	19.58	21.44	15.28
F/F+M	.147	.235	.181	.238	.270	.223
	TiSal	TiSal	TiSal	TiSal	TiSal	TiSal

	9ESJ13A	9FSJ13A	10SJ13A	11SJ13A	11SJ6	12SJ6
SiO_2	47.89	48.23	48.96	50.98	48.25	48.04
TiO_2	1.67	1.59	1.43	1.70	1.59	1.55
Al_2O_3	6.65	6.14	5.64	3.60	6.59	6.06
FeO*3	8.58	5.70	5.70	6.44	6.25	5.95
MnO	.23	.12	.12	.14	.14	.13
MgO	12.98	14.04	14.65	15.52	14.09	14.13
CaO	19.75	20.91	20.95	21.54	20.68	21.04
Na_2O	.61	.42	.45	.31	.48	.44
Cr_2O_3	0	.72	1.05	.24	.37	.77
	98.36	97.87	98.95	100.46	98.46	98.11

Number of ions in the formula on the basis of 6 oxygens

Si	1.813	1.818	1.826	1.874	1.810	1.810
Ti	.046	.044	.039	.046	.044	.043
Al	.296	.272	.247	.155	.291	.269
Fe*	.271	.179	.177	.197	.196	.187
Mn	.006	.003	.003	.004	.004	.003
Mg	.732	.788	.814	.850	.788	.794
Ca	.801	.844	.837	.848	.831	.849
Na	.044	.030	.032	.021	.035	.031
Cr	0	.021	.030	.006	.011	.022
	4.009	3.998	4.006	4.002	4.010	4.007
Ca	45.43	46.98	46.58	45.31	46.68	47.57
Mg	41.52	43.87	45.31	45.41	44.24	44.44
Fe	13.05	9.15	8.11	9.28	9.08	7.99
Ti	16.59	17.32	15.92	23.66	16.28	16.12
NaM2	15.62	11.80	12.91	11.12	12.67	11.80
Al4	67.79	70.88	71.17	65.22	71.06	72.07
Other	19.36	18.42	17.89	12.93	19.53	19.57
F/F+M	.270	.185	.178	.188	.199	.190
	TiSal	TiSal	TiSal	TiSal	TiSal	TiSal

	8ANC17	8BNC17	9NC17	8JB202	5NC12C	6NC12C
SiO_2	49.00	49.08	49.78	48.99	47.27	46.08
TiO_2	1.39	1.53	1.89	1.35	1.78	2.07
Al_2O_3	5.60	5.07	4.26	5.16	8.45	8.45
FeO*	5.81	5.91	7.26	7.14	6.36	6.42
MnO	.07	.10	.29	.17	.14	.15
MgO	14.26	14.09	14.14	13.94	13.21	13.09
CaO	21.85	22.50	22.11	20.75	20.99	20.78
Na_2O	.26	.37	.54	.38	.35	.40
Cr_2O_3	.22	.33	.01	.04	.21	.38
	98.46	98.99	100.27	97.91	98.75	97.82

Number of ions in the formula on the basis of 6 oxygens

Si	1.836	1.836	1.849	1.851	1.767	1.746
Ti	.038	.042	.052	.038	.049	.059
Al	.246	.223	.186	.229	.372	.376
Fe*	.181	.184	.224	.225	.198	.202
Mn	.002	.002	.008	.004	.004	.004
Mg	.796	.786	.782	.785	.736	.739
Ca	.876	.901	.879	.839	.840	.843
Na	.019	.026	.038	.026	.024	.029
Cr	.005	.008	0	.001	.005	.011
	4.000	4.008	4.019	4.000	3.995	4.009
Ca	47.80	49.49	48.49	45.95	47.72	48.45
Mg	43.39	43.11	43.13	42.93	41.77	42.45
Fe	8.81	7.40	8.39	11.12	10.51	9.10
Ti	17.41	17.84	20.69	17.65	16.20	16.88
NaM2	8.40	11.13	15.24	12.81	8.21	8.41
Al4	74.19	71.03	64.06	69.54	75.59	74.72
Other	16.66	17.07	16.24	15.10	23.34	26.02
F/F+M	.185	.189	.222	.222	.212	.214
	TiSal	TiSal	TiSal	TiSal	TiSal	TiSal

	10ASJ15A	12ASJ15A	8ANC20	9ANC15	1ANC27L	2ANC27L
SiO_2	47.86	46.52	46.99	47.98	49.36	49.47
TiO_2	2.54	3.07	2.82	1.94	1.69	1.55
Al_2O_3	5.82	6.60	6.35	6.85	4.04	5.32
FeO*	6.74	7.81	7.51	6.51	7.35	5.84
MnO	.16	.17	.13	.16	.14	.11
MgO	13.80	12.86	12.97	14.03	14.38	14.70
CaO	22.13	21.73	22.18	21.29	21.75	22.06
Na_2O	.32	.39	.33	.60	.39	.28
Cr_2O_3	.24	.11	.13	.09	.02	.10
	99.60	99.26	99.40	99.45	99.13	99.44
	Number of ions in the formula on the basis of 6 oxygens					
Si	1.788	1.755	1.767	1.786	1.853	1.836
Ti	.071	.086	.079	.053	.047	.042
Al	.255	.293	.281	.300	.178	.232
Fe*	.210	.246	.236	.202	.230	.181
Mn	.004	.004	.003	.004	.004	.003
Mg	.768	.723	.727	.779	.804	.813
Ca	.884	.878	.893	.849	.875	.876
Na	.023	.027	.023	.042	.028	.020
Cr	.006	.002	.003	.002	0	.002
	4.010	4.015	4.011	4.018	4.020	4.005
Ca	49.00	49.36	49.80	48.56	47.56	47.79
Mg	42.50	40.63	40.51	44.51	43.74	44.30
Fe	8.50	10.01	9.69	6.93	8.70	7.91
Ti	22.69	23.48	23.09	16.83	20.33	18.61
NaM2	7.37	7.69	6.97	13.42	12.10	8.67
Al4	69.93	68.83	69.94	69.75	67.57	72.73
Other	21.90	25.40	24.05	22.38	15.76	16.87
F/F+M	.210	.253	.245	.205	.222	.182
	TiAug-R	TiAug-R	TiAug-R	TiAug-R	TiAug-R	TiAug-R

	6NC27L	10ASJ6	5ANC22	13SJ15A	12SJ20B	13SJ20B
SiO_2	47.14	50.02	48.37	48.49	48.21	47.99
TiO_2	2.68	1.80	2.57	2.49	2.66	1.79
Al_2O_3	5.88	4.63	6.19	5.58	7.01	5.71
FeO*	7.61	6.96	8.48	7.40	7.89	6.36
MnO	.15	.12	.21	.14	.16	.11
MgO	13.23	15.00	13.18	13.49	13.13	13.89
CaO	21.93	21.08	21.48	21.95	21.32	21.37
Na_2O	.39	.29	.41	.38	.54	.29
Cr_2O_3	.03	.41	.07	.10	.16	.57
	99.03	100.32	100.96	100.02	101.09	98.08
	Number of ions in the formula on the basis of 6 oxygens					
Si	1.781	1.845	1.792	1.807	1.777	1.812
Ti	.075	.050	.070	.069	.073	.050
Al	.262	.201	.270	.245	.304	.253
Fe*	.240	.214	.262	.229	.242	.200
Mn	.004	.003	.006	.004	.004	.003
Mg	.745	.825	.727	.749	.722	.781
Ca	.887	.833	.852	.876	.842	.864
Na	.027	.021	.029	.026	.038	.021
Cr	0	.012	.001	.002	.004	.017
	4.022	4.002	4.009	4.006	4.005	4.000
Ca	49.45	45.04	47.42	48.22	47.61	47.59
Mg	41.50	44.58	40.47	41.22	40.78	43.02
Fe	9.05	10.38	12.11	10.55	11.61	9.39
Ti	22.60	21.88	22.61	23.52	21.66	19.33
NaM2	8.48	9.09	9.30	9.25	11.34	8.07
Al4	68.92	69.03	68.09	67.23	67.00	72.60
Other	23.07	15.74	21.48	19.89	22.75	19.06
F/F+M	.243	.206	.264	.234	.251	.203
	TiAug-R	TiAug-R	TiAug-R	TiAug-G	TiAug-G	TiAug-G

	9NC20	10NC20	13NC15	13SJ6	10NC17	11NC17
SiO_2	44.69	49.68	48.36	50.25	43.63	49.35
TiO_2	3.02	2.15	2.54	1.79	4.44	2.23
Al_2O_3	9.48	4.89	5.23	3.90	9.20	4.55
FeO*	7.48	7.95	9.52	7.55	9.48	8.88
MnO	.16	.16	.25	.19	.18	.19
MgO	12.39	14.28	13.63	15.39	10.96	14.20
CaO	21.57	21.33	21.10	20.58	21.53	21.04
Na_2O	.38	.30	.30	.30	.43	.36
Cr_2O_3	.16	.08	.01	.35	.02	0
	99.31	100.81	100.93	100.30	99.88	100.79

Number of ions in the formula on the basis of 6 oxygens

Si	1.683	1.833	1.800	1.857	1.654	1.831
Ti	.085	.059	.070	.048	.125	.062
Al	.420	.212	.228	.169	.410	.198
Fe*	.235	.245	.296	.233	.300	.274
Mn	.004	.004	.007	.005	.005	.005
Mg	.695	.785	.756	.848	.620	.785
Ca	.870	.842	.841	.814	.874	.835
Na	.027	.021	.021	.021	.031	.025
Cr	.004	.002	0	.009	0	0
	4.024	4.002	4.020	4.005	4.020	4.015
Ca	50.96	45.71	46.24	43.86	51.10	45.57
Mg	40.71	42.57	41.54	45.62	36.18	42.78
Fe	8.32	11.72	12.22	10.51	12.73	11.65
Ti	19.24	23.67	23.32	22.68	24.52	23.24
NaM2	6.24	8.51	7.10	9.80	6.12	9.67
Al4	74.51	67.82	69.58	67.52	69.36	67.09
Other	32.89	17.06	21.09	14.77	35.59	17.87
F/F+M	.252	.237	.281	.215	.326	.258
	TiAug-G	TiAug-G	TiAug-G	TiAug-G	TiAug-G	TiAug-G

	11NC34B	7JB202	12SJ25B	13SJ25B	14SJ25B
SiO_2	44.50	45.61	50.46	49.66	51.01
TiO_2	3.75	4.24	.38	.34	.35
Al_2O_3	7.55	6.87	2.30	4.10	.97
FeO*	8.96	10.45	14.38	13.27	16.08
MnO	.16	.23	2.45	2.30	2.72
MgO	11.36	10.96	10.45	10.71	9.83
CaO	20.61	20.55	19.04	18.66	18.92
Na_2O	,46	.52	.71	.70	.77
Cr_2O_3	.07	.03	0	0	0
	97.41	99.45	100.17	99.75	100.65

Number of ions in the formula on the basis of 6 oxygens

Si	1.720	1.737	1.936	1.901	1.966
Ti	.109	.121	.010	.009	.009
Al	.344	.307	.104	.184	.044
Fe*	.289	.332	.460	.424	.518
Mn	.004	.006	.079	.074	.088
Mg	.654	.623	.598	.611	.564
Ca	.853	.838	.782	.765	.780
Na	.034	.038	.053	.051	.056
Cr	.001	0	0	0	0
	4.008	4.001	4.021	4.020	4.026
Ca	48.64	47.26	44.43	44.18	43.82
Mg	37.29	35.06	33.92	35.27	31.67
Fe	14.07	17.67	21.65	20.55	24.51
Ti	25.37	28.48	7.81	5.67	9.08
NaM2	8.02	9.01	37.64	30.11	51.49
Al4	66.61	62.51	54.55	64.21	39.44
Other	28.53	26.61	11.77	15.21	9.09
F/F+M	.306	.347	.434	.409	.478
	TiAug-G	TiAug-G	Aeg-Aug	Aeg-Aug	Aeg-Aug

FELDSPAR ANALYSES

	4SJ20B	5SJ20B	3ANC17	3BNC17	4NC17	5NC17	2ANC22	3NC22	3SJ15A
SiO_2	45.68	45.96	45.22	45.66	44.89	45.48	46.10	46.07	50.57
Al_2O_3	34.32	34.26	34.17	34.88	34.24	34.89	34.25	34.09	30.36
FeO*	.69	.67	.90	.79	.77	.52	.69	.70	.83
MgO	.13	.11	.04	.07	.07	.07	.10	.12	.02
CaO	17.25	17.41	17.37	17.58	17.63	17.54	16.86	17.00	13.93
Na_2O	1.43	1.40	1.28	1.36	1.23	1.27	1.48	1.46	3.42
K_2O	.19	.17	.13	.09	.09	.18	.16	.15	.21
BaO	.04	.04	.04	0	0	0	.02	.04	.07
	99.71	100.01	99.14	100.44	98.92	99.94	99.64	99.63	99.41

Number of ions in the formula on the basis of 32 oxygens

Si	8.459	8.482	8.431	8.396	8.388	8.396	8.521	8.526	9.301
Al	7.486	7.453	7.506	7.560	7.538	7.589	7.458	7.435	6.580
Fe*	.103	.103	.137	.119	.115	.076	.103	.103	.124
Mg	.032	.027	.005	.016	.016	.016	.021	.027	0
Ca	3.417	3.439	3.468	3.459	3.525	3.467	3.335	3.367	2.742
Na	.510	.498	.459	.485	.444	.449	.526	.521	1.214
K	.043	.038	.027	.016	.016	.038	.032	.032	.048
Ba	0	0	0	0	0	0	0	0	0
	20.051	20.039	20.034	20.052	20.042	20.031	19.996	20.012	20.010
Ca	86.07	86.52	87.71	87.35	88.46	87.68	85.67	85.89	68.48
Na	12.85	12.53	11.61	12.25	11.14	11.36	13.51	13.29	30.32
K	1.08	.95	.68	.40	.40	.96	.82	.82	1.20
	x	x	x	x	x	x	x	x	p

	4SJ15A	6SJ20B	3NC20	4NC20	4NC15	5NC15	6NC15	4SJ13A	5SJ13A
SiO_2	51.20	46.98	47.70	48.22	47.93	46.33	48.69	48.16	50.19
Al_2O_3	29.82	33.53	34.19	31.00	31.53	33.55	31.66	31.84	31.68
FeO*	.63	.59	.64	.93	.88	.72	.66	.89	.64
MgO	.04	.12	.07	.14	.12	.10	.12	.19	.18
CaO	13.16	16.93	17.09	14.79	15.45	16.25	15.29	14.18	14.52
Na_2O	3.91	1.85	1.84	2.73	2.27	2.05	2.73	2.86	3.04
K_2O	.25	.21	.16	.45	.15	.18	.39	.39	.42
BaO	.07	.05	.04	.05	0	.03	.05	.02	.11
	99.08	100.26	101.73	98.32	98.32	99.20	99.58	98.52	100.78

Number of ions in the formula on the basis of 32 oxygens

Si	9.427	8.636	8.633	9.017	8.949	8.604	8.985	8.959	9.127
Al	6.472	7.266	7.294	6.832	6.938	7.340	6.884	6.983	6.790
Fe*	.092	.086	.095	.143	.131	.109	.097	.136	.096
Mg	.005	.027	.016	.038	.033	.021	.027	.049	.042
Ca	2.593	3.333	3.315	2.963	3.091	3.231	3.022	2.822	2.829
Na	1.394	.658	.643	.988	.816	.735	.975	1.026	1.067
K	.054	.048	.032	.104	.033	.038	.086	.093	.096
Ba	0	0	0	0	0	0	0	0	.005
	20.037	20.055	20.028	20.084	19.991	20.080	20.076	20.069	20.052
Ca	64.17	82.52	83.08	73.07	78.45	80.69	74.01	71.61	70.87
Na	34.50	16.29	16.12	24.37	20.71	18.36	23.88	26.03	26.73
K	1.33	1.19	.80	2.56	.84	.95	2.11	2.36	2.40
	p	p	p	p	p	p	p	p	p

	6ASJ13A	6BSJ13A	3ASJ6	4SJ6	5SJ6	6SJ6	7SJ6	5ANC34B	5BNC34B
SiO_2	49.54	49.41	48.97	47.51	48.46	47.45	49.84	47.14	46.55
Al_2O_3	32.66	32.35	31.68	32.25	31.70	32.82	32.55	32.63	33.31
FeO*	.66	.75	.62	.73	.60	.70	.64	.63	.63
MgO	.18	.18	.14	.17	.10	.16	.17	.12	.12
CaO	15.22	14.94	15.22	14.73	15.26	14.77	15.09	16.52	17.16
Na_2O	2.71	2.82	2.74	2.85	2.73	2.68	2.96	2.03	1.76
K_2O	.33	.35	.26	.30	.18	.27	.28	.26	.21
BaO	.04	.02	.04	.02	.05	0	.05	.04	.05
	101.33	100.83	99.66	98.56	99.07	98.85	101.58	99.38	99.79
	Number of ions in the formula on the basis of 32 oxygens								
Si	8.970	8.985	9.014	8.856	8.971	8.806	8.996	8.743	8.613
Al	6.972	6.931	6.870	7.083	6.917	7.177	6.924	7.131	7.267
Fe*	.095	.112	.092	.109	.092	.103	.095	.092	.098
Mg	.042	.048	.032	.043	.021	.043	.042	.032	.032
Ca	2.949	2.908	2.997	2.943	3.026	2.935	2.919	3.283	3.399
Na	.946	.992	.978	1.028	.978	.964	1.033	.729	.630
K	.074	.080	.059	.065	.038	.060	.063	.060	.049
Ba	0	0	0	0	0	0	0	0	0
	20.048	20.056	20.041	20.129	20.044	20.088	20.072	20.070	20.088
Ca	74.30	73.07	74.29	72.92	74.86	74.13	72.70	80.63	83.35
Na	23.84	24.92	24.25	25.47	24.20	24.35	25.73	17.90	15.45
K	1.86	2.01	1.46	1.61	.94	1.52	1.57	1.47	1.20
	p	p	p	p	p	p	p	p	p

	6ANC34B	6BNC34B	7ANC34B	7BNC34B	8NC34B	2AJB202	3JB202	4JB202	2NC12C
SiO_2	47.25	47.21	47.51	47.12	47.86	47.57	47.24	46.62	50.63
Al_2O_3	32.94	32.63	32.17	32.60	33.37	32.63	33.38	33.15	31.59
FeO*	.69	.70	.65	.64	.63	.70	.62	.63	.71
MgO	.11	.11	.09	.10	.12	.14	.12	.11	.14
CaO	16.76	16.54	16.14	16.66	16.49	15.66	16.55	16.68	14.33
Na_2O	1.94	2.05	2.09	1.94	1.94	2.31	1.93	1.73	3.34
K_2O	.25	.27	.27	.25	.27	.34	.27	.25	.30
BaO	.06	.08	.05	.05	.06	.10	.01	.01	.08
	100.00	99.59	98.98	99.36	100.75	99.44	100.12	99.17	101.12
	Number of ions in the formula on the basis of 32 oxygens								
Si	8.713	8.740	8.833	8.744	8.742	8.804	8.691	8.660	9.162
Al	7.160	7.116	7.049	7.127	7.182	7.114	7.233	7.258	6.734
Fe*	.103	.108	.098	.098	.096	.103	.091	.098	.106
Mg	.027	.027	.021	.021	.032	.032	.032	.027	.037
Ca	3.312	3.275	3.213	3.310	3.227	3.101	3.260	3.315	2.777
Na	.692	.733	.753	.697	.686	.825	.686	.622	1.168
K	.054	.060	.060	.060	.059	.076	.059	.054	.069
Ba	0	.005	0	0	0	.005	0	0	.005
	20.060	20.064	20.027	20.057	20.023	20.061	20.053	20.034	20.059
Ca	81.62	80.51	79.81	81.39	81.24	77.49	81.40	83.06	69.18
Na	17.05	18.02	18.70	17.14	17.27	20.61	17.13	15.59	29.10
K	1.33	1.47	1.49	1.47	1.49	1.90	1.47	1.35	1.72
	p	p	p	p	p	p	p	p	p

	1ASJ2B	2ASJ2B	3ASJ2B	4SJ2B	5SJ2B	6SJ2B	1AJB1I	1BJB1I	1CJB1I
SiO_2	62.25	60.28	58.75	60.04	62.88	58.70	58.02	56.67	55.71
Al_2O_3	22.80	24.14	25.48	24.99	23.88	25.82	27.05	27.34	28.28
FeO*	.29	.48	.50	.43	.32	.41	.44	.48	.48
MgO	.02	.03	.04	.03	0	.04	.04	.05	.05
CaO	3.56	5.10	6.61	6.13	5.08	6.92	9.04	9.74	10.27
Na_2O	7.66	7.36	6.66	7.13	7.27	6.63	5.72	5.32	5.32
K_2O	2.19	1.29	1.07	1.04	1.71	.95	.87	.78	.70
BaO	.54	.73	.48	.22	.40	.27	.22	.23	.16
	99.30	99.39	99.58	100.01	101.55	99.73	101.40	100.62	100.89
	Number of ions in the formula on the basis of 32 oxygens								
Si	11.190	10.871	10.594	10.738	11.048	10.549	10.305	10.163	9.986
Al	4.828	5.128	5.414	5.264	4.944	5.469	5.661	5.779	5.977
Fe*	.042	.068	.074	.063	.046	.058	.063	.068	.068
Mg	0	.005	.005	.005	0	.005	.005	.010	.010
Ca	.686	.984	1.275	1.170	.954	1.329	1.720	1.868	1.973
Na	2.664	2.572	2.323	2.472	2.475	2.305	1.970	1.847	1.815
K	.501	.296	.243	.236	.381	.216	.192	.173	.158
Ba	.037	.047	.032	.010	.025	.016	.010	.016	.010
	19.947	19.973	19.959	19.958	19.873	19.946	19.926	19.925	19.997
Ca	17.81	25.55	33.19	30.17	25.04	34.52	44.31	48.05	50.00
Na	69.18	66.77	60.48	63.74	64.96	59.87	50.75	47.50	46.00
K	13.01	7.68	6.33	6.09	10.00	5.61	4.94	4.45	4.00
	p	p	p	p	p	p	p	p	p

	4JB1I	1SJ25B	2SJ25B	3SJ25B	4SJ25B	5SJ25B	11BSJ25B	3BSJ6	2BNC22
SiO_2	54.14	65.46	62.42	63.81	66.79	67.30	55.64	52.44	54.61
Al_2O_3	27.04	19.91	22.15	21.39	19.90	18.57	27.65	29.07	28.30
FeO*	.58	.18	.37	.27	.42	.52	.64	.80	.67
MgO	.05	.01	.05	.05	.01	.01	.07	.17	.10
CaO	8.98	.17	.48	.20	.93	.03	6.00	12.91	10.34
Na_2O	6.06	7.33	6.98	7.34	7.11	5.88	6.47	4.37	5.04
K_2O	.66	5.45	4.88	5.13	4.94	8.33	.94	.39	.62
BaO	.26	.10	.91	.06	.07	.05	.14	.01	.10
	97.78	98.61	98.25	98.25	100.17	100.70	97.55	100.16	99.77
	Number of ions in the formula on the basis of 32 oxygens								
Si	10.032	11.822	11.401	11.573	11.862	12.038	10.223	9.559	9.905
Al	5.905	4.233	4.765	4.570	4.164	3.915	5.984	6.243	6.046
Fe*	.087	.026	.053	.037	.057	.073	.097	.118	.101
Mg	.011	0	.010	.010	0	0	.016	.042	.021
Ca	1.783	.032	.091	.037	.172	.005	1.181	2.520	2.006
Na	2.175	2.564	2.471	2.575	2.444	2.036	2.302	1.541	1.772
K	.152	1.255	1.136	1.187	1.115	1.899	.215	.085	.138
Ba	.016	.005	.064	0	0	0	.005	0	.005
	20.161	19.938	19.991	19.989	19.814	19.965	20.023	20.107	19.995
Ca	43.38	.83	2.46	.97	4.61	.13	31.94	60.78	51.23
Na	52.92	66.58	66.82	67.78	65.51	51.68	62.25	37.17	45.25
K	3.70	32.59	30.72	31.25	29.88	48.19	5.71	2.05	3.52
	p	p	p	p	p	p	p	r	r

	5CNC34B	6CNC34B	7CNC34B	2BJB202	5JB202	1BSJ2B	2BSJ2B	3BSJ2B	11ASJ25B
SiO_2	50.60	52.58	51.41	52.30	48.98	65.27	62.02	59.08	64.92
Al_2O_3	30.07	29.12	29.59	29.74	30.36	19.86	22.33	24.60	19.11
FeO*	.71	.75	.84	.73	.71	.47	.48	.51	.72
MgO	.14	.09	.12	.09	.14	.01	.05	.03	.02
CaO	13.36	12.26	13.16	12.56	14.31	.56	3.61	5.67	0
Na_2O	3.67	4.36	3.64	4.26	2.99	6.88	7.63	7.01	6.20
K_2O	.62	.81	.64	.55	.52	6.06	2.23	1.09	7.41
BaO	.11	.09	.10	.07	.05	.48	.44	.30	.02
	99.29	100.05	99.50	100.31	98.07	99.59	98.80	98.29	98.39

Number of ions in the formula on the basis of 32 oxygens

Si	9.330	9.594	9.451	9.520	9.164	11.775	11.221	10.747	11.872
Al	6.532	6.258	6.408	6.378	6.693	4.219	4.758	5.274	4.117
Fe*	.108	.112	.124	.106	.109	.068	.069	.075	.107
Mg	.038	.021	.032	.021	.033	0	.010	.005	0
Ca	2.635	2.393	2.589	2.446	2.866	.105	.695	1.105	0
Na	1.310	1.542	1.294	1.501	1.082	2.403	2.676	2.472	2.195
K	.146	.187	.146	.128	.121	1.392	.510	.250	1.728
Ba	.005	.005	.005	0	0	.032	.026	.021	0
	20.103	20.112	20.049	20.101	20.066	19.995	19.965	19.949	20.019
Ca	64.41	58.05	64.26	60.02	70.44	2.69	17.91	28.88	0
Na	32.02	37.41	32.12	36.83	26.59	61.62	68.95	64.59	55.95
K	3.57	4.54	3.62	3.14	2.97	35.69	13.14	6.53	44.05
	r	r	r	r	r	r	r	r	r

	5SJ15A	6SJ15A	7SJ15A	8SJ15A	9SJ15A	7SJ20B	5NC20	6NC20	7NC15
SiO_2	49.16	49.82	49.76	50.24	49.68	49.59	46.88	50.39	50.54
Al_2O_3	31.29	30.21	31.51	30.95	31.41	30.60	33.29	31.66	30.71
FeO*	.69	.64	.92	.69	.73	.76	.98	.73	1.03
MgO	.15	.16	.24	.18	.19	.13	.21	.18	.04
CaO	14.97	13.65	15.13	14.21	14.67	13.50	13.91	14.37	13.39
Na_2O	2.79	3.18	2.87	2.87	2.91	3.14	2.55	3.25	3.54
K_2O	.40	.64	.40	.46	.44	.62	.50	.57	.30
BaO	.03	.01	.02	.05	0	.13	.06	.08	.09
	99.48	98.32	100.85	99.64	100.03	98.46	98.39	101.23	99.68
	Number of ions in the formula on the basis of 32 oxygens								
Si	9.063	9.272	9.068	9.221	9.101	9.221	8.745	9.128	9.272
Al	6.801	6.624	6.763	6.695	6.778	6.705	7.321	6.762	6.639
Fe*	.103	.098	.139	.102	.107	.114	.147	.106	.156
Mg	.038	.043	.064	.043	.048	.033	.055	.047	.021
Ca	2.954	2.719	2.951	2.790	2.875	2.684	2.781	2.786	2.627
Na	.995	1.141	1.010	1.018	1.032	1.129	.919	1.138	1.254
K	.092	.153	.091	.102	.102	.147	.115	.127	.070
Ba	0	0	0	0	0	.005	0	.005	.005
	20.045	20.050	20.086	19.971	20.044	20.039	20.083	20.100	20.045
Ca	73.10	67.76	72.83	71.36	71.72	67.78	72.90	68.77	66.49
Na	24.62	28.43	24.93	26.04	25.74	28.51	24.09	28.09	31.74
K	2.28	3.81	2.24	2.60	2.54	3.71	3.01	3.14	1.77
	g	g	g	g	g	g	g	g	g

	7SJ13A	8SJ6	9SJ6	6NC17	7NC17	4NC22	9NC34B	10NC34B	6JB202
SiO_2	50.61	49.54	50.14	51.51	50.75	53.54	50.29	51.04	52.41
Al_2O_3	31.57	31.89	31.91	31.04	30.46	28.75	30.19	30.98	29.46
FeO*	.82	.73	.60	.83	.83	.94	.89	.73	.65
MgO	.20	.15	.13	.05	.05	.13	.12	.14	.13
CaO	14.58	14.95	14.47	13.24	12.98	10.89	13.86	13.90	12.04
Na_2O	2.93	3.04	3.22	4.17	4.05	4.73	3.29	3.26	4.20
K_2O	.41	.18	.27	.23	.21	.59	.54	.56	.63
BaO	.04	.08	.04	.14	.04	.18	.08	.09	.05
	101.15	100.56	100.78	101.21	99.37	99.75	99.25	100.70	99.57
	Number of ions in the formula on the basis of 32 oxygens								
Si	9.160	9.034	9.104	9.304	9.322	9.759	9.285	9.271	9.581
Al	6.733	6.856	6.824	6.605	6.594	6.171	6.565	6.632	6.346
Fe*	.122	.107	.090	.122	.124	.139	.135	.106	.096
Mg	.053	.037	.032	.010	.011	.032	.032	.032	.032
Ca	2.825	2.922	2.813	2.561	2.556	2.123	2.735	2.703	2.355
Na	1.024	1.070	1.129	1.458	1.439	1.668	1.175	1.146	1.486
K	.090	.037	.059	.047	.048	.133	.125	.128	.145
Ba	0	.005	0	.005	0	.010	.005	.005	0
	20.007	20.068	20.050	20.111	20.094	20.035	20.059	20.023	20.041
Ca	71.72	72.52	70.31	62.99	63.22	54.10	67.78	67.97	59.08
Na	26.00	26.56	28.22	35.86	35.59	42.51	29.12	28.81	37.28
K	2.28	.92	1.47	1.15	1.19	3.39	3.10	3.22	3.64
	g	g	g	g	g	g	g	g	g

	3NC12C	4NC12C	7SJ2B	8SJ2B	9SJ2B	10SJ2B	2JB1I	3JB1I	6SJ25B
SiO_2	51.13	49.68	61.45	59.16	64.12	62.71	63.72	60.63	66.14
Al_2O_3	31.25	32.36	24.41	24.67	22.39	23.63	21.92	25.20	20.01
FeO*	.81	.84	.57	.52	.45	.26	.52	.57	.37
MgO	.07	.18	.03	.01	.01	0	.06	.02	0
CaO	13.63	15.05	5.51	6.29	3.33	4.76	3.00	6.56	.68
Na_2O	3.71	2.76	6.88	6.76	7.06	7.13	6.63	6.43	6.28
K_2O	.26	.20	1.69	1.32	2.62	1.84	3.43	1.08	6.44
BaO	.05	.10	.63	.44	.65	.39	.66	.63	.05
	100.90	101.16	101.16	99.16	100.63	100.71	99.93	101.11	99.98
	Number of ions in the formula on the basis of 32 oxygens								
Si	9.256	9.003	10.896	10.718	11.361	11.094	11.409	10.750	11.832
Al	6.668	6.908	5.099	5.263	4.674	4.926	4.622	5.266	4.215
Fe*	.122	.127	.083	.074	.062	.036	.073	.083	.052
Mg	.016	.042	.005	0	0	0	.010	0	0
Ca	2.641	2.919	1.045	1.217	.629	.898	.572	1.243	.126
Na	1.296	.968	2.362	2.371	2.423	2.440	2.300	2.206	2.178
K	.058	.042	.379	.303	.587	.410	.782	.244	1.470
Ba	0	.005	.042	.026	.042	.026	.042	.042	0
	20.058	20.016	19.911	19.973	19.778	19.830	19.811	19.833	19.873
Ca	66.11	74.29	27.60	31.28	17.29	23.96	15.65	33.66	3.34
Na	32.44	24.64	62.39	60.93	66.58	65.10	62.95	59.73	57.71
K	1.45	1.07	10.01	7.79	16.13	10.94	21.40	6.61	38.95
	g	g	g	g	g	g	g	g	g

OPAQUE ANALYSES

	12NC17	7NC12C	7SJ25B	8SJ25B	9SJ25B	10SJ25B
SiO_2	.16	.77	.16	.40	.13	.45
TiO_2	19.11	23.57	48.90	7.39	50.23	21.22
Al_2O_3	6.11	1.82	.14	.61	.17	1.21
FeO*	68.18	66.96	39.39	79.14	39.81	66.81
MnO	.63	.70	5.56	1.46	5.10	1.91
MgO	3.14	1.07	1.22	.04	1.15	.40
CaO	0	.12	.08	.16	.11	.23
Cr_2O_3	.04	.02	.03	.07	.04	.04
	97.37	95.03	95.48	89.28	96.75	92.28

Number of ions in the formula on the basis of 32 oxygens

Si	.034	.186	.031	.113	.024	.113
Ti	3.369	4.318	7.760	1.647	7.839	4.094
Al	1.688	.521	.031	.209	.036	.362
Fe*	13.388	13.641	6.949	19.658	6.907	14.356
Mn	.124	.143	.991	.366	.895	.415
Mg	1.095	.386	.377	.017	.353	.150
Ca	0	.028	.012	.043	.024	.060
Cr	0	0	0	.017	.006	.007
	19.699	19.222	16.151	22.071	16.084	19.557

APPENDIX V

MINERAL CHEMISTRY

(OTHER AUTHORS)

OLIVINE ANALYSES

	NC15K	NC19A	NC19B	NC19C	NC22I	NC22K	NC22O	NC12CG	NC12CF
SiO_2	41.40	41.28	40.95	41.18	40.49	40.39	40.78	41.55	40.74
Al_2O_3	.05	.03	.05	.07	.01	.03	.01	.03	.05
FeO*	10.03	11.46	11.73	10.56	10.13	10.49	10.06	16.26	15.36
MnO	.24	.25	.24	.23	.18	.20	.17	.37	.42
MgO	48.68	47.99	46.86	47.67	48.25	47.79	48.06	43.16	43.44
CaO	.42	.39	.40	.36	.37	.40	.36	.32	.31
K_2O	.01	.02	.01	.01	.02	.02	.01	.01	.02
NiO	.26	.24	.25	.28	.21	.17	.17	.12	.13
Cr_2O_3	.05	.02	.02	.07	.05	.03	.06	.01	.03
	101.18	101.68	100.51	100.43	99.71	99.51	99.68	101.87	100.50

Number of ions in the formula on the basis of 4 oxygens

Si	1.006	1.004	1.008	1.010	.999	1.000	1.005	1.027	1.019
Al	.001	.001	.002	0	0	.001	0	.001	.002
Fe*	.204	.233	.242	.217	.209	.217	.207	.336	.321
Mn	.005	.005	.005	.005	.004	.004	.004	.008	.009
Mg	1.761	1.739	1.719	1.742	1.774	1.763	1.765	1.589	1.619
Ca	.011	.010	.011	.010	.010	.011	.010	.009	.008
K	0	.001	0	0	.001	.001	0	0	.001
Ni	.005	.005	.005	.006	.004	.003	.003	.002	.003
Cr	.001	0	0	.001	.001	.001	.001	0	.001
	2.994	2.998	2.992	2.991	3.002	3.001	2.995	2.972	2.983
Fo	89.62	88.18	87.66	88.92	89.46	89.04	89.50	82.55	83.44
F/F+M	.104	.118	.123	.111	.105	.110	.105	.175	.166

	NC15L
SiO_2	40.93
Al_2O_3	.05
FeO*	12.96
MnO	.31
MgO	45.85
CaO	.41
K_2O	.01
NiO	.24
Cr_2O_3	0
	100.56

Number of ions in the formula on the basis of 4 oxygens

Si	1.010
Al	.002
Fe*	.268
Mn	.007
Mg	1.687
Ca	.011
K	0
Ni	.005
Cr	0
	2.990
Fo	86.31
F/F+M	.137

CLINOPYROXENE ANALYSES

	JM5-1D	JM5-2B	JM5-2C	JM5-1A	JM5-3A	JM5-3B
SiO_2	52.6	51.7	52.5	52.0	51.9	52.3
TiO_2	.5	.8	.7	.5	.6	.7
Al_2O_3	2.0	2.8	2.6	2.0	2.7	2.5
FeO*	3.3	4.3	4.1	3.5	3.8	4.0
MnO						
MgO	19.3	17.2	18.0	17.9	17.7	17.3
CaO	22.1	22.4	22.0	22.1	22.2	22.2
Na_2O						
Cr_2O_3						
NiO						
	99.0	99.8	99.2	99.9	98.8	99.0

Number of ions in the formula on the basis of 6 oxygens

Si	1.916	1.906	1.915	1.931	1.913	1.925
Ti	.014	.022	.019	.014	.017	.019
Al	.085	.120	.111	.087	.116	.107
Fe*	.101	.133	.125	.109	.117	.123
Mn						
Mg	1.048	.945	.979	.991	.972	.949
Ca	.863	.885	.860	.879	.877	.876
Na						
Cr						
Ni						
	4.027	4.011	4.009	4.011	4.012	3.999
Ca	42.89	45.08	43.79	44.42	44.61	44.96
Mg	52.09	48.14	49.85	50.08	49.44	48.72
Fe	5.02	6.78	6.36	5.50	5.95	6.31
F/F+M	.088	.123	.113	.099	.108	.115
	CrDi	CrDi	CrDi	CrDi	CrDi	CrDi

	JM6-6A	JM6-6B	JM7-3J	JM7-3K	JM7-5B	NC12CA
SiO_2	51.7	52.2	52.7	52.3	52.4	52.44
TiO_2	.6	.7	.5	.7	.7	.74
Al_2O_3	2.6	3.3	2.5	2.5	2.8	2.09
FeO*	4.2	4.3	3.7	4.0	3.7	4.34
MnO			.1	.1	.1	.11
MgO	17.5	16.6	17.7	17.4	17.4	16.52
CaO	22.4	22.3	22.1	22.2	22.1	22.75
Na_2O						.45
Cr_2O_3			.2	.2	.4	.11
NiO						.03
	99.0	99.4	99.5	99.4	99.6	99.72
	Number of ions in the formula on the basis of 6 oxygens					
Si	1.909	1.915	1.927	1.920	1.918	1.932
Ti	.017	.019	.014	.019	.019	.005
Al	.112	.141	.107	.107	.116	.091
Fe*	.130	.132	.113	.123	.113	.124
Mn			.003	.003	.003	.003
Mg	.963	.908	.965	.952	.949	.907
Ca	.886	.877	.866	.873	.867	.898
Na						.032
Cr			.006	.006	.011	.003
Ni						.001
	4.017	3.992	4.001	4.003	3.996	4.006
Ca	44.77	45.75	44.55	44.82	44.94	47.05
Mg	48.66	47.37	39.64	48.87	49.20	46.04
Fe	6.56	6.89	5.81	6.31	5.86	6.91
F/F+M	.119	.127	.105	.114	.107	.128
	CrDi	CrDi	CrDi	CrDi	CrDi	CrDi

	NC22H	NC22L	BAT	NC15M	NC15N	NC19D
SiO_2	51.68	52.86	52.17	52.44	52.63	51.01
TiO_2	.67	.50	.64	.49	.50	.74
Al_2O_3	2.55	2.08	3.35	1.69	1.82	3.08
FeO*	3.60	3.33	3.84	3.09	3.21	4.53
MnO	.14	.10		.10	.07	.11
MgO	16.61	17.13	17.12	16.83	17.00	15.97
CaO	22.84	22.80	22.12	22.94	22.81	23.11
Na_2O	.45	.45	.27	.45	.45	.45
Cr_2O_3	.15	.71	.70	.75	.69	.49
NiO	.03			.02	.05	.02
	98.83	100.06	100.38	98.88	99.32	99.65

Number of ions in the formula on the basis of 6 oxygens

Si	1.909	1.925	1.89	1.933	1.931	1.881
Ti	.019	.014	.02	.014	.014	.021
Al	.111	.089	.05	.074	.079	.134
Fe*	.111	.102	.12	.095	.098	.139
Mn	.004	.003		.003	.002	.003
Mg	.914	.930	.92	.925	.930	.877
Ca	.904	.890	.85	.906	.897	.913
Na	.032	.032	.02	.032	.032	.032
Cr	.004	.020	.01	.022	.020	.014
Ni	.001			.001	.001	.001
	4.009	4.005	3.99	4.005	4.004	4.015
Ca	47.51	46.67	45.43	47.33	46.93	47.76
Mg	46.64	48.06	48.59	47.74	48.00	45.04
Fe	5.85	5.28	5.98	4.94	5.06	7.19
F/F+M	.108	.098	.112	.093	.096	.137
	CrDi	CrDi	CrDi	CrDi	CrDi	CrDi

	NC19G	NC150	NC15P	NC19H	NC19I	NC19J
SiO_2	53.01	51.28	49.12	48.04	46.33	48.91
TiO_2	.42	.91	.91	1.86	2.78	1.76
Al_2O_3	1.78	3.37	4.70	5.79	6.72	3.99
FeO*	3.32	4.58	6.23	6.96	8.53	8.26
MnO	.10	.13	.13	.19	.23	.26
MgO	17.42	16.03	14.19	13.63	12.12	13.84
CaO	22.28	23.01	22.80	22.37	22.24	21.67
Na_2O	.45	.50	.50	.50	.50	.50
Cr_2O_3	.58	.15	.15	.04	.02	
NiO		.01	.01	.03	.04	.03
	99.76	100.10	98.87	99.54	99.64	99.45

Number of ions in the formula on the basis of 6 oxygens

Si	1.938	1.881	1.842	1.797	1.748	1.840
Ti	.012	.025	.026	.052	.079	.050
Al	.077	.146	.208	.255	.300	.177
Fe*	.102	.141	.196	.217	.270	.263
Mn	.003	.004	.004	.006	.007	.008
Mg	.949	.876	.793	.760	.682	.780
Ca	.873	.905	.916	.896	.899	.873
Na	.032	.036	.036	.036	.037	.036
Cr	.017	.004	.004	.001	.001	
Ni		0	0	.001	.001	.001
	4.003	4.018	4.025	4.021	4.024	4.028
Ca	45.82	47.86	48.89	48.66	49.40	46.58
Mg	48.89	44.81	40.90	39.70	36.04	39.72
Fe	5.28	7.34	10.21	11.64	14.56	13.70
F/F+M	.096	.138	.197	.223	.283	.251
	CrDi	TiSal	TiSal	TiSal	TiSal	TiSal

	JM6-9S	JM6-11A	KAPPTR	JM6-11B	JM6-11C	JM6-12C
SiO_2	48.5	48.6	45.13	49.0	50.5	49.5
TiO_2	1.8	1.7	2.57	1.7	1.8	1.9
Al_2O_3	5.5	5.3	10.44	5.3	3.7	4.2
FeO*	7.5	6.8	7.16	6.7	8.5	7.4
MnO						
MgO	14.1	14.3	12.35	14.1	13.3	14.6
CaO	21.6	21.9	21.53	21.8	22.0	22.6
Na_2O			.47			
Cr_2O_3						
NiO						
	99.0	98.6	100.08	98.6	99.8	100.2
	Number of ions in the formula on the basis of 6 oxygens					
Si	1.820	1.827	1.67	1.839	1.885	1.840
Ti	.051	.048	.07	.048	.051	.053
Al	.241	.233	.44	.231	.161	.182
Fe*	.235	.214	.22	.210	.265	.230
Mn						
Mg	.789	.801	.68	.788	.740	.809
Ca	.869	.882	.85	.876	.880	.900
Na			.01			
Cr						
Ni						
	4.005	4.005	3.94	3.992	3.982	4.014
Ca	45.91	46.49	49.69	46.74	46.68	46.42
Mg	41.68	42.23	38.00	42.05	39.26	41.72
Fe	12.41	11.28	12.31	11.21	14.06	11.86
F/F+M	.229	.211	.245	.211	.264	.221
	TiSal	TiSal	TiSal	TiSal	TiSal	TiSal

	JM7-4E	NC12CC	NC12CD	NC12CE	NC22	JM7-4B
SiO_2	49.4	51.26	51.89	47.61	49.65	46.6
TiO_2	1.6	1.12	1.29	1.59	1.37	3.0
Al_2O_3	4.7	3.68	3.82	6.40	3.75	6.4
FeO*	7.4	5.72	5.75	5.98	8.02	9.3
MnO	.2	.17	.14	.15	.33	.2
MgO	14.4	15.15	15.09	13.52	14.19	11.8
CaO	21.6	21.90	21.83	22.44	21.30	21.4
Na_2O		.50	.50	.50	.50	
Cr_2O_3		.26	.48	.46		
NiO		.01				
	99.3	99.90	100.92	99.78	99.24	98.7

Number of ions in the formula on the basis of 6 oxygens

Si	1.847	1.886	1.889	1.783	1.863	1.775
Ti	.045	.031	.035	.045	.039	.086
Al	.205	.160	.164	.281	.166	.285
Fe*	.231	.176	.175	.200	.251	.296
Mn	.006	.005	.004	.005	.011	.006
Mg	.802	.831	.819	.755	.794	.670
Ca	.865	.863	.851	.900	.856	.874
Na		.036	.035	.036	.036	
Cr		.008	.014	.014		
Ni		0				
	4.001	3.996	3.986	4.019	4.016	3.992
Ca	45.57	46.89	46.74	49.42	45.85	47.50
Mg	42.26	43.68	43.83	40.48	40.71	36.41
Fe	12.17	9.43	9.43	10.10	13.43	16.09
F/F+M	.224	.175	.176	.199	.241	.307
	TiSal	TiSal	TiSal	TiSal	TiSal	TiAug-R

	JM7-4B	JM7-8B	JM5-1B	JM5-1C	JM5-3D	JM7-3B
SiO_2	46.3	45.9	45.1	45.7	45.0	43.4
TiO_2	3.4	3.0	3.1	2.9	3.0	3.5
Al_2O_3	7.2	7.6	7.4	6.9	6.5	7.8
FeO*	8.0	8.6	8.9	9.2	7.8	8.7
MnO	.2	.2				.2
MgO	12.7	12.3	12.0	12.6	13.4	12.5
CaO	21.2	21.6	22.0	22.0	22.4	21.9
Na_2O						
Cr_2O_3						
NiO						
	99.0	99.2	98.5	99.3	98.1	98.0

Number of ions in the formula on the basis of 6 oxygens

Si	1.748	1.737	1.725	1.735	1.725	1.676
Ti	.097	.085	.089	.083	.086	.102
Al	.317	.336	.330	.306	.281	.351
Fe*	.253	.272	.285	.292	.250	.281
Mn	.006	.006				.007
Mg	.714	.694	.684	.713	.766	.719
Ca	.857	.876	.902	.895	.920	.906
Na						
Cr						
Ni						
	3.992	4.006	4.015	4.024	4.028	4.042
Ca	46.98	47.55	48.21	47.10	47.53	47.54
Mg	39.14	37.68	36.56	37.53	39.56	37.72
Fe	13.88	14.77	15.23	15.37	12.91	14.74
F/F+M	.261	.282	.294	.291	.246	.281
	TiAug-R	TiAug-R	TiAug-R	TiAug-R	TiAug-R	TiAug-R

	JM7-8	JM6-9	JM6-13
SiO_2	44.7	47.4	46.2
TiO_2	3.2	2.5	2.6
Al_2O_3	6.2	5.8	5.5
FeO*	8.2	9.5	8.7
MnO	.2		
MgO	14.1	12.3	14.8
CaO	22.3	21.1	21.4
Na_2O			
Cr_2O_3			
NiO			
	98.9	98.6	99.2

Number of ions in the formula on the basis of 6 oxygens

Si	1.707	1.803	1.751
Ti	.092	.072	.074
Al	.276	.258	.243
Fe*	.262	.302	.276
Mn	.006		
Mg	.802	.697	.836
Ca	.913	.860	.869
Na			
Cr			
Ni			
	4.058	3.992	4.049
Ca	46.18	46.26	43.87
Mg	40.57	37.49	42.20
Fe	13.25	16.25	13.92
F/F+M	.246	.302	.248
	TiAug-G	TiAug-G	TiAug-G

APPENDIX VI

RESULTS OF LEAST SQUARES MAGMA MIXING

NC15

	Observed	Calculated
SiO_2	48.34	48.15
TiO_2	2.02	2.21
Al_2O_3	8.28	9.06
FeO*	9.37	8.55
MnO	.14	.18
MgO	14.86	15.21
CaO	14.05	14.27
Na_2O	1.52	1.61
K_2O	1.08	1.20
P_2O_5	.32	.26

Estimated Weight Percentages

Liq	NC22	39.54
Ol	3NC15	13.54
CrDi	8CNC15	7.28
TiSal	12NC15	39.63

Sum of Squares of Residuals

1.5418

NC20

	Observed	Calculated
SiO_2	45.99	46.35
TiO_2	2.20	2.06
Al_2O_3	10.03	9.68
FeO*	9.77	8.80
MnO	.14	.16
MgO	15.44	15.35
CaO	13.35	13.12
Na_2O	1.53	1.62
K_2O	1.21	1.17
P_2O_5	.34	.26

Estimated Weight Percentages

Liq	NC22	39.09
Ol	1NC22	16.16
TiSal	7CNC20	42.73
Feld	2ANC22	2.03

Sum of Squares of Residuals

1.2891

NC27L

	Observed	Calculated
SiO_2	47.47	48.13
TiO_2	2.02	1.66
Al_2O_3	10.88	10.50
FeO*	9.06	7.19
MnO	.18	.14
MgO	13.16	13.02
CaO	14.08	13.10
Na_2O	1.66	1.93
K_2O	1.18	1.49
P_2O_5	.30	.33

Estimated Weight Percentages

Liq	NC22	50.54
Ol	1NC22	9.71
CrDi	3NC27L	37.57
Feld	2ANC22	2.17

Sum of Squares of Residuals

5.3557

NC23

	Observed	Calculated
SiO_2	49.43	49.41
TiO_2	2.14	2.23
Al_2O_3	14.24	14.24
FeO*	8.56	8.52
MnO	.17	.17
MgO	9.01	9.04
CaO	10.75	10.78
Na_2O	2.65	2.89
K_2O	2.28	2.29
P_2O_5	.78	.50

Estimated Weight Percentages

Liq	NC22	75.64
Ol	1NC22	5.96
CrDi	5BNC22	9.42
TiSal	9NC17	3.51
Feld	2ANC22	5.47

Sum of Squares of Residuals

0.1488

NC12C

	Observed	Calculated
SiO_2	47.34	47.95
TiO_2	2.57	2.36
Al_2O_3	14.14	13.60
FeO*	10.42	8.58
MnO	.12	.17
MgO	8.67	8.56
CaO	12.10	11.58
Na_2O	2.48	2.65
K_2O	1.70	2.11
P_2O_5	.47	.46

Estimated Weight Percentages

Liq	NC22	71.05
Ol	1NC22	3.83
TiSal	5NC12C	23.60
Feld	2ANC22	1.52

Sum of Squares of Residuals

4.5557

SJ15A

	Observed	Calculated
SiO_2	46.74	47.44
TiO_2	2.20	1.15
Al_2O_3	11.08	10.47
FeO*	9.17	8.44
MnO	.19	.16
MgO	12.48	12.12
CaO	14.29	13.18
Na_2O	2.26	1.92
K_2O	1.25	1.01
P_2O_5	.35	.40

Estimated Weight Percentages

Liq	SJ1A	50.68
Ol	1BSJ15A	8.62
CrDi	10BSJ15A	35.75
Feld	3SJ15A	4.95

Sum of Squares of Residuals

4.0308

SJ20B

	Observed	Calculated
SiO_2	47.28	47.30
TiO_2	2.35	1.83
Al_2O_3	12.02	11.91
FeO*	9.87	10.11
MnO	.14	.17
MgO	11.01	10.92
CaO	13.45	13.49
Na_2O	1.95	2.06
K_2O	1.55	1.13
P_2O_5	.36	.46

Estimated Weight Percentages

Liq	SJ1A	55.71
Ol	1SJ20B	6.30
CrDi	8SJ13A	1.80
TiSal	8ASJ20B	36.19

Sum of Squares of Residuals

0.5559

SJ6

	Observed	Calculated
SiO_2	47.46	48.05
TiO_2	1.30	1.27
Al_2O_3	12.90	12.56
FeO*	10.73	9.64
MnO	.16	.17
MgO	11.15	10.99
CaO	12.29	11.18
Na_2O	2.29	2.44
K_2O	1.23	1.38
P_2O_5	.50	.55

Estimated Weight Percentages

Liq	SJ1A	68.45
Ol	1SJ6	8.22
CrDi	10CSJ6	20.76
Feld	6SJ6	2.57

Sum of Squares of Residuals

2.9701

APPENDIX VII

SAMPLE LOCATIONS

Ankaramite

SJ14B lava from the base of cliffs just east of Svand Foynbreen, Krossbukta, Nord Jan, 71°8'42"N, 8°06'38"W. Fitch, written commun.

SJ15A lava from 8m above base of cliffs just east of Svand Foynbreen, Krossbukta, Nord Jan, 71°8'42"N, 8°06'38"W. Fitch, written commun.

SJ20B lava from within the tillite sequence east of Svand Foynbreen, Nord Jan, 71°8'42"N, 8°6'10"W. Fitch, written commun.

NC20 lava from a cinder/lava whaleback come exposed in cross-section within the Storfjellet formation near the base of the cliff below Tvillingkrateret, Nord Jan, 71°6'50"N, 8°2'50"W. Fitch, written commun.

NC15 lava from top of Kraterlia cliff behind Nordbukta, Nord Jan, 71°9'00"N, 8°0'40"W. Fitch, written commun.

NC27L lava from the upper part of the cliff section at Kvalnosa, Nord Jan, 71°8'20"N, 8°8'00"W. Fitch, written commun.

NC19 lava from the Storfjellet cliff below Tvillingkrateret, Nord Jan. Roberts and Hawkins, 1965.

NC15* lava from the Kraterlia cliff south of Nordbukta, Nord Jan. Roberts and Hawkins, 1965.

7^T probably a lava, west of Cape Hope, Jan Mayen. Tyrrell, 1926.

C9 lava from Krossbukta, Nord Jan. Lussia-Berdou-Polve and Vidal, 1973.

Alkali Olivine Basalt - Sor Jan

SJ1A lava from the base of the cliff at the southern end of Sorbukta, Sor Jan, 70°50'35"N, 9°2'30"W. Fitch, written commun.

SJ13A lava from 10m above base of cliffs at Ullringbukta, Sor Jan, 70°50'50"N, 8°56'00"W. Fitch, written commun.

SJ5A lava from base of cliffs at southern end of Kvalrossbukta, Sor Jan, 70°57'50"N, 8°41'30"W. Fitch, written commun.

SJ6 lava from the same locality as SJ5A. Fitch, written commun.

SJ9B lava from the same locality as SJ13A. Fitch, written commun.

3^T lava scarp south of the Saule, Jan Mayen. Tyrrell, 1926.

5^T lava from Turn Bay, Jan Mayen. Tyrrell, 1926.

5^C lava from Sorbukta, Jan Mayen. Carstens, 1961.

Alkali Olivine Basalt - Nord Jan

NC12C lava from Tromsoryggen 'window' through the Kokssletta formation lavas, small inland cliff behind Nordbukta, Nord Jan, 71°9'20"N, 7°59'30"W. Fitch, written commun.

NC12C* lava from same locality as NC12C. Roberts and Hawkins, 1965.

NC17 lava from the same locality as NC20. Fitch, written commun.

NC17* lava from the same locality as NC20. Fitch, written commun.

NJ17 lava from the upper aa-lava of the Kokssletta lava platform near Youngneat, Nord Jan, 71°9'25"N, 8°1'40"W. Fitch, written commun.

NJ17* lava from the same locality as NJ17. Roberts and Hawkins, 1965.

NC27K lava from the Kvalnosa buttress of the Nordvestkapp formation, Nord Jan. Hawkins and Roberts, 1972.

NC27K* lava from the same locality as NC27K. Roberts and Hawkins, 1965.

JB202 lava flow from Nunataken, at 1550m on the southwest flank of Beerenberg, 71°4'2"N, 8°11'50"W. Fitch, written commun.

JB202* lava from the same locality as JB202. Hawkins and Roberts, 1972.

NC22 lava from the same locality as NC20. Fitch, written commun.

NC23 lava from the same locality as NC20. Fitch, written commun.

NC34B lava from an inland cliff exposure at the southern end of Marmadukeflya, Nord Jan, 71°8'00"N, 7°58'35"W. Fitch, written commun.

NC35B lava from the northwestern end of Marmadukeflya, Nord Jan, 71°8'25"N, 7°58'40"W. Fitch, written commun.

NC30C lava from the northern tip of the main fissure at Nordkapp, Nord Jan, 71°9'12"N, 7°58'00"W. Fitch, written commun.

NC3 lava from the Storfjellet cliff near Krossbukta, Nord Jan. Roberts and Hawkins, 1965.

NC13 lava from the Kraterlia cliff south of Nordbukta, Nord Jan. Roberts and Hawkins, 1965.

SJ48 lava from Bastionen, Beerenberg, Nord Jan. Hawkins and Roberts, 1972.

SJ53 lava from the same locality as SJ48. Hawkins and Roberts, 1972.

JM5 lava flow from the Trinityberget crater (Sept.-Oct. 1970 eruption), Nord Jan. Weigand, 1972.

JM6 lava flow from the same locality as JM5. Weigand, 1972.

JM7 lava flow from the Dufferinbreen crater (Sept.-Oct. 1970 eruption), Nord Jan. Weigand, 1972.

JM3 an ejected bomb from the Tollnerodden crater (Sept.-Oct. 1970 eruption), Nord Jan. Weigand, 1972.

4T lava, the Nunatak, Beerenberg, Jan Mayen. Tyrrell, 1926.

6T Mary Muss Bay, Jan Mayen. Tyrrell, 1926.

C15 lava from Krossbukta, Nord Jan. Lussia-Berdou-Polve and Vidal, 1973.

C10 lava from Krossbukta, Nord Jan. Lussia-Berdou Polve and Vidal, 1973.

C11 lava from Krossbukta, Nord Jan. Lussia-Berdou-Polve and Vidal, 1973.

C12 lava from Krossbukta, Nord Jan. Lussia-Berdou-Polve and Vidal, 1973.

1^{S} from a lava stream from the Dufferinbreen crater one of the first days of eruption in 1970, Nord Jan. Siggerud, 1972.

2^{S} from the eruption of the Sigurdbreen crater in the morning of October 3, 1970, Nord Jan. Siggerud, 1972.

Trachyandesite

NC22 lava from the same locality as NC20. Roberts and Hawkins, 1965.

3^{C} from Dollartoppen, Jan Mayen. Carstens, 1961.

2^{H} near Skrukkefjell, Jan Mayen, Carstens, 1962.

2^{T} block in agglomerate of Egg Bluff, Jan Mayen. Tyrrell, 1926.

C13 lava from Krossbukta, Nord Jan. Lussia-Berdou-Polve and Vidal, 1973.

C14 lava from Krossbukta, Nord Jan. Lussia-Berdou-Polve and Vidal, 1973.

Latite Andesite

SJ2B lava from 10m above the base of the cliffs at the southern end of Sorbukta, Sor Jan, 70°50'35"N, 9°2'29"W. Fitch, written commun.

JB1I ejected lava block from Eggoya, Nord Jan, 70°58'27"N, 8°22'30"W. Fitch, written commun.

Trachyte

SJ25B	from a volcanic dome forming the hill Bombelle-stoppen, Sor Jan, 70°54'10"N, 8°52'15"W. Fitch, written commun.
1^{C}	from Inndalsmoya, Jan Mayen. Carstens, 1961.
1^{T}	from Bombelle Mountain, Jan Mayen. Tyrrell, 1926.

APPENDIX VIII

PETROGRAPHY OF THE INDIVIDUAL SAMPLES (THIS STUDY)

Ankaramites

SJ14B (Krossbukta formation) has a K-Ar age of 0.19 ± 0.10 my (Fitch, Grasty and Miller, 1965) and is a dark gray, slightly to moderately vesicular, pilotaxitic, seriate porphyritic ankaramite. Common xenocrysts present are subhedral to anhedral chromium diopside, anhedral to euhedral titaniferous salite, and resorbed olivine.

Chromium diopside xenocrysts (maximum of 5.0 mm in size) are light yellow green, resorbed, polygonized and may contain inclusions of plagioclase, olivine, or magnetite. The chromium diopside is rimmed by purple brown titaniferous augite (0.02 mm) and may be simply twinned.

Light brown titaniferous salite xenocrysts are reversely zoned (average composition of $Wo_{49}En_{43}Fs_8$) and rimmed by titaniferous augite. They occur as both euhedral and embayed crystals up to 5.0 mm in size, sometimes containing unaltered red brown glass. Larger crystals may be characterized by discontinuous poikilitic rims, while smaller ones may have poikilitic cores of devitrified or partially crystallized glass, that often takes on an appearance to the groundmass (any mention hereafter of poikilitic titaniferous salite refers to this description).

Olivine xenocrysts (up to 2.0 mm) may also be polygonized and contain magnetite and devitrified glass inclusions. They are resorbed and iddingsitized on the edges.

The xenocrysts and microphenocrysts of magnetite (up to 0.30 mm) and anhedral, brown biotite (up to 0.15 mm long) lie in an aphanitic, intergranular groundmass of purple brown titaniferous augite prisms (some of which are sector zoned), plagioclase laths, euhedral or rounded olivine (some of which are surrounded by iddingsite), and magnetite cubes.

Glomerocrysts of clinopyroxene (diameter = 3.0-5.0 mm) are abundant, but clinopyroxene+olivine glomerocrysts may also be found. Generally, the volume percent of clinopyroxene > plagioclase = olivine.

SJ15A (Krossbukta formation) has a K-Ar age of 0.19 ± 0.10 my (Fitch, Grasty and Miller, 1965) and is a dark gray, moderately vesicular, pilotaxitic, seriate porphyritic ankaramite. Xenocrystal phases present in this rock are euhedral to anhedral chromium diopside, euhedral to anhedral titaniferous salite, and embayed olivine.

Xenocrysts of yellow green chromium diopside ($Wo_{47}En_{48}Fs_5$) attain a maximum of 5.5 mm and are resorbed, polygonized, and timmed (0.10 mm) by a purple brown titani-

ferous augite ($Wo_{49}En_{42}Fs_9$). They contain inclusions of plagioclase, olivine, or magnetite and may be simply twinned.

Light brown titaniferous salite xenocrysts are reversely zoned (core: $Wo_{48}En_{43}Fs_9$, edge: $Wo_{48}En_{44}Fs_8$) and occur up to a size of 5.5 mm. The crystals are both euhedral and resorbed and are rimmed by titaniferous augite ($Wo_{46}En_{44}Fs_{10}$). Sometimes this rim is discontinuously poikilitic. They may contain slightly altered dark red brown glass associated with a few minute opaques.

Olivine xenocrysts (Fo_{84}) are up to 2.0 mm in size, may contain inclusions of magnetite or partially crystallized glass (microlites are oriented in such a manner as to produce a wavy extinction), and are resorbed and iddingsitized.

These xenocrysts and microxenocrysts of resorbed plagioclase (up to 0.35 mm in size, zoned with altered cores, some with combined Carlsbad-albite twins), and rounded magnetite (up to 0.30 mm) sit in a fine grained, intergranular matrix of euhedral purple brown titaniferous augite ($Wo_{48}En_{41}Fs_{11}$), plagioclase laths ($Ca_{71}Na_{26}K_3$), euhedral olivine, and magnetite.

Glomerocrysts of clinopyroxene (diameter = 0.5-4.0 mm) are predominant, but olivine (diameter = 0.25-1.0 mm), clinopyroxene+olivine (diameter = 1.0-2.0 mm), and some plagioclase (diameter = 1.0 mm) glomerocrysts ($Ca_{69}Na_{30}K_1$) are also present. Volumetrically, the amount of clinopyroxene is greater than plagioclase and olivine, where plagioclase = olivine.

SJ20B (Kapp Fishburn Tillite) is a dark gray, slightly vesicular, pilotaxitic, seriate porphyritic ankaramite. Common xenocrysts are subhedral chromium diopside, euhedral to anhedral titaniferous salite, subhedral to anhedral plagioclase, and embayed olivine.

Yellow green chromium diopside xenocrysts (up to 4.0 mm in size) are resorbed and rimmed by a light purple brown titaniferous augite (0.06 mm) around the embayed edges. They may contain plagioclase, olivine, or magnetite and may be simply twinned.

Light brown titaniferous salite xenocrysts attain a maximum of 4.0 mm in size and are found as euhedral and resorbed crystals. They may be sector zoned or reversely zoned in a concentric manner. The cores of the smaller crystals are poikilitic. A sector zoned titaniferous salite appears to be poikilitic on only one side of one of the sectors. The composition of the reversely zoned crystals varies from $Wo_{48}En_{42}Fs_{10}$ in the core to $Wo_{48}En_{43}Fs_9$ on the edges. Clear unaltered red brown glass may occur as inclusions in some titaniferous salites.

Olivine xenocrysts (Fo_{83} and Fo_{78}) attain maximum sizes of 3.5 mm. They may contain magnetite or devitrified glass inclusions and may be polygonized. They are resorbed and iddingsitized about the edges.

Xenocrysts of plagioclase ($Ca_{86}Na_{13}K_1$) are up to 0.75 mm in size, are resorbed and have a rim (0.01 mm) of a more sodic plagioclase around the embayed edges. A few may contain devitrified glass inclusions.

Microphenocrysts of anhedral, brown green-dark brown biotite (up to 0.75 mm long and surrounded by a reaction rim of magnetite), microphenocrysts of plagioclase ($Ca_{83}Na_{16}K_1$), rounded magnetite microxenocrysts (up to 0.6 mm), and xenocrysts occur in a fine grained, intergranular groundmass of light purple brown titaniferous augite prisms ($Wo_{48}En_{41}Fs_{11}$), plagioclase laths ($Ca_{68}Na_{28}K_4$), euhedral and rounded olivine, and magnetite.

Glomerocrysts of clinopyroxene (diameter = 0.5-1.5 mm), olivine (diameter = 0.25 mm), and clinopyroxene+olivine (diameter = 0.3-4.0 mm) are common, though plagioclase, clinopyroxene+plagioclase, olivine+magnetite, and some plagioclase+magnetite are also present. Volumetrically, clinopyroxene > olivine = plagioclase.

NC20 (Storfjellet formation) is a dark gray, slightly vesicular, weakly pilotaxitic, seriate porphyritic ankaramite. Common xenocrysts in NC20 are subhedral to anhedral chromium diopside, subhedral to anhedral titaniferous salite, and embayed olivine.

Yellow green chromium diopside xenocrysts have a composition of $Wo_{46}En_{50}Fs_4$, are up to 6.0 mm in size and may contain inclusions of plagioclase, olivine, or magnetite. They are resorbed and have a 0.08 mm rim of purple brown titaniferous augite ($Wo_{50}En_{40}Fs_{10}$) about the embayed edges. A few are simply twinned.

Xenocrysts of light brown titaniferous salite are reversely zoned (core: $Wo_{49}En_{42}Fs_9$, near rim: $Wo_{46}En_{46}Fs_8$) and are rimmed by titaniferous augite about the edges ($Wo_{46}En_{42}Fs_{12}$). They occur as euhedral and embayed crystals with discontinuous poikilitic rims up to 6.0 mm in size.

Olivine xenocrysts (maximum of 3.0 mm) are resorbed, iddingsitized along the edges, polygonized, and may contain magnetite inclusions. They have a composition of Fo_{89}. One olivine grain contains the 'ghost' of a pyroxene crystal as deduced by the 90° orientation of lines of fine grained opaques.

These xenocrysts, microxenocrysts of resorbed plagioclase up to 0.35 mm in size ($Ca_{83}Na_{16}K_1$), and rounded magnetite, microphenocrysts of euhedral yellow brown-green brown biotite (up to 0.50 mm long with a reaction rim of magnetite), and microphenocrysts of plagioclase ($Ca_{73}Na_{24}K_3$), occur in a fine grained, intergranular groundmass composed of prismatic purple brown, sector zoned titaniferous augite ($Wo_{46}En_{42}Fs_{12}$), plagioclase laths ($Ca_{71}Na_{26}K_3$), olivine hexagons and equant magnetite grains.

Clinopyroxene (diameter = 1.0-3.0 mm) and clinopyroxene+olivine (diameter = 0.5-4.0 mm) glomerocrysts are most abundant, however, olivine and olivine+magnetite glomerocrysts are also found. The volume percent of clinopyroxene > olivine > plagioclase.

NC15 (Nordvestkapp formation) is a dark gray, slightly vesicular, weakly pilotaxitic, seriate porphyritic ankaramite. Xenocrystal phases present are subhedral to anhedral chromium diopside, euhedral to anhedral titaniferous salite, and embayed olivine.

Xenocrysts of yellow green chromium diopside ($Wo_{46}En_{49}Fs_5$) are up to 4.0 mm in size and are resorbed and rimmed (0.03 mm) by a light purple brown titaniferous augite ($Wo_{49}En_{44}Fs_7$) about the embayed edges. They are polygonized and may contain plagioclase, olivine, or magnetite. A few are simply twinned.

Resorbed xenocrysts and euhedral microphenocrysts of titaniferous salite ($Wo_{50}En_{41}Fs_9$) are light brown to light purple brown reversely zoned crystals rimmed by titaniferous augite. The xenocrysts occur up to 4.0 mm in size and may contain brown yellow-brown pleochroic kaersutite(?). Some microphenocrysts are simply twinned.

Olivine xenocrysts (Fo_{88}) attain a maximum size of 2.0 mm and are resorbed, may be polygonized, and may contain inclusions of magnetite. Some are partially altered to hematite along cracks and cleavages.

Microxenocrysts of resorbed and rimmed plagioclase ($Ca_{80}Na_{19}K_1$) containing glass inclusions, rounded and resorbed magnetite (up to 0.5 mm), microphenocrysts of euhedral olivine (Fo_{86}) and equant hematite, and the xenocrysts occur in a fine grained, intergranular groundmass of light purple brown titaniferous augite prisms ($Wo_{46}En_{42}Fs_{12}$), plagioclase laths ($Ca_{66}Na_{32}K_2$), euhedral olivine, ragged red brown biotite plates, and magnetite.

Glomerocrysts of clinopyroxene (diameter = 0.3-2.0 mm) and plagioclase with devitrified glass inclusions ($Ca_{74}Na_{24}K_2$ with a diameter = 0.3-2.0 mm) are common. Clinopyroxene+plagioclase, clinopyroxene+olivine, clinopyroxene+olivine+plagioclase, and sometimes olivine+magnetite also occur in this ankaramite. Generally, the volume percent of clinopyroxene > olivine = plagioclase.

NC27L (Nordvestkapp formation) is a dark gray, moderately vesicular, nonpilotaxitic, seriate porphyritic ankaramite. Common xenocrysts in NC27L are subhedral to anhedral chromium diopside, anhedral to euhedral titaniferous salite, subhedral plagioclase, and embayed olivine.

Chromium diopside xenocrysts ($Wo_{47}En_{48}Fs_5$) have a maximum size of 4.0 mm, are yellow green, polygonized,

resorbed, and have a 0.04 mm rim of a light purple brown titaniferous augite ($Wo_{47}En_{43}Fs_{10}$) about embayed edges. They may contain inclusions of plagioclase, olivine, magnetite, or carbonate (alteration of rounded plagioclase inclusions). They may be simply twinned.

Xenocrysts of light brown titaniferous salite (up to 4.0 mm in size) occur as reversely zoned euhedral and resorbed crystals with a rim of titaniferous augite. Some are sector zoned and have either a poikilitic core or rim of glass inclusions. They may also contain inclusions of yellow brown-brown pleochroic kaersutite(?).

Olivine xenocrysts (up to 2.0 mm) are resorbed, polygonized (as are some olivine glomerocrysts), and may contain magnetite or partially crystallized glass inclusions (with wavy extinction).

Plagioclase xenocrysts (0.05 mm maximum) are resorbed and rimmed (0.02 mm) around the embayed edges. The rims on some crystals may be discontinuously poikilitic with devitrified glass.

These xenocrysts and microxenocrysts of rounded magnetite are set in a very fine grained, intergranular groundmass of tabular, light purple brown titaniferous augite, plagioclase laths, olivine hexagons, and magnetite grains.

Glomerocrysts of clinopyroxene (diameter = 0.3-2.0 mm) and clinopyroxene+olivine (diameter = 0.5-2.0 mm) are common, but plagioclase and clinopyroxene+plagioclase glomerocrysts are also present. Volumetrically, clinopyroxene > olivine > plagioclase.

Alkali Olivine Basalts - Sor Jan

SJ1A (Lower Volcanic Series) has K-Ar ages of 0.49 ± 0.12 my and 0.31 ± 0.12 my (Fitch, Grasty and Miller, 1965) and is a gray, moderately vesicular, trachytic, seriate porphyritic alkali olivine basalt.

Subhedral plagioclase xenocrysts (up to 1.5 mm) are concentrically zoned and contain inclusions of glass. A rim of a more Na rich plagioclase (0.02 mm) surrounds the embayed edges of the plagioclase xenocrysts. Glomerocrysts of plagioclase (diameter = 0.3-1.2 mm) and olivine (diameter = 0.3-0.7 mm) are also resorbed. Other glomerocrysts occurring in SJ1A are composed of plagioclase+ olivine, olivine+magnetite, and plagioclase+olivine+ magnetite.

Microxenocrysts of plagioclase, olivine, and magnetite (up to 0.35 mm) occur in an intergranular groundmass of euhedral purple brown titaniferous augite prisms, plagioclase laths, fork shaped olivine needles and diamonds, rods of ilmenite, and magnetite grains. Groundmass diamond shaped olivines have an opaque core indicating that they crystallized about this pre-existing surface. Generally, the volume percent of plagioclase > clinopyroxene > olivine.

SJ13A (Lower Volcanic Series) has a K-Ar age of less than 0.24 my (Fitch, Grasty and Miller, 1965) and is a gray, slightly vesicular, pilotaxitic, seriate porphyritic alkali olivine basalt.

Xenocrysts of subhedral to anhedral chromium diopside, euhedral titaniferous salite, anhedral plagioclase, and embayed olivine occur in an intergranular matrix of prismatic light purple brown titaniferous augite, plagioclase laths ($Ca_{72}Na_{26}K_2$), and skeletal and diamond shaped olivine.

Light yellow green chromium diopside xenocrysts ($Wo_{43}En_{51}Fs_6$) are up to 3.0 mm in size and are rimmed by a light purple brown titaniferous augite around previously resorbed edges (0.10 mm). They are also polygonized and may contain inclusions of plagioclase, olivine, and magnetite. A few are simply twinned.

Euhedral light brown titaniferous salite (3.0 mm maximum) crystals are reversely zoned (core: $Wo_{45}En_{42}Fs_{13}$, edge: $Wo_{47}En_{45}Fs_8$) or sector zoned. Microphenocrysts of titaniferous salite have a composition of $Wo_{45}En_{45}Fs_{10}$, and may have poikilitic cores.

Olivine xenocrysts (maximum of 1.0 mm) are polygonized, resorbed (some are skeletal), and iddingsitized along the outer edges with a magnetite rim about the crystal. They have a composition of Fo_{88}. Microphenocrysts of olivine have a composition of Fo_{86}.

Xenocrysts of plagioclase (up to 0.70 mm in size) are resorbed and rimmed by a more sodic plagioclase (0.01 mm) around embayed edges. Some are zoned and have altered cores. Microprobe analyses could not be obtained from the core, but the clear edges have a composition of $Ca_{73}Na_{35}K_2$.

Glomerocrysts of clinopyroxene (diameter = 0.2-0.5 mm), olivine (diameter = 0.3-2.0 mm), and clinopyroxene+olivine (diameter = 0.4-1.5 mm) are common in SJ13A. Minor amounts of olivine+magnetite, and clinopyroxene+olivine+magnetite glomerocrysts are also present. The volume percent of plagioclase > clinopyroxene > olivine.

SJ9B (Lower Volcanic Series) is an alkali olivine basalt and has an age of less than 0.24 my (Fitch, Grasty and Miller, 1965). Xenocrysts present in this rock are anhedral to subhedral chromium diopside, anhedral to subhedral titaniferous salite, resorbed olivine and resorbed plagioclase.

Light yellow green chromium diopside crystals are rimmed by a titaniferous augite, and may be polygonized. Xenocrysts of light yellow brown titaniferous salite are reversely zoned and also rimmed by titaniferous augite. The core of a few crystals are poikilitic. Some clinopyroxenes have green cores and colorless rims and are sector zoned.

Olivine xenocrysts are resorbed, polygonized, and iddingsitized.

Plagioclase xenocrysts are rounded, resorbed, and rimmed by a more sodic plagioclase (which is poikilitic with devitrified glass). They attain sizes up to 1.5 mm in diameter. One plagioclase xenocryst exhibits undulatory extinction along with bent Carlsbad-albite twins.

The xenocrysts lie in an intergranular groundmass of euhedral purple brown titaniferous augite, plagioclase laths, partially to totally iddingsitized olivine, and magnetite cubes.

Olivine glomerocrysts (4.0 2.0 mm), plagioclase glomerocrysts, and clinopyroxene glomerocrysts (3.5 3.0 mm) are found in this rock. Generally, the volume of clinopyroxene > olivine > plagioclase.

SJ5A (Middle Volcanic Series) is a gray, moderately vesicular, pilotaxitic, seriate porphyritic alkali olivine basalt. Xenocrystal phases are subhedral to anhedral chromium diopside, euhedral to anhedral titaniferous salite, anhedral plagioclase, and embayed olivine.

Xenocrysts of yellow green chromium diopside (up to 3.0 mm in size) contain inclusions of plagioclase, olivine, magnetite, or carbonate (alteration of rounded plagioclase

inclusions). They are resorbed, polygonized, and have a light purple brown rim (0.10 mm) occurring along embayed edges. A few are simply twinned.

Light brown titaniferous salite xenocrysts (up to 3.0 mm maximum) and microphenocrysts are reversely zoned, and have a rim of titaniferous augite. The rim of some microphenocrysts are poikilitic, whereas the cores of the larger crystals are poikilitic. Titaniferous salite xenocrysts may contain bright red brown clear isotropic inclusions of glass.

Olivine xenocrysts (maximum size of 2.0 mm) may contain magnetite inclusions and are commonly intergrown. Olivines are resorbed, polygonized, iddingsitized along the edges, and sometimes have a reaction rim of magnetite.

Plagioclase xenocrysts (up to 0.75 mm in size) may have altered cores, are resorbed, and have a rim of a more sodic plagioclase (0.02 mm) around the embayed edges.

These xenocrysts, microphenocrysts of plagioclase, tabular anhedral yellow brown biotite (up to 0.35 mm long with a magnetite reaction rim), and rounded magnetite microxenocryst occur in an intergranular groundmass of light purple brown titaniferous augite prisms, forked olivine needles, plagioclase laths, magnetite grains, and ilmenite rods. A groundmass size wedge-shaped crystal with red brown-yellowbrown pleochroism appears similar to kaersutite and lies partially within a microphenocryst of plagioclase.

Clinopyroxene (diameter = 1.0-2.5 mm), olivine (diameter = 0.5-2.0 mm), clinopyroxene+olivine (diameter = 1.0-1.5 mm), and some plagioclase glomerocrysts are found in this rock. Volumetrically, plagioclase > clinopyroxene > olivine.

SJ6 (Middle Volcanic Series) is a gray, moderately to highly vesicular, pilotaxitic, seriate porphyritic alkali olivine basalt. Common xenocrysts are subhedral to anhedral chromium diopside, euhedral to anhedral titaniferous salite, and embayed olivine.

Chromium diopside xenocrysts ($Wo_{44}En_{51}Fs_5$) are up to 4.0 mm in size, are yellow green and may contain inclusions of plagioclase, olivine, magnetite, or carbonate (from alteration of rounded plagioclase inclusions). They are resorbed, may be polygonized, may be simply twinned, and have a 0.06 mm rim of light purple brown titaniferous augite ($Wo_{45}En_{45}Fs_{10}$).

Xenocrysts of brown titaniferous salite are resorbed and attain a maximum size of 4.0 mm. Euhedral light purple brown microphenocrysts of titaniferous salite have a composition of $Wo_{47}En_{44}Fs_9$. Titaniferous salite crystals are reversely zoned or sector zoned and have a rim of titaniferous augite. Some may have poikilitic cores and some may contain red brown-yellow brown pleochroic kaersutite(?).

Olivine xenocrysts (Fo_{84}) are 4.0 mm maximum in size and are commonly intergrown, resorbed, polygonized, and iddingsitized along the edges with a magnetite reaction rim. Some olivines are completely replaced by a magnetite-hematite mass. They also contain inclusions of magnetite and chromium diopside.

These xenocrysts, microphenocrysts of olivine, anhedral red brown-dark red brown biotite (up to 0.20 mm long and rimmed by magnetite), euhedral hematite, microxenocrysts up to 0.75 mm in size of resorbed and rimmed plagioclase containing devitrified glass inclusions ($Ca_{74}Na_{25}K_1$ core rimmed by $Ca_{61}Na_{37}K_2$), and microxenocrysts of rounded magnetite lie in an intergranular groundmass of light purple brown prisms of titaniferous augite ($Wo_{44}En_{46}Fs_{10}$), plagioclase laths ($Ca_{71}Na_{28}K_1$), magnetite grains, amorphous hematite, and some ilmenite rods. It is almost impossible to distinguish plagioclase microxenocrysts from groundmass plagioclase because they span the same size range.

Clinopyroxene (diameter = 0.5-1.5 mm), olivine (diameter = 0.5-1.5 mm), and clinopyroxene+olivine (diameter = 1.0-2.0 mm) glomerocrysts are common. Other glomerocrysts are olivine+magnetite, plagioclase+clinopyroxene+magnetite, plagioclase, and clinopyroxene+olivine+magnetite. Clinopyroxene and plagioclase are volumetrically dominant over olivine, but clinopyroxene = plagioclase.

Alkali Olivine Basalts - Nord Jan

NC17 (Storfjellet formation) is a gray, slightly to moderately vesicular, pilotaxitic, seriate porphyritic alkali olivine basalt. Xenocrysts occurring in NC17 are anhedral to subhedral chromium diopside, anhedral titaniferous salite, anhedral plagioclase, and embayed olivine.

Xenocrysts of yellow green chromium diopside (maximum of 4.0 mm) are resorbed and rimmed (0.04 mm) by a purple brown titaniferous augite along the embayed edges. They may contain inclusions of olivine or magnetite, and some are simply twinned.

Resorbed light brown titaniferous salite (up to 4.0 mm) xenocrysts and euhedral purple brown microphenocrysts are concentrically zoned (core: $Wo_{50}En_{43}Fs_7$, edge: $Wo_{48}En_{43}Fs_9$).

Olivine xenocrysts (Fo_{88}) are up to 4.0 mm in size and glomerocrysts are resorbed and polygonized.

Plagioclase xenocrysts (1.5 mm maximum) may have glass inclusions and may be zoned. They have a composition of $Ca_{88}Na_{11.5}K_{0.5}$. They are resorbed and rimmed by a more sodic plagioclase (0.02 mm) about the embayed edges.

Microphenocrysts of euhedral olivine, anhedral yellow brown to red brown biotite (up to 0.15 mm in size), and microxenocrysts of rounded, resorbed magnetite (up to 0.35 mm) sit in a fine grained, intergranular groundmass of prismatic purple brown titaniferous augite ($Wo_{51}En_{36}Fs_{13}$), laths of plagioclase ($Ca_{63}Na_{36}K_1$), euhedral forked olivine needles (Fo_{58}), and equant magnetite.

Plagioclase glomerocrysts (diameter = 0.25-1.0 mm) are very common in NC17, but glomerocrysts of clinopyroxene (diameter = 0.5-1.5 mm), clinopyroxene+olivine (diameter = 0.5-3.0 mm), and some olivine (diameter = 1.0-3.0 mm) are also present. Generally, the volume percent of plagioclase = clinopyroxene = olivine.

NC22 (Storfjellet formation) is a gray, slightly vesicular, pilotaxitic, porphyritic alkali olivine basalt. Xenocrystal phases present are anhedral chromium diopside, anhedral plagioclase, anhedral titaniferous salite, and resorbed olivine.

Yellow green chromium diopside xenocrysts ($Wo_{45}En_{50}Fs_5$) attain sizes up to 1.5 mm and may have inclusions of plagioclase, olivine, or magnetite and may be polygonized. They are resorbed and rimmed (0.02 mm) by a purple brown titaniferous augite ($Wo_{47}En_{41}Fs_{12}$) about the embayed edges.

A few zoned titaniferous salite xenocrysts form an anhedral glomerocryst which has a rim of titaniferous augite about it.

Olivine xenocrysts (Fo_{90}) attain a maximum size of 1.5 mm and may be polygonized and may contain inclusions of magnetite. They are surrounded by a magnetite reaction rim.

Resorbed plagioclase xenocrysts have a composition of $Ca_{86}Na_{13}K_1$ and have a 0.01 mm rim of a more sodic and potassic feldspar ($Ca_{51}Na_{45}K_4$). They attain a maximum size of 1.3 mm and may contain inclusions of glass.

These xenocrysts, microphenocrysts of subhedral biotite and microxenocrysts of rounded magnetite (up to 0.10 mm in size) are set in an intergranular groundmass of purple brown titaniferous augite prisms, plagioclase laths ($Ca_{54}Na_{43}K_3$), olivine hexagons, needles, and diamonds and magnetite grains.

Plagioclase glomerocrysts (diameter = 0.5-1.5 mm) are predominant over clinopyroxene+magnetite and olivine+ magnetite glomerocrysts. Clinopyroxene and plagioclase are volumetrically dominant over olivine, but clinopyroxene = plagioclase.

NC23 (Storfjellet formation) is a dark gray, moderately to highly vesicular, pilotaxitic, seriate porphyritic alkali olivine basalt. Common xenocrysts are anhedral chromium diopside, euhedral to anhedral titaniferous salite, anhedral plagioclase, and embayed olivine.

Yellow green chromium diopside xenocrysts (maximum of 6.0 mm in size) may contain inclusions of plagioclase, olivine, or magnetite. They are resorbed, rimmed by a purple brown titaniferous augite (0.07 mm) around the embayed edges, and may be simply twinned.

Euhedral to resorbed light brown titaniferous salite xenocrysts (up to 6.0 mm maximum) and euhedral purple brown microphenocrysts are sector zoned or reversely zoned with a rim of titaniferous augite which may be poikilitic. Some may contain red-brown glass or altered kaersutite(?) which is distinguished by lines of opaques parallel to 124° - 56° cleavage angles.

Olivine xenocrysts (Fo_{89}) attain sizes up to 4.0 mm and are resorbed, may contain magnetite inclusions and may be polygonized (as are some olivine glomerocrysts).

Xenocrysts of plagioclase (3.0 mm maximum) are resorbed and have a rim of a more sodic plagioclase (0.01 mm) about the embayed edges. They may be zoned having cores that are poikilitic with devitrified glass inclusions. Some exhibit combined Carlsbad-albite twins.

These xenocrysts and rounded magnetite microxenocrysts (up to 0.50 mm) are set in an intergranular groundmass of prismatic purple brown titaniferous augite, plagioclase laths, olivine hexagons (formed about tiny opaque points) and equant magnetite.

Clinopyroxene (diameter = 0.5-1.0 mm) and clinopyroxene+ olivine (diameter = 0.5-3.0 mm) glomerocrysts are most common but clinopyroxene+plagioclase, clinopyroxene+plagioclase+magnetite, and some plagioclase glomerocrysts are present. Generally, the volume percent of clinopyroxene > plagioclase > olivine.

NC34B (Nordvestkapp formation) is a dark gray, highly vesicular, glomeroporphyritic alkali olivine basalt. Phenocrysts present in NC34B are euhedral titaniferous salite, euhedral to subhedral plagioclase, and euhedral olivine.

Plagioclase phenocrysts and glomerocrysts ($Ca_{81}Na_{17.5}K_{1.5}$) are predominant and are surrounded by a rim 0.02 mm wide of a more sodic plagioclase ($Ca_{62}Na_{34}K_4$). Twinned and untwinned zoned plagioclase phenocrysts exhibit strong undulatory extinction, and some contain devitrified glass inclusions. Small phenocrysts (up to 0.35 mm in size) and glomerocrysts of olivine have a composition of Fo_{76} and some contain magnetite inclusions.

Euhedral dark purple brown sector zoned titaniferous salite microphenocrysts (up to 0.50 mm in size) and glomerocrysts of plagioclase (diameter = 0.5-1.0 mm) and olivine (diameter = 0.25-0.50 mm) rest in an intergranular matrix of prismatic dark purple brown, sector zoned titaniferous augite ($Wo_{49}En_{37}Fs_{14}$), plagioclase ($Ca_{68}Na_{29}K_3$), olivine diamonds and forked needles, ilmenite rods, and equant magnetite. Glomerocrysts of plagioclase+olivine also are present. Volumetrically, plagioclase = clinopyroxene > olivine.

JB202 (Sentralkrateret formation) is a gray to gray brown, highly vesicular, glomeroporphyritic alkali olivine basalt. Phenocrystal phases present are subhedral titaniferous salite and anhedral plagioclase.

Titaniferous salite phenocrysts ($Wo_{46}En_{43}Fs_{11}$) attain a maximum size of 1.1 mm, are sector zoned, and may be simply twinned. They may contain plagioclase and magnetite inclusions.

Plagioclase phenocrysts (up to 1.0 mm in size) and glomerocrysts (diameter = 0.1-2.0 mm) are abundant ($Ca_{82.5}Na_{16}K_{1.5}$) and may have a more sodic plagioclase rim of $Ca_{60}Na_{37}K_3$ (0.01 mm) about apparently resorbed edges. Some have combined Carlsbad-albite twins and appear zoned with inclusions of devitrified glass in the core. Twinned and untwinned zoned plagioclase phenocrysts exhibit strong undulatory extinction.

The phenocrysts and microphenocrysts of iddingsitized olivine (up to 0.20 mm with a magnetite reaction rim) and pseudomorphous magnetite after olivine (up to 0.75 mm) lie in an intergranular groundmass of dark purple brown, sector zoned titaniferous augite prisms ($Wo_{47}En_{35}Fs_{18}$) occasionally altering to a yellow brown amphibole, plagioclase laths ($Ca_{59}Na_{37}K_4$), euhedral olivine (Fo_{72}) surrounded by magnetite, rods of ilmenite and magnetite grains.

Lesser amounts of clinopyroxene (diameter = 0.5-2.0 mm), clinopyroxene+plagioclase, clinopyroxene+plagioclase+olivine, plagioclase+magnetite, clinopyroxene+plagioclase+magnetite, olivine, and plagioclase+olivine glomerocrysts also occur. Generally, the volume percent of plagioclase > clinopyroxene > olivine.

NC12C (Tromsoryggen formation) is a gray, moderately to highly vesicular, pilotaxitic, seriate porphyritic alkali olivine basalt. Xenocrysts occurring in this rock are subhedral to euhedral titaniferous salite, anhedral plagioclase, and olivine.

Light brown subhedral titaniferous salite xenocrysts (up to 1.4 mm in size) and euhedral purple brown microphenocrysts ($Wo_{48}En_{42}Fs_{10}$) are sector zoned, and may contain inclusions of hematite, plagioclase, olivine or magnetite. They are slightly resorbed and some are also simply twinned. The rock consists primarily of titaniferous salite glomerocrysts and chromium diopside xenocrysts appear to be absent.

Olivine xenocrysts (maximum of 1.0 mm) are resorbed and may contain magnetite inclusions. Euhedral olivine phenocrysts are also present and may contain magnetite inclusions.

Plagioclase xenocrysts (0.65 mm maximum) are resorbed and rimmed (0.01 mm) by a more sodic plagioclase about the embayed edges. One plagioclase xenocryst shows bent and strained albite twins.

These xenocrysts and microphenocrysts of plagioclase ($Ca_{69}Na_{29}K_2$), and olivine (Fo_{85}) are set in an intergranular matrix of prismatic purple brown titaniferous augite, plagioclase laths ($Ca_{66}Na_{32.5}K_{1.5}$), diamond shaped and skeletal olivine, and equant magnetite.

Glomerocrysts of clinopyroxene+olivine (diameter = 0.25-3.0 mm) are most common, but other glomerocrysts of clinopyroxene, plagioclase, olivine, clinopyroxene+plagioclase, and clinopyroxene+plagioclase+olivine also are found. Volumetrically, plagioclase and clinopyroxene exceed olivine, but plagioclase = clinopyroxene.

NC35B (Tromsoryggen formation) is a gray, highly vesicular, pilotaxitic, seriate porphyritic alkali olivine basalt. Xenocrystal phases present are subhedral chromium diopside, anhedral titaniferous salite, subhedral to anhedral plagioclase, and embayed olivine.

Yellow green chromium diopside xenocrysts (maximum size of 2.5 mm) are resorbed and rimmed (0.04 mm) by a light purple brown titaniferous augite along the embayed edges. They may have plagioclase and magnetite inclusions.

Xenocrysts of titaniferous salite are reversely zoned and unrimmed.

Olivine xenocrysts (0.70 mm maximum) are resorbed and may be polygonized. Plagioclase xenocrysts (up to 1.0 mm in size) are resorbed and have a distinct rim of a more sodic plagioclase (0.01 mm) about the embayed edges. Some contain glass inclusions. Both plagioclase and olivine xenocrysts may have magnetite inclusions.

The xenocrysts, rounded magnetite microxenocrysts, and euhedral magnetite phenocrysts lie in a very fine grained, intergranular groundmass composed of purple brown sector

zoned titaniferous augite prisms (sometimes in radiating groups), plagioclase laths, olivine diamonds and forked needles, and magnetite grains.

Glomerocrysts of plagioclase (diameter = 0.3-1.0 mm) are predominant, though some consisting of clinopyroxene+ olivine+magnetite also occur. Generally, the volume percent of plagioclase > clinopyroxene > olivine.

NC30C (Tromsoryggen formation) is a gray to dark gray, moderately to highly vesicular, pilotaxitic, porphyritic alkali olivine basalt. Xenocrysts occurring in NC30C are subhedral chromium diopside, subhedral to anhedral plagioclase, anhedral titaniferous salite, and embayed olivine.

Light green chromium diopside xenocrysts (up to 3.0 mm in size) are resorbed and rimmed by a purple brown titaniferous augite (0.03 mm). They may have olivine, plagioclase, or magnetite as inclusions.

Rounded, embayed light brown titaniferous salite xenocrysts rimmed by a titaniferous augite are also present.

Olivine xenocrysts (2.0 mm maximum) are resorbed and may be faintly polygonized as are some olivine glomerocrysts.

Plagioclase xenocrysts (maximum size of 0.5 mm) are resorbed and rimmed by a more sodic plagioclase (0.01 mm). They may contain inclusions of glass.

The xenocrysts, microphenocrysts of subhedral, red brown-yellow brown biotite (up to 0.15 mm long with a reaction rim of magnetite), and microxenocrysts of resorbed, rounded magnetite (up to 0.7 mm in size) occur in a very fine grained, intergranular groundmass of prismatic purple brown, simply twinned titaniferous augite (sometimes found in radiating glomerocrysts), plagioclase laths, olivine diamonds and forked needles, and magnetite grains.

Plagioclase glomerocrysts (diameter = 0.2-1.5 mm) are most common, but clinopyroxene and some clinopyroxene+ olivine glomerocrysts are present. Volumetrically, plagioclase > clinopyroxene > olivine.

Latite Andesites

SJ2B (Lower Volcanic Series) has a K-Ar age of 0.49 ± 0.12 my or 0.31 ± 0.12 my (Fitch, Grasty and Miller, 1965) and is a light gray, nonvesicular, trachytic, porphyritic latite andesite.

Phenocrysts of anhedral, equant Na-K rich plagioclase (up to 3.0 mm in size) appear to be resorbed and have a thin rim (0.03 mm) about the embayed edges. They exhibit an undulatory extinction and some may contain inclusions of clinopyroxene or magnetite. The composition of the feldspars varies widely. Core compositions are: $Ca_{34}Na_{60}K_6$, $Ca_{25}Na_{66}K_9$, $Ca_{18}Na_{69}K_{13}$ and their respective rim compositions are: $Ca_{29}Na_{65}K_6$, $Ca_{18}Na_{69}K_{13}$, and $Ca_3Na_{61}K_{36}$.

Na-K rich plagioclase phenocrysts and microphenocrysts of subhedral, dark brown to brown biotite (up to 1.5 mm long surrounded by a magnetite reaction rim), dark brown anhedral hornblende (which also has a magnetite reaction rim), and rounded resorbed magnetite (0.35 mm maximum in size) sit in a flow aligned groundmass of zoned sodic plagioclase laths ($Ca_{31}Na_{61}K_8$), interstitial potassium feldspar laths ($Ca_{17}Na_{67}K_{16}$), and magnetite grains.

Glomerocrysts of plagioclase (diameter = 1.0-3.0 mm) and Na-K rich plagioclase (diameter = 0.25-1.0 mm) are predominant. Generally, the volume percent of plagioclase+ potassium feldspar is greater than that of clinopyroxene.

JB1I (Sentralkrateret formation) is an ejected lava block from Eggoya and may be equivalent to a late Middle Volcanic Series lava. It is a light gray to gray, nonvesicular, trachytic, seriate porphyritic biotite latite andesite. Common phenocrysts in JB1I are euhedral altered clinopyroxene, anhedral plagioclase, subhedral to anhedral biotite and anhedral hornblende.

Phenocrysts of clinopyroxene (up to 1.2 mm in size) are completely altered to calcite, hematite, and a felty mass (actinolite-tremolite?). The clinopyroxene 'ghosts' contain inclusions of plagioclase, magnetite, and biotite.

Plagioclase phenocrysts (maximum of 3.0 mm in size) are zoned, resorbed, and have a rim of potassium feldspar (0.02 mm) around the resorbed edges. Chemically, the zonation varies from $Ca_{50}Na_{46}K_4$ in the core to $Ca_{44}Na_{51}K_5$ near the rim. They may contain inclusions of clinopyroxene or magnetite. Some have combine Carlsbad-albite twins.

Biotite phenocrysts (up to 1.2 mm long) display a dark brown-yellow brown pleochroism and are surrounded by a reaction rim of magnetite. Some biotite crystals contain plagioclase as an inclusion.

Hornblende phenocrysts (maximum of 1.5 mm long) are dark red brown and are altered to magnetite and hematite on the outer edges. Magnetite microphenocrysts (0.5 mm

maximum in size) appear resorbed in some cases and are often pseudomorphous after biotite or hornblende.

These phenocryst phases lie in a flow aligned groundmass of plagioclase laths ($Ca_{34}Na_{60}K_6$), intersitial potassium feldspar laths ($Ca_3Na_{58}K_{39}$), magnetite, and amorphous hematite staining the groundmass red.

Glomerocrysts which occur in this rock are combinations of clinopyroxene, plagioclase, magnetite, biotite, and hornblende. Glomerocryst sizes range from 0.5 to 3.0 mm in diameter.

Trachytes

SJ25B (Middle Volcanic Series) is a light gray to white nonvesicular, trachytic, seriate porphyritic alkali trachyte. Phenocryst phases present in this rock are subhedral aegirine-augite, anhedral plagioclase, anhedral equant anorthoclase, and subhedral to anhedral biotite.

Phenocrysts of bright green aegirine-augite ($Wo_{44}En_{34}Fs_{22}$) attain sizes up to 1.0 mm and may contain inclusions of hematite, plagioclase, or magnetite.

Plagioclase phenocrysts ($Ca_{32}Na_{62}K_6$) are a maximum of 4.5 mm in size, appear resorbed and are rimmed by 0.12 mm of potassium feldspar ($Ca_0Na_{56}K_{44}$) around the embayed edges. They may contain clinopyroxene, magnetite, or biotite inclusions.

Anorthoclase phenocrysts have a composition of $Ca_1Na_{67}K_{32}$ and are up to 4.0 mm in size. They also appear to be resorbed and rimmed (0.03 mm) and may contain inclusions of magnetite, clinopyroxene, or biotite. They also exhibit an undulatory extinction.

Euhedral squares of sanidine ($Ca_{0.1}Na_{51.9}K_{48}$) microphenocrysts are also present.

Biotite phenocrysts (up to 1.4 mm long) display a brown green to dark brown pleochroism and are surrounded by a reaction rim of magnetite and hematite. Rounded magnetite microphenocrysts attain a maximum size of 0.35 mm.

The groundmass consists of flow aligned plagioclase laths, anhedral alkali feldspar ($Ca_3Na_{58}K_{39}$), and magnetite grains.

Glomerocrysts which occur in SJ25B are combinations of anorthoclase, aegirine-augite, magnetite, and biotite. They range in size from 0.5 to 4.0 mm in diameter. Generally, the volume percent of plagioclase+potassium feldspar is greater than that of clinopyroxene.